Alma Mater Studiorum – University of Bologna

Submitted in accordance with the requirement for the degree of

DOCTOR OF PHILOSOPHY IN BIOENGINEERING

XXVI CYCLE

IN VIVO EVALUATION OF THE TRANSLATIONS OF THE GLENO-HUMERAL JOINT USING MAGNETIC RESONANCE IMAGING

Manuela Calderone

Supervisor
Prof. Ugo Della Croce

Co-supervisor
Dr. Andrea Cereatti

Examiners
Prof. Luca Cristofolini
Dr. Ara Nazaria

Alma Mater Studiorum – Università di Bologna

DOTTORATO DI RICERCA IN

BIOINGEGNERIA

Ciclo XXVI

Settore Concorsuale di afferenza: 09/G2

Settore Scientifico disciplinare: ING-INF/06

IN VIVO EVALUATION OF THE TRANSLATIONS OF THE GLENO-HUMERAL JOINT USING MAGNETIC RESONANCE IMAGING

Presentata da: Manuela Calderone

Coordinatore Dottorato
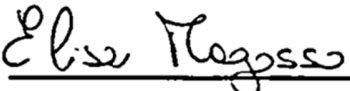
Relatore
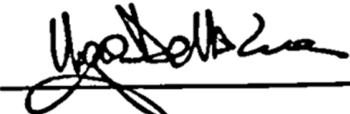
Esame finale anno 2014

TABLE OF CONTENTS

SUMMARY

Gleno-humeral joint (GHJ) is the most mobile joint of the human body. This is related to the incongruence between the large humeral head articulating with the much smaller glenoid (ratio 3:1). The GHJ laxity is the ability of the humeral head to be passively translated on the glenoid fossa and, when physiological, it guarantees the normal range of motion of the joint. Three-dimensional GHJ linear displacements have been measured, both *in vivo* and *in vitro* by means of different instrumental techniques. *In vivo* gleno-humeral displacements have been assessed by means of stereophotogrammetry, electromagnetic tracking sensors, and bio-imaging techniques. Both stereophotogrammetric systems and electromagnetic tracking devices, due to the deformation of the soft tissues surrounding the bones, are not capable to accurately assess small displacements, such as gleno-humeral joint translations. The bio-imaging techniques can ensure for an accurate joint kinematic (linear and angular displacement) description, but, due to the radiation exposure, most of these techniques, such as computer tomography or fluoroscopy, are invasive for patients. Among the bio-imaging techniques, an alternative which could provide an acceptable level of accuracy and that is innocuous for patients is represented by magnetic resonance imaging (MRI). Unfortunately, only few studies have been conducted for three-dimensional analysis and very limited data is available in situations where preset loads are being applied.

The general aim of this doctoral thesis is to develop a non-invasive methodology based on open-MRI for *in-vivo* evaluation of the gleno-humeral translation components in healthy subjects under the application of external loads. To achieve this goal it was necessary to take action on two critical points related to the use of MR scanner: (1) the definition of scapula and humerus anatomical coordinate systems which are suitable to be used with 3D incomplete bone models obtained from MRI images; (2) the development of a device for applying an external force during a MRI exam and which was compatible, in terms of material, with the MR scanner.

For the research study thirteen asymptomatic shoulders were acquired using a horizontal open magnetic resonance scanner. Recordings were made with the subjects in the supine position both at 15 deg and 90 deg of arm abduction with and without an anterior force of 20 N applied to the humerus. The results showed that when no load was applied, from 15 deg to 90 deg of arm abduction, the translation of the humeral head center with respect the glenoid fossa were greater in the anterior and superior direction

than in the medio-lateral direction. Under the application of the anterior force no statistically significant differences were found in the GHJ laxity between 15 deg and 90 deg of arm abduction. The translations observed *in vivo* in this study were significantly smaller than those observed in previous cadaver studies under the application of an anterior load of 20 N. This discrepancy can be ascribed to the total or partial lack of the shoulder muscles and differences in muscular tone. The results also showed a level of precision associated to the GHJ translation estimates of one order of magnitude smaller than the relevant translations.

SOMMARIO

L'articolazione gleno-omerale rappresenta l'articolazione più mobile del corpo umano. Le ragioni di ciò sono da ricondursi alla parziale congruenza tra la testa omerale che si articola con la più piccola cavità glenoidea (rapporto 3:1). La lassità dell'articolazione gleno-omerale rappresenta l'attitudine della testa omerale a essere traslata passivamente rispetto alla cavità glenoidea; essa garantisce, quando fisiologica, il normale range di movimento dell'articolazione. Gli spostamenti lineari tridimensionali (lassità) sono stati misurati, sia *in vivo* sia *in vitro* per mezzo di diverse tecniche strumentali. *In vivo* gli spostamenti dell'articolazione gleno-omerale sono stati valutati con sistemi stereofotogrammetrici, sensori di tracciamento elettromagnetici, e tecniche di *bio-imaging*.

Sia i sistemi stereofotogrammetrici sia i dispositivi di tracciamento elettromagnetici, a causa della deformazione dei tessuti molli che circondano le ossa, non sono adatti a stimare accuratamente piccoli spostamenti, come possono essere le traslazioni dell'articolazione gleno-omerale. Le tecniche di *bio-imaging* possono garantire un'accurata descrizione della cinematica articolare (spostamenti lineari e angolari), ma a causa dell'esposizione alle radiazioni molte di queste tecniche, come la tomografia assiale computerizzata e la fluoroscopia, sono invasive per i pazienti. Tra le tecniche di *bio-imaging*, un'alternativa che può garantire un accettabile livello di accuratezza e che risulta innocua per i pazienti è rappresentata dall'*imaging* di risonanza magnetica (RM). Sfortunatamente, solo pochi studi sono stati condotti sull'analisi tridimensionale e pochi dati sono disponibili in situazioni in cui l'articolazione è soggetta all'azione di carichi esterni noti.

L'obiettivo generale di questa tesi di dottorato è di sviluppare una metodologia non invasiva basata sulla RM aperta per la valutazione in vivo delle componenti traslazionali dell'articolazione gleno-omerale in soggetti sani e con l'applicazione di carichi esterni. Per raggiungere quest'obiettivo è stato necessario intervenire su due punti critici legati all'uso della RM: (1) la definizione dei sistemi di riferimento anatomici di scapola e omero, compatibili con l'uso di modelli ossei 3D incompleti ottenuti da immagini di RM; (2) lo sviluppo di un dispositivo per l'applicazione di carichi esterni durante gli esami di RM e che fosse compatibile, in termini di materiali, con lo scanner di RM.

Per lo studio sono state acquisite tredici spalle asintomatiche per mezzo uno scanner di RM aperta orizzontale. Le acquisizioni sono state fatte con il soggetto in posizione supina con il braccio abdotto a 15 e a 90 gradi, in presenza e in assenza di un carico esterno di intensità pari a 20 N applicato all'omero

e diretto anteriormente. I risultati hanno mostrato che in assenza di carco, da 15 a 90 gradi di abduzione dell'omero, le traslazioni del centro della testa dell'omero rispetto alla cavità glenoidea erano maggiori in direzione anteriore e superiore rispetto alla direzione medio laterale. Non sono state trovate differenze significative nella lassità dell'articolazione gleno-omerale nelle due posizioni del braccio analizzate (15 e 90 gradi di abduzione) a seguito dell'applicazione del carico. Le traslazioni osservate in vivo in questo studio sono significativamente più piccole rispetto a quelle osservate in studi precedenti svolti su cadavere e con l'applicazione di un carico esterno d'intensità pari a 20 N diretto anteriormente. Questa discrepanza può essere attribuita alla totale o parziale mancanza dei muscoli della spalla e alle differenze nel tono muscolare. I risultati hanno mostrato inoltre un livello di precisione associata alla stima delle traslazioni dell'articolazione gleno-omerale di un ordine di grandezza più piccolo rispetto alle effettive traslazioni.

STRUCTURE OF THE THESIS

The present doctoral thesis fits in the broader context of the gleno-humeral joint laxity evaluation which represents a topic of high relevance both in biomechanics and orthopedic medicine. Specifically, the general objective of the present thesis concerns the evaluation of the translational components of the joint under the action of an anterior directed force.

Primary and secondary aims of the doctoral thesis and the main issues addressed during the research work were discussed in CHAPTER 1.

In CHAPTER 2, a brief description of the shoulder joint complex and a detailed description of the anatomy and biomechanics of the gleno-humeral joint are reported.

The CHAPTER 3 reports a literature review of the *in vivo* and *in vitro* techniques proposed for the evaluation and quantification of the translation of the gleno-humeral joint. This section also focuses on the magnetic resonance imaging technique by covering the following topics physical principles, image formation, and acquisition parameters.

The CHAPTER 4 contains a review of the literature on scapula and humerus anatomical reference systems. In addition a novel proposal for the definition of scapula and humerus anatomical reference systems is presented. In this chapter it is also investigated an alternative method for the definition of the humerus anatomical coordinate system.

In CHAPTER 5 is presented a MRI based methodology for the evaluation of the translations of the gleno-humeral joint. The thesis ends with a section reporting the general conclusions.

GLOSSARY OF TERMS

3D: Three-dimensional

AA: Angulus Acromialis

ACS: Anatomical Coordinate System

AL: Anatomical landmark

AN: anatomical Neck

A-P: Anterior-Posterior

AR: Anatomical Region

B_0: Magnetic Field Strength

CP: Tip of Coracoid Process

CT: Computed Tomography

DoF: Degree of Freedom

DRRs: Digitally Reconstructed Radiographs

EBCT: Electron Beam Computed Tomography

FFT: Fast Fourier Transform

FoV: Field of View

GHJ: Gleno Humeral Joint

GHJC: Gleno Humeral Joint Center

G: Glenoid

GT: Greater tubercle

HHC: Humera Head Center

IA: Inferior Angle

LB: Lateral Border

LE: Lateral Epicondyle

LT: Lesser Tubercle

$MAD_{x,y,z}^{\theta}$ / $MAD_{x,y,z}^{\phi}$: Mean Absolute Angular Deviation Value

MEc: Medial epicondyle (central)

M-L: Medio-Lateral

MRI: Magnetic Resonance Imaging

NMV: Net Magnetization Vector

RSA: Radio Stereometric Analisis

RF: Radio Frequency

SBP: Portion of the Subject Specific Bone Model

SD: Standard Deviation

S-I: Superior-Inferior

SS: Root of Scapula Spine

TBC: Template of a Complete Bone Model

TE: Echo Time

TR: Repetition Time

TS: Trigonium Spinae Scapula

CHAPTER 1

AIMS OF THE THESIS

Traumatic joint dislocations represent a frequent and important problem in orthopaedic surgery and sports medicine. The most frequently dislocated joint by far is the shoulder, or the gleno-humeral joint (GHJ), which is characterized by the widest range of motion among the human joints and by very little coverage of the humeral head by the joint socket. The incidence of gleno-humeral dislocations has been reported to be 11.2 per 100`000 per year and a high number of recurrences after the first dislocation have been reported, especially in young patients. The investigation of gleno-humeral kinematics of the shoulder, in terms of rotations and translations and joint stability, has been a primary focus of orthopaedic research and it is instrumental in understanding and thus preventing primary and repeated shoulder dislocations. *In vivo* kinematics of the shoulder joint has been studied by means of different instrumental techniques (Hill et al., 2007). Both using stereo-photogrammetric systems and electromagnetic tracking devices, the orientation and position of the relevant body segments are estimated using sensors placed on the skin of the subject. Due to the deformation of the soft tissues surrounding the bones, there is an ongoing debate about the capability to accurately track the movement of the underlying bony segments from sensors attached to the skin (van Andel et al., 2009). It is especially true, when small displacements, such as gleno-humeral joint translations, need to be assessed. An alternative approach is offered by the use of technologies based on ionizing radiation such as computer tomography (Baeyens et al., 2001), biplanar X-rays (Lagacé et al., 2012), fluoroscopy (San Juan and Karduna, 2010) or a combination of dual-plane fluoroscopy and 3D bone models derived from CT. Major limitations of such techniques include the image geometric distortion and invasiveness due to the radiation exposure. A further alternative, which could provide an acceptable level of accuracy and that is innocuous for patients, is the use of magnetic resonance imaging (MRI) (von Eisenhart-Rothe et al., 2010). GHJ translations have been investigated both in healthy subjects (Rohad et al, 1998; Graichen et al., 2000; Sahara et al., 2007) and patients (von Eisenhart-Rothe et al., 2002; Chhadia et al., 2010) using MRI. However, none of the latter *in vivo* studies analyzed the GHJ translations under the action of selected external forces. This doctoral research aims at developing and testing a MRI based methodology for *in vivo* estimation of the GHJ translations with and without an external load. The images from an open-MRI system were used, along with three-dimensional post-processing methods, to analyze gleno-humeral displacements (1) in different shoulder positions and (2) under the application of an anterior load in healthy volunteers. In contrast to earlier conducted cadaveric studies and anatomical studies using bone pin markers, the assessment with open-MRI allowed us to observe and document joint motion at high resolution and with all passive restraints

(ligaments, joints capsule) and active stabilizers (musculature) in place and fully, physiologically functioning.

This research represents the first step of a wider research aimed at developing and validating both experimental and analytical methods for evaluating and comparing the outcome of different surgical techniques and rehabilitation protocols for the treatment of gleno-humeral joint dislocation using bio-imaging techniques as an ultimate goal.

While pursuing, the main aim of the present doctoral thesis, the following secondary aims were also considered:

Anatomical coordinate systems definition

The description of joint kinematics requires the definition of anatomical reference systems of the bone segments forming the joint. Most of the definitions in the literature are based either on the identification of anatomical landmarks, or anatomical regions located in the distal portions of the bones under analysis. Often, the relevant anatomical landmarks or anatomical regions are not included in the images acquired using bio-imaging techniques for the clinical examination of the joint. In fact, these techniques have the limitation of being characterized by a restricted field of view (FoV) which may prevent the acquisition of the entire bones.

Development of a device for applying an external force during a MRI exam

To study the gleno-humeral joint in different configurations while an external force is applied, a device for fixing the arm at different degrees of abduction and applying a selected force to the proximal humerus was developed. Since the recordings have to be carried out under high intensity magnetic fields and in small measurement volumes, particular attention was paid in the selection of non-ferromagnetic materials for the construction of the device for the shoulder loading.

CHAPTER 2

THE SHOULDER JOINT COMPLEX AND THE GLENO-HUMERAL JOINT

2.1 Anatomy of the shoulder joint complex

The shoulder joint complex is formed by the shoulder girdle and the humerus. The shoulder or pectoral girdle is the set of bones which connects the upper limb to the axial skeleton. It consists of the clavicle, scapula and sternum. The pectoral girdle is a complex of five joints that can be divided into two groups. Three of these joints are true anatomical joints, while two are physiological joints. Within each group, the joints are mechanically linked so that both groups simultaneously contribute to the different movements of the shoulder to variable degrees.

The scapulo-thoracic joint is not a true joint in anatomical sense, it has no capsule or ligamentous attachments, but is a physiological joint formed by articulation of the anterior scapula with the posterior thoracic rib cage. The scapula attachment to the axial skeleton in a healthy shoulder is purely musculo-tendinous, formed by the trapezius and serratus muscles. Its gliding movement patterns consist of elevation/depression, retraction/protraction, and superior/inferior rotation. Scapulo-thoracic joint function enhances arm-trunk motion and gleno-humeral stability as the scapula orients the glenoid to the humeral head.

Sterno-clavicular joint represents the single bony articulation between the axial skeleton and upper extremity (Dempster, 1965). It is formed by the articulation of the manubrium of the sternum and the first costal cartilage with the medial end of the clavicle. The sterno-clavicular joint serves as the pivot point for scapular elevation-depression and abduction-adduction (Doody et al., 1970).

Acromio-clavicular joint is a plane synovial joint formed by the articulation of the distal clavicle with the acromion of the scapula. The acromion of the scapula rotates on the acromial end of the clavicle. Three degrees of freedom are available at the acromio-clavicular joint. Movement can occur between the acromion and lateral end of the clavicle, about a vertical axis, around a frontal axis, and about a sagittal axis (Peat, 1986).

*Supra-humeral joint (*subacromial joint) is a physiological joint formed by an articulation of the coraco-acromial ligament and the head of the humerus. It is formed by the gap between the humerus and the acromion process of the scapula. This joint plays a role during complex movements while the arm is fully flexed at the gleno-humeral joint.

Gleno-humeral joint is the articulation between the head of the humerus and the glenoid cavity of the scapula. It is a ball-and-socket type of synovial joint. It represents the most important joint of the shoulder. In this chapter we will focus on the gleno-humeral joint, its components and the mechanism which confer mobility to the joint.

Plane of motion of the shoulder complex

Motion of the shoulder complex is described in relation to the cardinal planes, sagittal, coronal, and horizontal (Fig. 2.1). Shoulder flexion and extension occur in the sagittal plane, abduction and adduction in the coronal plane, and horizontal abduction and adduction in the horizontal plane. Internal and external rotation occurs through the long axis of the humerus, affording a high degree of mobility in an in finite number of planes. This is typically assessed at 90 deg of coronal plane abduction or with the arm at the side (Kelley et al., 1995).
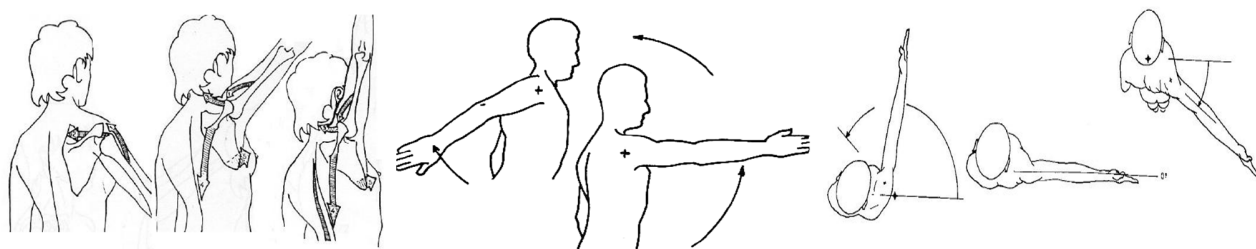
Figure 2.1: Motion of the shoulder in the coronal (abduction-adduction), sagittal (flexion-extension) and horizontal (internal-external rotation) planes.

Scapulo-humeral rhythm

During arm elevation the humerus rotates around the scapula, at the gleno-humeral joint, and the scapula moves around the thorax, at the scapulo-thoracic joint. The result is a synchronized movement of the shoulder girdle and humerus, described as the scapulo-humeral rhythm (Inman et al., 1944; Groot et al., 1999; McQuade et al., 1998; Meskers et al., 1998).

The scapulo-humeral rhythm describes the relationship of motion between the scapula and humerus, and is influenced by the movement of the sterno-clavicular and acromio-clavicular joints.

With active humeral elevation up to 30 degrees (deg) in the coronal or scapular abduction planes and up to 60 deg of sagittal plane flexion, the scapula seeks a position of stability (setting phase). The setting phase is variable and individualized (Inman et al., 1944). Following the setting phase, the humerus and scapula maintain a particular relationship during arm elevation (a ratio of movement). The relationship between gleno-humeral and scapulo-thoracic motion is critical and is generally considered to be 2:1, culminating in 120 and 60 deg, respectively.

4

Taking into account only the GHJ, the active abduction up to 120 deg occurs only if the humerus extra rotates of 90 deg. Then, the movement is due to the tilting of the scapula. The shoulder blade glides over the thoracic wall thanks to the scapulo-thoracic and acromion-clavicular joints, and the muscular activity. The full abduction of the arm in the frontal plane is therefore the consequence of a harmonic sequence of actions, for every 15 deg of abduction 10 deg achieved on the gleno-humeral joint and 5 deg at scapulo-thoracic level, with an integrated scheme and rhythm. For the deltoid, the main muscle of abduction, it is important the scapular rotation to maintain the tension necessary for its contraction. The stability of the shoulder, especially after the first 90 deg of abduction, is guaranteed by the tilting of the scapula that changes the relationship between the humeral head and the glenoid so that at 180 deg the deltoid almost does not work because the glenoid socket is located below the humeral head. In this rhythm also the sterno-clavicular joint steps in. In the excursion between 0 deg and 90 deg the scapula rotates 30 deg and the clavicle rises equally; beyond 90 deg of abduction (at sterno-clavear level), however, it is no longer possible for the scapula to move. For this reason the clavicle rotates 45 deg around the axis of the diaphysal, in order to raise its lateral end of the remaining 30 deg required to complete the movement of abduction.

2.2   Gleno-humeral joint
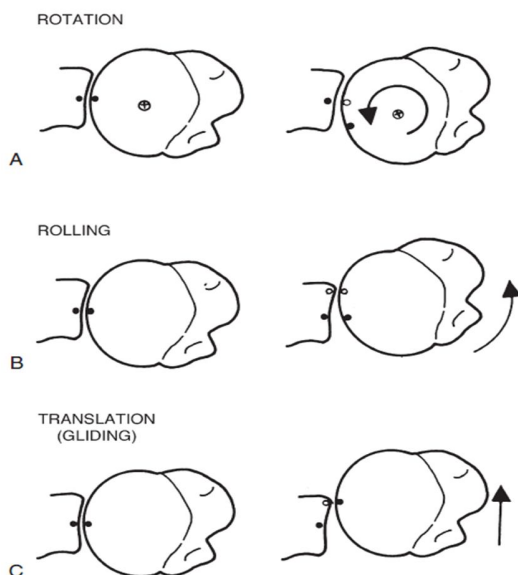
Figure 2.2: Three types of articular movement occur at the gleno-humeral joint. A, Rotation. B, Rolling. C, Gliding. *(From Matzen FA III, Zuckerman J: Biomechanics of the shoulder. In Frankel VH, Mordin M [eds]: Basic Biomechanics of the Musculoskeletal System, 2nd ed. Philadelphia, Lea & Febiger, 1989, p 231).*

The gleno-humeral joint is an enarthrosis (ball-and-socket joint). The bones entering into its formation are the humeral head and the glenoid cavity of the scapula. Only 25% to 30% of the humeral head is covered by the glenoid surface in any given anatomic position. Although the bony surfaces of the humeral head and glenoid fossa have slightly different curvatures, their cartilaginous articular surfaces have approximately the same radius of curvature. This joint has three rotational axes of motion along the cardinal planes of the body: sagittal, frontal, and horizontal.

The humeral head spins, rotates, and glides or translates, on the face of the glenoid during arm elevation and rotation (Fig. 2.2) (Hart and Carmichael, 1985).

The direction of rolling and gliding components is dependent on whether the concave or convex surface is moving. The more congruent the surfaces, the more gliding occur and the more incongruent, the more rolling takes place (Kaltenborn, 1980). If a convex surface moves on a concave surface, then gliding occurs in the opposite direction to the rolling; if a concave surface moves on a convex surface, then rolling and gliding occur in the same direction. Therefore, due to the disproportion between the gleno-humeral articular surfaces rolling would be dominant.

Humerus

Figure 2.3: Humerus.
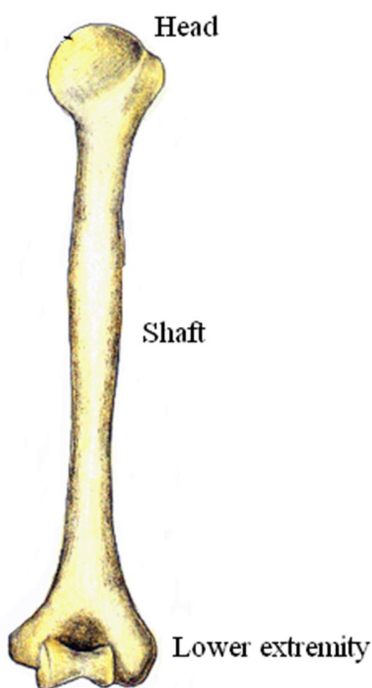
The humerus (Fig. 2.3) is the longest and largest bone of the upper extremity. Three parts can be distinguished: the body and two extremities. The upper extremity consists of a large rounded head joined to the body by a constricted portion called the neck, and two eminences, the greater and lesser tubercles.

The head (nearly hemispherical in form) is the humeral portion that articulates with the glenoid cavity of the scapula. The circumference of its articular surface is slightly constricted and it is referred to as the anatomical neck, in contradistinction to a constriction below the tubercles called the surgical neck. The anatomical neck is obliquely directed, forming an obtuse angle with the body. It is best marked in the lower half of its circumference; in the upper half, it is represented by a narrow groove separating the head from the tubercles. It affords attachment to the articular capsule of the shoulder-joint.

The greater tubercle (greater tuberosity) is situated laterally to the head and lesser tubercle. Its upper surface is rounded and marked by three flat impressions which give insertion to the muscle tendons (supra-spinatus; infra-spinatus and teres minor).

The lesser tubercle (lesser tuberosity) although smaller, is more prominent than the greater and it is located anteriorly.

The body or shaft is almost cylindrical in the upper half of its extent, prismatic and flattened below, and has three borders and three surfaces.

The lower extremity includes, projected on either side, the lateral and medial epicondyles. The lateral epicondyle is a small, tuberculated eminence, curved a little forward. The medial epicondyle, larger and

more prominent than the lateral, is directed slightly backwards. The epicondyles serve as insertion points for tendons and ligaments of the elbow-joint (Standring, 2008).

Scapula

The scapula forms the posterior part of the shoulder girdle. It is a flat, triangular bone, with two surfaces, three borders, and three angles.

The costal or ventral surface (Fig. 2.4) presents a broad concavity, the sub-scapular fossa. The medial two-thirds of this fossa are marked by several oblique ridges, which run laterally and upward. The ridges provide the attachment to the tendinous insertions.

The dorsal surface (Fig.2.4) is arched from above downward, and it is divided into two
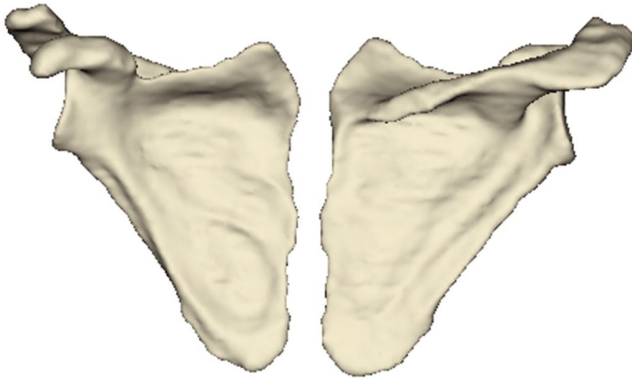
Figure 2.4: Scapular ventral and dorsal surfaces.

unequal parts by the spine; the portion above the spine is called the supra-spinatous fossa, and that below it is the infra-spinatous fossa.

The spine is a prominent plate of bone, which crosses obliquely the medial four-fifths of the dorsal surface of the scapula at its upper part, and separates the supra- from the infra-spinatous fossa. It begins at the vertical border by a smooth triangular area and ends in the acromion. The spine is triangular, and flattened from above downward. It presents two surfaces (superior and inferior) and three borders (anterior, posterior and lateral).

The acromion forms the summit of the shoulder. It is a large, somewhat triangular or oblong process, curving forward and upward, so as to overhang the glenoid cavity.

The scapula has three borders and three angles. The superior is the shortest and thinnest of the three borders of the scapula, it is concave, and it extends from the medial angle to the base of the coracoid process. The axillary border is the thickest of the three. It begins above at the lower margin of the glenoid cavity, and inclines obliquely downward and backward to the inferior angle. The vertebral border is the longest of the three, and extends from the medial to the inferior angle.

The inferior angle is formed by the union of the vertebral and axillary borders. The lateral angle is the thickest part of the bone, and it is sometimes called the head of the scapula. The articular surface, the glenoid cavity, is directed laterally and forward and articulates with the head of the humerus; it is broader at the bottom than at the top and its vertical diameter is the longest. The surface is covered with

cartilage in the fresh state; and its margins, slightly raised, give attachment to a fibro-cartilaginous structure, the glenoidal labrum, which deepens the cavity. At its apex is a slight elevation, the supra-glenoid tuberosity. The neck of the scapula is the slightly constricted portion which surrounds the head. The coracoid process is a thick curved process attached by a broad base to the upper part of the neck of the scapula; it runs at first upward and medially, then, becoming smaller, it changes its direction and it projects forward and laterally (Standring, 2008).

The scapula is involved in various movements of the shoulder. In particular, Kibler et al. (1998) have described five roles attributed to the scapula: (1) it represents a stable part of the gleno-humeral joint; (2) it allows for retraction and protraction along the thoracic wall; (3) it elevates the acromion to decrease impingement and coraco-acromial arch compression in the throwing and serving motion; (4) it serves as a base for muscle attachment; and (5) it functions as a link in the proximal to distal sequencing of the kinetic chain (Fig. 2.5).
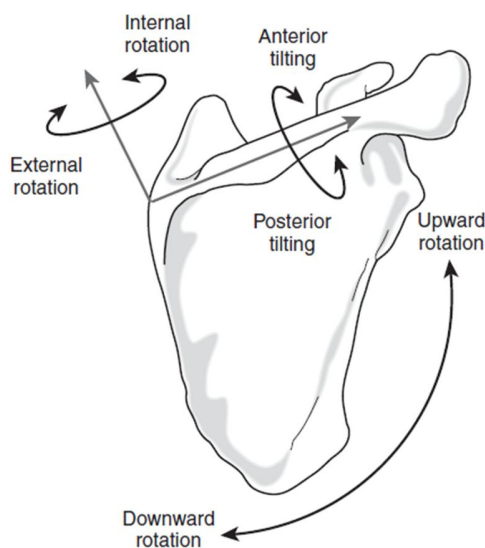
Figure 2.5: Scapular variables: posterior tilt, upward rotation, and external rotation. *(From Dayanidhi S, Orlin M, Kozin S, et al: Scapular kinematics during humeral elevation in adults and children. Clin Biomech (Bristol, Avon) 20:600-606, 2005).*

- *Posterior and anterior tilt:* posterior and anterior tilt is the scapular rotation about an oblique medial-lateral axis (Karduna et al., 2000); posterior tilt occurs as the acromion moves backward and anterior tilt occurs as the acromion moves forward.

- *Internal and external rotation:* internal and external rotation are described as scapular rotation about an oblique superior-inferior axis (Karduna et al., 2000); external rotation can be visualized as the acromion moving posteriorly with the medial border of the scapula moving in an anterior direction.

- *Downward (medial) and upward (lateral) rotation*: scapular downward and upward rotation occurs about an axis in the scapular body (Karduna et al., 2000); downward rotation is defined by the rotation of the glenoid downward and the inferior angle of the scapula toward the spine; upward rotation is the rotation of the glenoid superiorly and movement of the inferior angle away from the spine.

- *Abduction and adduction:* abduction is the movement of the medial border of the scapula away from the vertebral column; adduction is defined as movement of the medial border of the scapula toward the vertebral column (Oatis, 2004).

- *Elevation and depression:* scapular elevation is the movement of the scapula superiorly on the thorax; depression is the movement of the scapula inferiorly on the thorax (Oatis, 2004). When a patient assumes the prone position, the shoulder girdle falls into a relatively elevated and protracted state.

2.2.1 Normal gleno-humeral relationship

The gleno-humeral joint is a multi-axial ball-and-socket synovial joint. The articular surfaces, the head of the humerus and the glenoid fossa of the scapula, although reciprocally curved, are oval and are not sections of true spheres. It was estimated that the articular surface of the glenoid fossa is one third to one fourth that of the humeral head (Iannotti et al., 1992).

Because the head of the humerus is larger than the glenoid fossa, only part of the humeral head can be in articulation with the glenoid fossa in any position of the joint.

The gleno-humeral congruence (conformity) is the relationship between the radius of curvature of the humeral head and the glenoid (Iannotti et al., 1998). If the radii of curvature of the humeral head and glenoid were the same, i.e. congruency ratio of 1, and then there would be maximum contact between the two surfaces. The most common configuration (90%) is a smaller radius of curvature for the humeral head relative to the glenoid, such that the congruency ratio is less than one. This implies an increased range of movement but a decreased stability. The design characteristics of the joint are typical of an "incongruous" joint. The surfaces are asymmetrical, the joint has a movable axis of rotation, and muscles related to the joint are essential in maintaining stability of the articulation (O'Brien et al., 1990).

The mean humeral head radius and the mean humeral head thickness are correlated with the humeral head offset, which is the distance between the center of the humeral head and the longitudinal axis of the humeral shaft. The ratio of the humeral head thickness to humeral head radius is reliably consistent at 0.7–0.9 (Howell et al., 1989; O'Connell et al., 1990). This ratio is directly proportional to the amount of humeral head which articulates with the glenoid, irrespective of other variables such as length of the humeral shaft or the size of the patient (O'Connell et al., 1990).

The normal glenoid has a pear shaped appearance with a shorter anterior-posterior dimension in the superior half (mean 23 mm) than in the inferior half (mean 29 mm) (Howell et al., 1989). The glenoid offset is the distance between the base of the coracoid and the deepest portion of the glenoid articular surface (Howell et al., 1989). This measurement determines the location of the gleno-humeral joint line and again is not related to the size of the patient. The lateral gleno-humeral offset is the distance

between the base of the coracoid and the most lateral aspect of the greater tuberosity. This measurement is important as it determines the resting tension of the rotator cuff and the moment arm of the deltoid.

Gleno-humeral index

This is defined as the maximum transverse diameter of the glenoid divided by the maximum transverse diameter of the humeral head. This ratio is approximately 0.75 in the sagittal plane and 0.6 in the transverse plane (Saha et al., 1971). A low gleno-humeral index is associated with recurrent anterior instability (Randelli et al., 1986).

Gleno-humeral articular constraint

The constraint is the amount of humeral head which is in direct articulation with the glenoid cavity (Iannotti et al., 1998). It is related to the depth of the glenoid but it is independent of articular congruence. The normal glenoid has a depth of 9 mm in the superior-inferior direction and 5 mm in the anterior-posterior direction. As a result, the glenoid is more constrained in the superior-inferior direction than anterior-posterior direction, accounting for the more frequently observed anterior-posterior dislocation (Lam et al., 2006).

2.2.2 Gleno-humeral joint stability

The term "gleno-humeral joint stability" refers to the process by which the humeral head remains centered on the glenoid during motion (Halder et al., 2001).

The stability of the joint is maintained by an interconnecting network of static and dynamic restraints (Lam et al., 2006) and it is provided by the articulating surfaces, capsular and ligamentous structures (static stabilizers), and synchronous activity of the rotator cuff, biceps, deltoid, and scapular muscles (dynamic stabilizer). The role of any specific component of the stabilizing system varies with gleno-humeral joint position and direction of the opposing force. A functional interplay or interdependence exists between anterior and posterior and between superior and inferior components of the capsule-ligamentous system. For the stability two aspects are important: conformity and constraint. Conformity is the relative match between the radii of the humeral head and glenoid; i.e. a completely conforming joint has 0 mm mismatch between the respective radii. Constraint is the threshold to dislocation which is related to the depth and size of the socket. Experimental evidence shows greater gleno-humeral translation in non-conforming articular surface (Iannotti et al., 1999). This means that the relationship

between gleno-humeral translation and joint conformity only applies under active, not passive joint loading.

Capsulo-ligamentous complex

The gleno-humeral joint capsule originates from the labrum and the margin of the glenoid fossa. It is attached laterally to the anatomical neck of the humerus. It maintains the negative intra-articular pressure, contributing to the stability of the gleno-humeral joint (Lam et al., 2006).

The gleno-humeral joint capsule provides passive stability at the extremes of gleno-humeral motion (Werner et al., 2004). The capsule does not only limit rotation and prevent excessive translations, but also causes a coaptation and obligate translation of the humeral head on the glenoid at the end of passive movements. The superior part of the capsule, together with the coraco-humeral ligament, is important in strengthening the superior aspect of the joint and resisting the effect of gravity on the dependent limb.

Anteriorly and posteriorly the capsule is strengthen by ligaments and tendons. Inferiorly, the capsule is thin and weak and contributes little to the stability of the joint. The inferior part of the capsule is subject to considerable strain because it is tightly stretched across the head of the humerus when the arm is elevated; moreover it is lax and lies in folds when the arm is adducted. The frequency of anterior dislocation seen clinically demonstrates the weakness of the inferior part of the capsule (Lam et al., 2006). The integrity of the capsule and the maintenance of the normal gleno-humeral relationship depend on the reinforcement of the capsule by ligaments and the attachment of the muscle tendons of the rotator cuff mechanism.

Glenoid labrum

The glenoid labrum is a rim of fibro-cartilaginous tissue attached around the margin of the glenoid fossa, deepening the glenoid cavity and serving to bridge bone to the gleno-humeral ligaments and biceps tendon. The inner surface of the labrum is covered with synovium; the outer surface attaches to the capsule and is continuous with the periosteum of the scapular neck (Lam et al., 2006). The glenoid labrum accounts for about 10–20% of the static stability by deepening the glenoid socket 50%, and detachment of the labrum anteriorly may reduce the depth of the socket in the anterior-posterior direction. The shape of the labrum adapts to accommodate rotation of the humeral head, adding flexibility to the edges of the glenoid fossa. Resection of the glenoid labrum has been reported to reduce the effectiveness of compression-stabilization by approximately 10% to 20% (Halder et al., 2001).

Compression by muscle activity and capsule-ligamentous tightening increases the stability of the labrum. Superior labral defects have been found to decrease torsional rigidity and increase inferior gleno-humeral ligament strain, which contributes to anterior instability (Abboud et al., 2002).

Gleno-humeral ligaments

The gleno-humeral ligaments are thickenings of the joint capsule and consist of superior, middle and inferior portions. The superior gleno-humeral ligament functions as the primary restraint to inferior translation of the humeral head. The middle gleno-humeral ligament is the most variable and it limits external rotation and anterior subluxation of the humeral head when the arm is in mid-abduction. The inferior gleno-humeral ligament is the most important ligament in maintaining joint stability (Lam et al., 2006).

Coraco-humeral ligament

The coraco-humeral ligament is one of the most important ligamentous structures in the shoulder complex as it is involved in maintaining the gleno-humeral relationship. The downward pull of gravity on the arm is counteracted largely by the superior capsule and the coraco-humeral ligament. Because the coraco-humeral ligament is located anterior to the vertical axis about which the humerus rotates axially, the ligament checks lateral rotation and extension. Shortening of the ligament would maintain the gleno-humeral relationship in medial rotation and would restrict lateral rotation severely.

Together with the acromion and the coracoid processes, the ligament forms an important protective arch over the gleno-humeral joint. The arch forms a secondary restraining socket for the humeral head, protecting the joint from trauma and preventing dislocation of the humeral head superiorly.

Rotator cuff

The rotator cuff is the musculo-tendinous complex formed by the attachment to the capsule of the supraspinatus muscle superiorly, the subscapularis muscle anteriorly, and the teres minor and infraspinatus muscles posteriorly. All of their tendons blend intricately with the fibrous capsule. They provide active support for the joint and can be considered true dynamic ligaments. The rotator cuff, acting as a dynamic compound musculo-tendinous unit, plays an essential role in movements of the gleno-humeral joint. The combined effect of the cuff muscles works as a force-couple to keep the humeral head centered on the glenoid. The dynamic restraints stabilize the joint by several mechanisms (Lam et al., 2006):

1. by a passive muscle tensioning effect;

2. by dynamic contraction thereby causing compression of the humeral head into the glenoid (Halder et al., 2001);

3. by determining a secondary tightening effect on the static constraints;

4. by exerting a direct barrier effect.

2.2.3 Gleno-humeral joint laxity and instability

The term shoulder laxity refers to the physiological motion of the gleno-humeral joint that allows a normal range of motion. It was defined as the ability of the humeral head to be passively translated on the glenoid fossa (Matsen et al., 1991). This obligate translation of the humeral head on the glenoid is physiologic and in fact necessary in order to achieve the large degrees of freedom afforded the highly mobile shoulder (Saurer et al., 2001). Translation can occur in any direction as the humeral head moves on the glenoid face during humeral elevation and rotation.

The position at which the maximal mobility occurs is defined resting position (Lin et al., 2007). The resting position is the position of a joint in which the joint tissues are under the least amount of stress and in which the joint capsule has its greatest laxity (Lin et al., 2007). It is also called the "loosely packed position" as opposed to the "closely packed position" (Lin et al., 2007). This position is also the position of minimal congruence between joint surfaces allowing the greatest passive separation between articular surfaces (Lin et al., 2007).

For the *in vivo* gleno-humeral joint, the resting position was found to be located at a position in neutral rotation between 30 and 60 deg of shoulder abduction with respect to the trunk in the plane of the scapula (commonly defined as the plane 30 deg anterior to the frontal plane) (Lin et al., 2007) .

Quantitative assessment of gleno-humeral laxity has been performed both *in vivo* and *in vitro*. Poppen and Walker (1976) observed from X-rays that the humeral head moved upward relative to the glenoid between 0 and 30 deg of abduction and translated inferiorly by 2-3 mm throughout the rest of abduction. Harryman et al. (1990) in their cadaveric study demonstrate the obligate nature of translation. In order to determine whether the observed translations were forced by asymmetrical tightness of the capsule, rather than being associated with laxity of the capsule, they attempted to prevent the anterior translation of the humeral head during flexion of shoulders that had an intact capsule by applying an oppositely directed (posterior) force to the humeral head. Herryman et al. (1990) concluded that given the obligate nature of these translations they may also occur with active motions. To confirm this, Howell et al. (1989) reported evidence that translation occurs with combined

abduction, extension, and external rotation and that normal translation is reduced or eliminated when there is gleno-humeral instability.

Rhoad et al. (1998) used MRI to examine normal relationships about the gleno-humeral joint in internal and external rotation. They found that during active motion the humeral head translation averaged 2.1 mm in the anterior-posterior plane and that during passive positioning average translations increased to 8.2 mm in the anterior-posterior plane.

Graichen et al. (2000) used 3D MRI to demonstrate the centering of the humeral head during abduction and rotation. They found that during passive elevation the humeral head translated slightly inferiorly at low angles of elevation (from +1.58 mm at 30 deg to +0.36 mm at 150 deg of abduction) and slightly posteriorly at higher angles of elevation (from +1.55 mm at 30 deg to -0.07 mm at 150 deg of abduction). With muscle activity, the respective translations were smaller, particularly at low angles of elevation (1.0±1.3 mm at 60 deg of abduction, 0.04±1.3 mm at 90 deg and of -0.02 ±1.4 mm at 120 deg of abduction). In their study, Graichen et al. (2000) reported an inferior translation of 1.2 mm (from 30 to 150 deg). While at 60 deg of abduction the humerus is still 1 mm superior to the glenoid, it is more centered at 90 and 120 deg. The superior position at 60 deg may be caused by the dominance of the deltoid with its cranial force direction, while at 90 deg and 120 deg the rotator cuff muscles with their centralizing effect are more active (Graichen 2000).

Saurer et al. (2001) in their study on the gleno-humeral joint laxity using an instrumented arthrometer found a greater posterior translation than anterior. This is probably due to the fact that the posterior capsule is thinner than the anterior capsulo-ligamentous structures and therefore may provide less resistance to translation than the thicker anterior capsule and supporting gleno-humeral ligaments (O'Brien et al., 1995). Additionally, the subscapularis tendon is also reported to resist anterior translation when the humerus is below 90 deg of abduction (McFarland et al., 1996).

Schiffern et al. (2002) conducted a study to analyze the humeral head centering in the absence of voluntary positioning. They found that the humeral head remained centered within the glenoid, especially in the midrange positions of passive rotation in which the gleno-humeral ligaments and capsule are known to be lax (from 0 deg to 45 deg of external rotation, 35 deg of gleno-humeral abduction, cadaveric studies) (Matsen et al., 1994; Matsen et al., 1998). Within this midrange of rotation, none of the humeral heads tested translated more than 2.2 mm either anteriorly or posteriorly in relation to the glenoid center.

The findings of the Schiffern et al. (2002) study demonstrate that active muscle effort is not required to stabilize the shoulder in midrange positions. They demonstrated that the humeral head remains centered

in the glenoid in the absence of voluntary muscle contraction when the shoulder is passively positioned in midrange positions in which the capsule and ligaments are lax. This observation leads to the consideration of what mechanisms other than ligament stabilization or dynamic neuromuscular control might maintain the desired position of the humeral head in the glenoid (Schiffern et al, 2002).

They justified their findings with the conformity of the joint. In a high conforming joint, the stability ratio (the ratio of force necessary to translate the humeral head to the load compressing the humeral head into the glenoid) is maximal when the humeral head is centered in the glenoid. In a system of this sort, the stabilizing effect of a given compressive load is greatest when the head is centered in the glenoid concavity, and very low compressive loads, such as those from resting muscle tone, may be sufficient to center the humeral head. Thus, a high degree of conformation of the glenoid concavity to the humeral head provides an anatomic situation that optimizes the centering effect of concavity compression (Schiffern et al, 2002).

This tendency for the gleno-humeral joint to become uncentred in positions near the end of the range of motion is thought to be related to an unopposed translatory force applied to the humeral head, forcing it from the centered position (Matsen et al., 1994; Matsen et al., 1998).

Alberta and colleagues (Alberta et al., 2006) tested six cadaver shoulders with an intact capsule and all muscles removed, under an external load of 15 and 20 N and found an anterior translation of 12.8 ± 1.9 mm and of 13.4 ± 2.0 mm at 90 deg of shoulder abduction, respectively. Sahara et al. (2007) in their *in vivo* study investigated the gleno-humeral joint motion during isometric arm abduction by means of an open and vertical MR scanner. As reported by the authors, in the superior-inferior direction, the humeral head translated inferiorly from 1.9 mm at 0 deg to 0.8 mm at the maximum abduction. In anterior-posterior direction, the humeral head translated anteriorly from 0 to 90 deg (mean 2.4 mm) and posteriorly from 90 to 150 deg of abduction (mean -1.4 mm). Marquardt et al. (2006) by means of robot-assisted shoulder simulator tested twelve cadaveric shoulders with all soft tissues removed except for the tendons of the rotator cuff, the pectoralis major and the deltoid muscle. They found a translation of 6.8 ± 2.4 mm at 0 deg and 5.1 ± 3.1 mm at 90 deg of gleno-humeral abduction. Su et al., (2009) investigate the translations in five cadaveric intact shoulders in both the superior and anterior-superior directions. The study design also provided the rotator cuff tendons were individually loaded, to simulate the muscle forces acting *in vivo*. They found an average translation of 2.0 ± 0.5 mm at 45 deg of gleno-humeral abduction. The studies on cadaver demonstrate the importance of muscle forces and joint conformity in the limitation of humeral head translations, which can lead to the instability.

Shoulder instability is the inability to maintain the humeral head within the center of the glenoid during active motion of the arm (Lippitt and Matsen, 1993).

As above mentioned, gleno-humeral stability is influenced by a variety of factors, such as adhesion-cohesion, concavity-compression, negative intra-articular pressure, and limited joint volume. All these factors are combined with the static ligamentous restraints and dynamic muscular control to provide stability within the large range of motion.

Gleno-humeral instability leads to shoulder dislocations in 2-8% of cases (Grumet et al., 2010). Although the natural history of the dislocated shoulder depends on a variety of factors, it is the age of the patient at the time of the initial dislocation that is most important (VandenBerghe et al., 2005). Shoulder dislocations most commonly occur in young males of less than 25 years of age, with a prevalence of anterior dislocations (about 90–95% of all shoulder dislocations). The etiology of shoulder instability is most commonly traumatic, and results in a Bankart lesion or disruption of the labrum and anterior-inferior gleno-humeral ligament complex from the glenoid as well as an impaction fracture on the postero-lateral aspect of the humeral head. Among the different dislocations the posterior are less common (only 3-5% of dislocations), instead the sub-acromial dislocation (humeral head posterior to the glenoid and inferior to the acromion) is the most common.

The incidence of shoulder dislocations has been reported to be 11.2 per 100`000 per year (Simonet et al., 1984). Major deficits in shoulder function and a high number of recurrences after the first dislocation have been reported especially in young patients (Robinson et al., 2006). According to Robinson et al. (2006), recurrences are found in 56% of young patients aged between 15 and 35 within the first year (Robinson et al., 2006).

Many classification systems have been developed to describe shoulder instability. Schemes related to direction (anterior, posterior, multidirectional), etiology (traumatic, atraumatic, overuse), degree of instability (subluxation versus dislocation), and duration of symptoms (acute, recurrent, fixed) are described in the literature.

A new classification, which distinguishes among static, dynamic, and voluntary dislocation, have been proposed (Gerber et al., 2002) and provides for a division into classes and subclasses.

- *Class A-static instabilities*: they are defined by the absence of classic symptoms of instability and are associated with rotator cuff tears and degenerative joint disease (radiological diagnosis) (VandenBerghe et al., 2005).

- *Classe B-dynamic instabilities*: they are symptomatic and have traumatic etiology (Hawkins et al., 1987).

- *Class C*: they are voluntary dislocation and are of two types: muscular and positional. This type of dislocation is most frequently among children and the preadolescent population. The first group of patients is able to sublux or dislocate the shoulder by selective muscle activation, whereas the others need to place the arm in appropriate position (such as forward flexion, adduction, and internal rotation for posterior instability) to induce the subluxation or dislocation.

CHAPTER 3

QUANTITATIVE MEASUREMENT OF THE GLENO-HUMERAL JOINT TRANSLATIONS

3.1   Background

Three-dimensional (3D) gleno-humeral joint linear displacements have been measured, both *in vivo* and *in vitro* by means of different instrumental techniques. *In vitro* studies allow for a very accurate and repeatable joint kinematics reconstruction permitted by the use of different invasive approaches (Bourne et al., 2010; Bull et al., 1997; Ludewig et al., 2009; Massimini et al., 2010; Milne et al., 1996; Nishinaka et al., 2008). Studies on anatomical specimens also enable researchers to study patterns of injury and changes in joint kinematics that would be impossible *in vivo* studies (Su et al., 2009). Cadaveric experiments (Halder et al., 2001; Payne et al., 1997; Sharkey et al., 1995; Wuelker et al., 1994; Wuelker et al., 1995) can provide highly accurate measures of joint position or motion, because of the use of bone-embedded sensors (pins drilled into the bone) (Karduna et al., 1997), but are unable to accurately duplicate the complex motions, muscle forces, or joint forces associated with dynamic *in vivo* conditions (Bey et al., 2006). Extensive analyses of the biomechanical role of soft tissues and articular surfaces as joint constraints under the application of selected external forces has been conducted on cadavers mainly by means of shoulder testing device that allow six degrees of freedom for gleno-humeral positioning (Grossman et al., 2005) coupled with microscribe, used to digitize three-dimensional anatomic landmarks on the bone and record the humeral shift and translation data (Grossman et al., 2005); linear transducers for linear displacements measurement, or magnetic tracking device to determine position and orientation of a user in the working space (Su et al., 2009, Lin et al., 2007).The main limitations associated with published *in vitro* models are the inactivity of the muscles involved and that the gleno-humeral joint is often analyzed in isolation, without consideration of scapulo-thoracic motion or, the position of the clavicle. *In vivo* kinematics of the shoulder joint has been studied by means of stereophotogrammetry, electromagnetic tracking sensors, single and dual-plane fluoroscopy and open-MRI. Due to various factors such as the total or partial lack of the shoulder muscles and differences in muscular tone in cadaveric experiments, there are discrepancies between the phenomena observed *in vivo* and *in vitro* conditions.

3.1.1   Instrumental techniques for the assessment of the gleno-humeral joint translations

After a brief overview on *in vivo* and *in vitro* studies and the main characteristics, in this chapter we will focus on the principal techniques employed, both *in vivo* and *in vitro,* for the assessment of the GHJ translations.

Stereophotogrammetry

Video-based optoelectronic systems represent conventional motion measurement methods used to track the instantaneous position of markers attached to the skin. These systems are used to track the 3D position of a set of fiducial points, constituted from either retro-reflective (passive) or light-emitting (active) markers. In order to reconstruct 3D positions of markers captured by two or more cameras, the extrinsic parameters of each camera have to be known. These extrinsic parameters describe the geometrical relation between the camera and the captured calibration body (Lujan et al., 2006; Everaert et al., 1999).

These systems are non-invasive, easy to use and represent a convenient solution for many clinical and research applications (Tashman et al., 2003). However, several studies have shown that markers affixed to the skin shift relative to underlying bone by as much as 30 mm, particularly during rapid movements (Holden et al., 1997; Reinschmidt et al., 1997; Lafortune et al., 1992). This marker tracking error varies with the body segment analyzed, the marker position, the type of motor task under analysis and the angular joint excursion. Due to the deformation of the soft tissues surrounding the bones, there is an ongoing debate about the capability to accurately track the movement of the underlying bony segments from sensors attached to the skin (van Andel et al., 2009). It is especially true, when small displacements, such as gleno-humeral joint translations, require to be assessed.

Electromagnetic tracking devices

Six-degree-of-freedom (DoF) electromagnetic trackers provide both the position and orientation of the sensor with respect to a laboratory coordinate system by exploiting orthogonal electromagnetic fields (Raab, Blood, Steioner, & Jones, 1979; Foxlin et al., 1998; Kindratenko et al., 1999, Kindratenko et al., 2000; Borstad et al., 2002; Karduna et al., 1996; Karduna et al., 1997; Karduna et al., 2000; Bull et al., 1998; Harryman et al., 1990; Herryman et al., 1992). The system is compound by a source (transmitter) and a detector (sensor attached to the skin). Similarly to the video-based optoelectronic systems, when using electromagnetic tracking devices for *in vivo* evaluation, the sensors are placed on the skin of the subject and the measurements are affected by the presence of soft tissue artifacts which can conceal the measurement of the small displacements involved (Bey et al., 2006). Moreover due to the dependence of the measurements on the local electromagnetic field, the tracking systems are sensitive to the ambient electromagnetic environment and the transmitter signals could be distorted and the resulting measurements contain errors (Kindratenko et al., 2001).

To overcome the error imparted by soft tissue deformation some *in vivo* studies have used bone-embedded sensors that is trans-cortical pins drilled into the bone to hold marker cluster (Bourne et al., 2010, S*tereophotogrammetry*) or sensors (Ludewing et al., 2009, *Electromagnetic tracking devices*). Since these systems use pins anchored directly to the bone segments, they allow obtaining a highly accurate estimation of joint kinematics. Unfortunately, bone-pin cluster markers are associated with the risk of infection, change in pattern of motion due to pain, and translational/rotational instability of the actual pin (Bourne et al., 2010). The pain intensity of 4 out of 10 (Visual Analog Scale, VAS) have been reported when bone pins were used (Ludewing et al., 2009).

Bio-imaging techniques

The term bio-imaging refers indiscriminately to a wide range of techniques either based on the use of ionizing (e.g. X-ray based techniques) and non-ionizing radiations (e.g. MRI) (Hill et al., 2007). Among the techniques based on ionizing radiation the main used for the shoulder analysis are: computer tomography (CT) (Baeyens et al., 2001), biplanar X-rays (Lagacé et al., 2012), fluoroscopy (Karduna et al., 1997; San Juan et al., 2010) or a combination of dual-plane fluoroscopy (Fleisig et al., 1995) and 3D bone models derived from CT. An alternative which avoid the radiation exposure and then is noninvasive for the patient is represented by the magnetic resonance imaging (MRI) (Bey et al., 2006; Nishinaka et al., 2008; Massimini et al., 2012).

- *Techniques based on ionizing radiation*

X-ray based techniques have been employed to measure the position of bones relative to one another, or the position of implanted markers (RSA), either from static or dynamic images. Below the main techniques employed for the assessment of the gleno-humeral joint displacement have been reported.

Planar rontegenography (planar X-ray) is more commonly used in the clinical practice for evaluating pathological abnormalities than as a tool for the kinematic study (Hill et al., 2007). Several studies used the X-ray for the imaging of the shoulder in the plane of the scapula (de Luca et al., 1973; Freedman et al., 1966; Poppen and Walker, 1976; Johnston et al., 1937; Saha et al., 1950) and the evaluation of the parameters of motion in normal and abnormal shoulders, such as the excursion of the humeral ball on the face of the glenoid (Poppen and Walker 1976).

However, this technique is affected by projective artifacts, which can be responsible of the many differences reported in the scapular-humeral rhythm in the different studies (de Groot et al., 1998). Moreover, for some applications, the 2D assessments of gleno-humeral joint motion, cannot be

sufficient to characterize the relative movement between the humerus and the glenoid which is characterized by rotations and translation along three axes (Bey et al., 2006)

Fluoroscopy is an imaging technique that uses X-rays to obtain real-time moving images of the internal body structures. Fluoroscopy can be mono-planar, which allows investigating a larger volume with a reduced dose of X-rays, or bi-planar which is more accurate but also expose the patient to a higher radiation dose. Mono- and bi-planar X-ray fluoroscopy besides allowing the acquisition of a wide range of motion (Anderst et al., 2009; Dennis et al., 2005; Torry et al., 2010) enable to measure the joint motion during dynamic activities (Burkhart et al., 1992; Mandalidis et al., 1999; Pfirrmann et al., 2002; Werner et al., 2004).

Unfortunately, the low quality of the fluoroscopic images and especially the motion artifact (blur) may introduce errors which could affect the estimation of the relevant variables. In fact, the errors associated to the geometry distortion are comparable to those found in static planar radiography, if not greater due to the dynamic nature of the modality (Hill et al., 2007). In addition to the image geometric distortion, another important limitation is related to the radiation exposure which makes this approach invasive for the patients (Massimini et al., 2010; Nishinaka et al., 2008).

Radiostereometric analysis consists in the implantation of tantalum spheres into the bony segments to be analyzed and to reconstruct their 3D positions from repeated multi-planar radiographic examinations. This methodology is very accurate (Selvik et al., 1983) and it has been applied to study prosthetic fixation (Ryd 1992) and joint stability (Uvehammer et al., 2000). RSA can be also used to dynamically study joint kinematics. Dynamic RSA has been used to study joint movements (Kärrholm et al. 1988; Brandsson et al., 2002; Saari et al., 2005), and in particular gleno-humeral joint kinematics (Bey et al., 2006; Hallström and Kärrholm, 2009). Use of biplane radiographic film methods (RSA) for 3D studies of static bone position has been well established (Kärrholm et al., 1988; Selvik et al., 1990), with precision reported in the ±10–250 μm range (Kärrholm et al., 1989). However, given the high invasiveness, the RSA is adopted only if there is the opportunity to insert marker of tantalum during the operating phase (such as in prosthetic implantation),

*X-ray computed tomog*raphy (x-ray CT) is a technology that uses computer-processed x-ray to form a series of electronically collected projections, which are later reconstructed to a topographic image of specific areas of the scanned body. Digital geometry processing is used to generate a three-dimensional image of the inside of the body from a large series of two-dimensional radiographic images taken around a single axis of rotation (Herman et al., 2009).

Thin (1mm or less) sections with multi-slice CT scanners provide high resolution multi-planar (axial, coronal, and sagittal) images along with 3D images. Because of the inherent high-contrast resolution of CT, differences between tissues that differ in physical density by less than 1% can be distinguished Computed tomography provides better bone detail than does roentgenography. Nevertheless with respect to MRI, CT provides worse contrast for evaluation of soft tissue. CT is regarded as a moderate-to high-radiation diagnostic technique. The radiation dose for a particular study depends on multiple factors: volume scanned, patient build, number and type of scan sequences, and desired resolution and image quality. In addition to the static 3D imaging of gleno-humeral joint position CT has been employed for the assessment joint kinematics mostly in combination with 2D biplane radiographic images as *model-based tracking* technique (Bey et al., 2006, Kon et al., 2008, Nishinaka et al., 2008). This technique takes advantage of the geometry of the biplane x-ray system and a 3D bone model (from a CT scan) to generate a pair of digitally reconstructed radiographs (DRRs) via ray-traced projection through the 3D bone model. This allows tracking the position of bones based on their 3D shape and texture (Bey et al., 2006). The results indicate that the proposed model-based tracking technique is accurate to within approximately ±0.5 mm of a high accuracy, validated dynamic RSA technique.

Electron beam computed tomography (EBCT): it is a fast scanning modality which generates twenty 180 x180 x 120 mm scan volumes throughout a 5s dynamic motion with minimal radiation exposure. It was employed in the volumetric dynamic and real-time imaging of different joints (Hill et al., 2003; Hill et al., 2004). With respect the traditional 3D imaging, the volumetric imaging involves the progressive capture of a number of contiguous stacked slices through a structural volume in order to approximate a 3D representation of the anatomy which can then be post-processed into slices. Using this technique, the need to infer spatial structure from a 2D image is reduced, and therefore, less error introduced (Hill et al., 2007)

- *Techniques base on non-ionizing radiation:*

Magnetic Resonance Imaging (MRI). It is a medical technique used in radiology to investigate the anatomy and function of the body. MRI scanners use strong magnetic fields and radio-waves to form images of the body. Based on MRI, GHJ translations were investigated for different shoulder configurations both in healthy subjects (Rohad et al, 1998; Graichen et al., 2000) and patients (von Eisenhart-Rothe et al., 2002; Chhadia et al., 2010), both with and without isometric muscle activity (von Eisenhart-Rothe et al., 2002; Sahara et al., 2007). The current literature describes two distinct methods of conducting this analysis: passive supine positioning (Graichen et al., 2000; Rhoad et al.,

1998; Von Eisenhart-Rothe et al., 2002) or seated weight-bearing (Hodge et al., 2001, Sahara et al., 2007). Since the use of closed shape tunnel (Kiss et al., 1997), do not allow investigating the arm in the clinically relevant positions (Kessel and Watson, 1977; 1983), recent several studies have employed low field open MRI scanner (Graichen et al., 1998). Due to the non-ionizing nature of MRI and the capability of providing multi-planar imaging with both anatomic and physiologic information this technique is often chosen in place of the CT. Farther on in this chapter in this chapter we will focus on the MRI technique.

Robot-assisted techniques

The shoulder testing device (jig) and the robot-assisted kinematic simulator are robot-assisted techniques for the *in vitro* assessment of gleno-humeral joint translations.

The jig measures the gleno-humeral translations and rotations (Remia et al., 2003). The testing apparatus allows for six degrees of freedom. Alternatively, a robot-assisted kinematic simulator allows to measure force and moments with the force moment sensor and to determine the joint kinematics in multiple directions (Marquardt et al., 2006, Burkart et al., 1992), is employed. Both these systems, allow to apply translational forces in the anterior, posterior, superior, and inferior directions; moreover they allow to apply loads to the muscle-tendon units in an attempt to simulate their contribution to stability (Su et al., 2009), even if *in vivo*, the muscle forces acting on the humeral head, such as the pectoralis major, biceps tendon, latissimus dorsi, and scapulothoracic stabilizers, are more complex than those modeled in cadaveric studies (Su et al., 2009).

3.2   Magnetic Resonance Imaging

MRI is an accurate non-invasive technique for the 3D visualization of muscles, tendons, and bones. It also provides 3D coordinate values (Sahara et al., 2007) and represents a powerful tool in those clinical applications where the joint motion can be analyzed in quasi-static conditions (Esfandiarpour et al., 2009) and small displacements need to be detected. Several studies on gleno-humeral joint translations have been conducted by means of a MR imaging.

3.2.1   Basic principles

MRI relies on the spinning motion of specific nuclei which are present in biological tissue. This spin derives from the individual spins of protons and neutrons within the nucleus. MRI active nuclei are that nuclei which have odd mass numbers (the number of neutrons is slightly more or less than the number

of protons) (Fig. 3.1). In these nuclei the spin directions are not equal and opposite, so the nucleus itself has a net spin or angular momentum. The hydrogen nucleus is the MR active nucleus used in clinical MRI, because it is very abundant in the human body, and because its solitary proton gives it a relatively large magnetic moment.
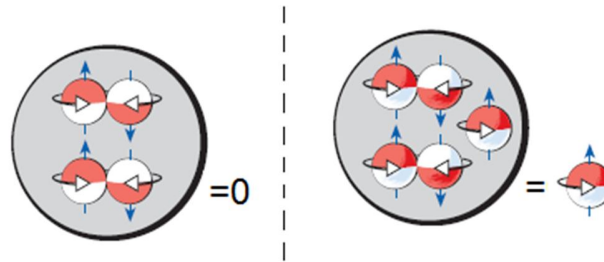
Figure 3.1: In the figure are represented the two situation of nuclei with even (left) and odd (right) mass numbers *(From Magnets, Spins, and Resonance. An introduction to the basics of Magnetic Resonance. Siemens medical).*

In absence of an applied magnetic field, the magnetic moments of the hydrogen nuclei are randomly oriented (Fig. 3.2a).
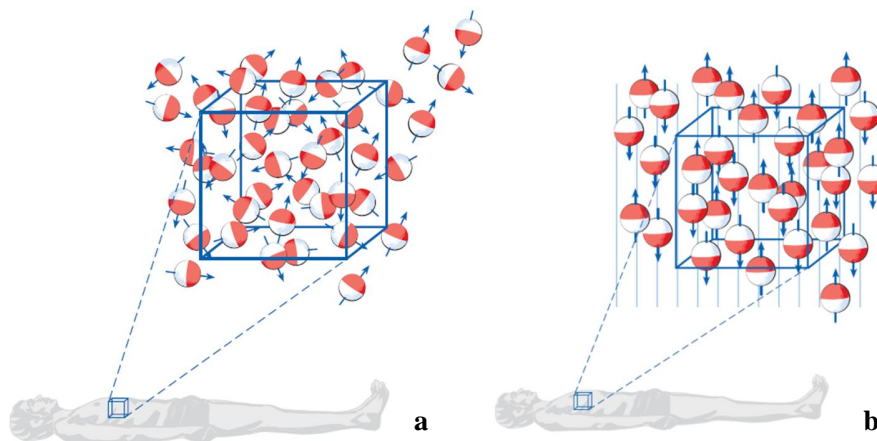
Figure 3.2: Magnetic moments of the hydrogen nuclei: (a) in absence of an applied magnetic field; (b) placed in a static magnetic *(From Magnets, Spins, and Resonance. An introduction to the basics of Magnetic Resonance. Siemens medical).*

When placed in a strong static external magnetic field, however the magnetic moments of the hydrogen nuclei align parallel with the magnetic field (in the same direction, high energy nuclei named *spin-up nuclei* Fig. 3.2b), while a smaller number of the nuclei align anti-parallel to the magnetic field (in the opposite direction, low energy nuclei named *spin-down* nuclei) as in Fig. 3.2b.

This is because they represent the only two possible energy states of hydrogen (thermal energy of the nucleus); the hydrogen nucleus itself does not change direction but merely spins on its axis. The thermal energy of the nucleus is mainly determined by the temperature of the patient.

In thermal equilibrium the magnetic moments of the nuclei aligned parallel to the magnetic field cancel out the smaller number of magnetic moments aligned anti-parallel. As there are a larger number aligned parallel, there is always a small excess in the direction that produces a net magnetic moment (Fig. 3.3).
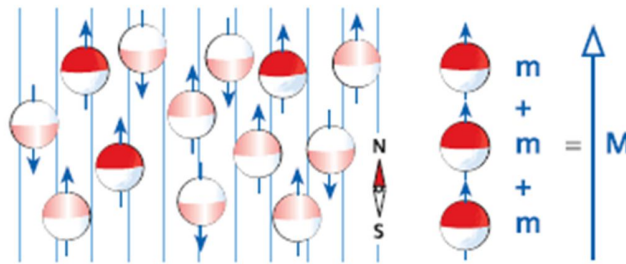
Figure 3.3: *Spin-up nuclei, spin-down nuclei and net magnetic vector (M) (From Magnets, Spins, and Resonance. An introduction to the basics of Magnetic Resonance. Siemens medical).*

The net magnetic moment of hydrogen produces a significant vector that is used in clinical MRI, the net magnetization vector (NMV: M in Fig. 3.3) which reflects the relative balance between spin-up and spin-down nuclei.

While each hydrogen nucleus is spinning on its axis, the presence of B_0 produces an additional spin, and then adds magnetic moments of hydrogen around B_0. This secondary spin is called precession and causes the magnetic moments to follow a circular path around B_0 (*precession path*) with a speed called the processional frequency (MHz: 1 million cycles per second). This rotation causes the emission of a radio signal from the sample. The frequency of this signal is identical to the precessional frequency and is termed the Larmor frequency (ω). The Larmor frequency is the product of the magnetic field strength (B_0) and the gyromagnetic ratio (γ) of the nuclei in the sample.

$$\omega = \gamma\, B_0$$

The Larmor frequency is unique for each type of nucleus; in a given magnetic field, therefore, all identical nuclei, such as in hydrogen, emit a signal of the same frequency. The frequency of this signal varies only with the magnetic field strength.

When a nucleus is exposed to an external perturbation, that has an oscillation similar to its own natural frequency, the nucleus gains energy from the external force and resonates. If the energy is delivered at a different precessional frequency, the resonance does not occur. Energy at the precessional frequency of hydrogen at all field strengths in clinical MRI corresponds to the radio frequency (RF) band of the electromagnetic spectrum. For resonance of hydrogen to occur, an RF pulse of energy at exactly the

Larmor frequency of hydrogen (*excitation*) must be applied. This absorption of energy causes an increase in the number of *spin-up* nuclei. The energy difference between the two populations corresponds to the energy required to produce resonance via excitation. As results of the resonance the NMV moves out of alignment away from B_0. As the NMV reflects the balance between the low and high-energy populations, resonance causes the NMV to no longer be parallel to B_0 but at given angle with respect to it. The angle to which the NMV moves out of alignment is the *flip angle* (Fig. 3.4). The magnitude of the flip angle depends upon the amplitude and duration of the RF pulse. Usually the flip angle is 90 deg. With a flip angle of 90 deg the longitudinal NMV is completely transferred into a transverse NMV (Fig. 3.4).
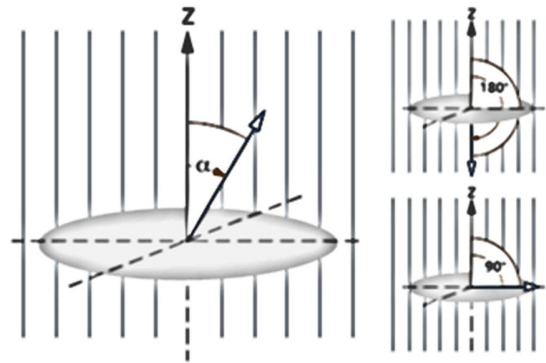
Figure 3.4: Angle to which the NMV moves out of alignment as consequence of the application of RF *(From Magnets, Spins, and Resonance. An introduction to the basics of Magnetic Resonance. Siemens medical).*

This transverse NMV rotates in the transverse plane at the Larmor frequency. When resonance occurs, all the magnetic moments move to the same position on the precessional path and are then in phase (or coherent) (Fig. 3.5).
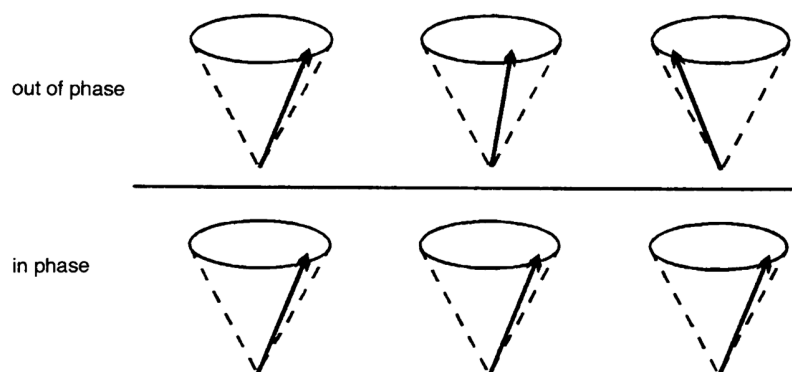
Figure 3.5: Magnetic moment in phase and magnetic moment out of phase *(From Catherine Westbrook and Carolyn Kaut, 1993. MRI in Practice 2nd edition. Blackwell Science Oxford.).*

The MR signal is produced when coherent magnetization cuts across the coil. Therefore the coherent moving transverse magnetization produces magnetic field fluctuation inside the coil that induces an electrical voltage in the coil (Faraday's law). This voltage is the MR signal. The frequency of the signal

is the same as the Larmor frequency, the magnitude of the signal depends on the amount of magnetization present in the transverse plane. When the RF pulse is switched off, the NMV is again influenced by B0 and it tries to realign with it. To do so, the hydrogen nuclei must lose the energy (*relaxation*) given to them by RF pulse.

As relaxation occurs, the NMV returns to realign with B_0. As the magnitude of transverse magnetization decrease, so does the magnitude of the voltage induced in the receiver coil. During relaxation hydrogen nuclei give up absorbed RF energy and the NMV returns to B_0. At the same time but independently the magnetic moments of hydrogen lose coherency due to dephasing. Relaxation results in recovery (gradually increment of amount of magnetization in the longitudinal plane, *T1 recovery*) in the longitudinal plane and decay (gradually decrement of amount of magnetization in the transverse plane, *T2 decay*). The rate of recovery is an exponential process, with a recovery time constant (*T1 relaxation time*). This is the time it takes 63% of longitudinal magnetization to recover in the tissue. The rate of decay is also an exponential process, so that the T2 relaxation time of a tissue is its time constant of decay. It is the time it takes 63% (Fig. 3.6) of the transverse magnetization to be lost (37% remains) (Fig. 3.7).
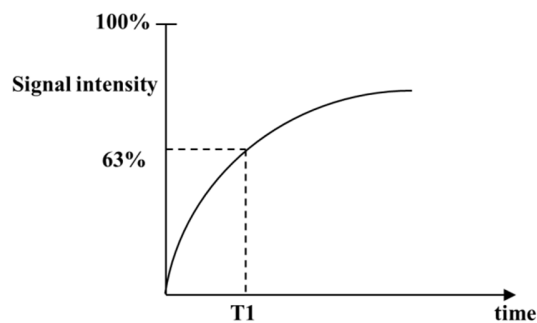
Figure 3.6: T1 relaxation time *(From Catherine Westbrook and Carolyn Kaut, 1993. MRI in Practice 2nd edition. Blackwell Science Oxford.).*
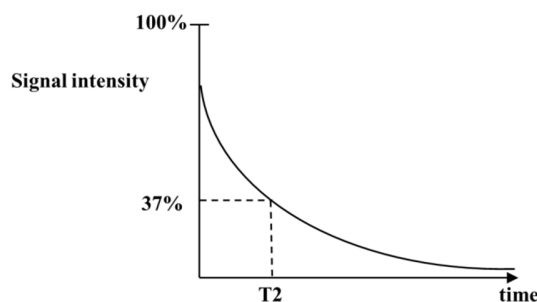
Figure 3.7: T2 relaxation time *(From Catherine Westbrook and Carolyn Kaut, 1993. MRI in Practice 2nd edition. Blackwell Science Oxford.).*

Any pulse sequence is a combination of RF pulses, signals and intervening periods of recovery. The two characterizing components a pulse sequence are the repetition time (TR) and the echo time (TE). TR is the time from the application of one RF pulse to the application of the next RF pulse for each slice and is measured in milliseconds (ms). It determines the amount of relaxation that is allowed to occur between the end of RF pulse and the application of the next. The TR thus determines the amount of T1 relaxation that has occurred when the signal is read. TE is the time from the application of the RF pulse to the peak included of the signal in the coil and is also measured in ms. It determines how much decay of transverse magnetization is allowed to occur. The TE thus controls the amount of T2 relaxation that has occurred when the signal is read (*Westbrook and Kaut, 1993*).

3.2.2 Image formation, contrast and weighting

Image formation

As previously described, for resonance to occur RF must be applied at 90 deg to B0 at the precessional frequency of hydrogen. This RF gives the NMV energy so that it is flipped into the transverse plane. The RF pulse also puts the individual magnetic moments that constitute the NMV into phase. The resultant coherent transverse magnetization precesses at the Larmor frequency of hydrogen in the transverse plane. A voltage or signal is therefore induced in the receiver coil that is positioned in the transverse plane. This signal has a frequency equal to the Larmor frequency of hydrogen, regardless of the origin of the signal in the patient. The system must be able to locate the signal spatially in three dimensions, so that it can position each signal at the correct point on the image. First it locates a slice. Once a slice is selected, the signal is located or encoded along both axes of the image. These tasks are performed by gradients.

Gradients are alterations to the main magnetic field and are generated by coils of wire located within the bore of the magnet through which current is passed. The passage of current through a gradient coil induces a gradient (magnetic) field around it, that alter (increase or decrease) the magnitude of B_0, so that the magnetic field strength and therefore the precessional frequency experienced by nuclei situated along the axis of the gradient can be predicted (spatial encoding).

Nuclei that experience an increased magnetic field strength due to the gradient speed up (their precessional frequency increases); whereas nuclei that experience a lower magnetic field strength due to the gradient slow down (their precessional frequency decreases). Therefore the position of a nucleus along a gradient can be identified according to its precessional frequency. There are three gradient coils situated within the bore of the magnet, and these are named according to the axis along which they act

when they are switched on, the Z, Y and X gradient which alter the magnetic field strength along the Z (long), Y (vertical) and X (horizontal) axis of the magnet respectively.

The magnetic field strength at the isocentre is always the same as B_0 (1.5 T, 1.0 T, 0.5 T), even when the gradients are switched on. When a gradient coil is switched on, the magnetic field strength is either subtracted from or added to B_0 relative to isocentre.

Gradients also perform the following three main tasks in encoding.

1. Slice selection - locating a slice within the scan plane selected.

2. Frequency encoding- spatially locating (encoding) signal along the long axis of the anatomy.

3. Phase encoding-spatially locating (encoding) signal along the short axis of the anatomy.

When data of each signal position are collected, the information is stored as data points in the array processor (K space) of the system computer. K space is a spatial frequency domain (where the information of frequencies related to the determinate point in the patient is stored). The acquired data held in K space are converted into an image. This conversion is made mathematically by a process known as Fast Fourier Transform (FFT). An MRI image consists of a matrix of pixels, the number of which is determined by the number of lines filled in K space (phase matrix) and the number of data points in each line (frequency matrix). As a result of FFT, each pixel is allocated a color on a grayscale corresponding to the amplitude of specific frequencies coming from the same spatial location as represented by that pixel. Each data point contains phase and frequency information from the whole slice at a particular moment in time during readout. In other words, frequency amplitude is represented in the time domain (*Westbrook and Kaut, 1993*).

Image contrast

One of the main advantages of MRI compared with other imaging modalities is the excellent soft tissue discrimination of the images. The contrast characteristics of each image depend on many variables.

Contrast in MRI is more complex and depends on many parameters, which can be classified into "intrinsic" and "extrinsic" parameters. Intrinsic contrast parameters are related directly to body's tissue and cannot be changed. They are T1 recovery time; T2 decay time; proton density; and many others.

Extrinsic contrast parameters are related to the physical characteristics of the imager and the details of the pulse sequence used for imaging. They are TR, TE, flip angle, and many others. These are selected by the operator and depend on the pulse sequence used. In this section we will focus on only the main parameters (*Westbrook and Kaut, 1993*).

Contrast mechanism: An MR image has contrast if there are areas of high signal (white on the image), areas of low signal (dark on the image) and areas of an intermediate signal (shades of gray in between white and black). The NMV can be separated into the individual vectors of the tissue present in the patient. A tissue has a high signal if it has a large transverse component of coherent magnetization at time TE. If that occurs the amplitude of the signal received by the coil is large, resulting in a bright area of the image. A tissue returns a low signal if it has a small transverse component of coherent magnetization at time TE. In this case the amplitude of the signal received by the coil is small, resulting in dark area on the image. Images obtain contrast mainly through the mechanism of T1 recovery, T2 decay and proton or spin density. The higher the proton density of a tissue, the more signal available from that tissue.

Relaxation in different tissues: T1 relaxation and T2 decay are exponential processes with a time constant T1 and T2. Generally, the two extremes of contrast are fat and water. The magnetic moments of fat nuclei are able to relax and regain their longitudinal magnetization quickly. The NMV of fat realigns rapidly with B0 so the T1 time of fat is short. Energy exchange is efficient in neighbor in fat as the molecular tumbling rate of fat is similar to the Larmor frequency and the molecules are packed closely together. As a result, spins diphase quickly and the loss of transverse magnetization is rapid. The T2 time of fat is therefore short. In water, molecular mobility is high, resulting in less efficient T1 recovery because the molecular tumbling rate does not match the Larmor frequency and does not allow efficient energy exchange from hydrogen nuclei to the surrounding molecular lattice. T2 of water is therefore long. The magnetic moments of water take longer to realign with B_0 and so the T1 of water is long.

T1 contrast: As the T1 time of fat is shorter than that of water, the fat vector realigns with B_0 faster than water vector. The longitudinal component of magnetization of fat is therefore larger than of water. After a certain TR that is shorter than the total relaxation times of the tissue, the next RF excitation pulse is applied. The RF excitation pulse flips the longitudinal component of magnetization of both fat and water into the transverse components (assuming a 90 deg pulse is applied). As there is more longitudinal magnetization in fat before the RF pulse, there is more transverse magnetization in fat after the RF pulse. Fat therefore has a high signal and appears bright on a T1 contrast image. As there is less longitudinal magnetization in water before RF pulse, there is less transverse magnetization in water after the RF pulse. Water therefore has a low signal and appears dark on a T1 contrast image. Such images are called *T1 weighted images*.

T2 contrast: The T2 time of fat is shorter than that of water, therefore the transverse component of magnetization of fat decays faster. The magnitude of transverse magnetization in water is large. Water has a high signal and appears bright on a T2 contrast image. However, the magnitude of transverse magnetization in fat is small. Fat therefore has a low signal, and appears dark on a T2 contrast image. Such images are called *T2 weighted images*.

Proton density contrast: Proton density contrast refers to differences in signal intensity between unit volumes. To produce contrast due to the differences in the proton densities between the tissues, the transverse component of magnetization must reflect these differences. Tissues with a high proton density (e.g. brain tissue) have a large transverse component of magnetization (and therefore a high signal), and are bright on a proton density contrast image. Tissues with a low proton density (e.g. cortical bone) have a small transverse component of magnetization (and therefore a low signal), and are dark on a proton density contrast image. Proton density contrast is always present and depends on the patient and the area being examined. It is the basic MRI contrast (*Westbrook and Kaut, 1993*).

Image weighting

To demonstrate either T1 proton density or T2 contrast, specific values of TR and TE are selected for a given pulse sequence. The selection of appropriate TR and TE weights an image so that one contrast mechanism predominates over the other two.

Four types of weighting:

1. T1 weighting: image wherein the contrast depends predominantly on the differences in the Tl times between fat and water. Because the TR controls how far each vector can recover before it is excited by the next RF pulse, to achieve T1 weighting the TR must be short enough so that neither fat nor water has sufficient time to fully return to B_0 (Fig. 3.8).
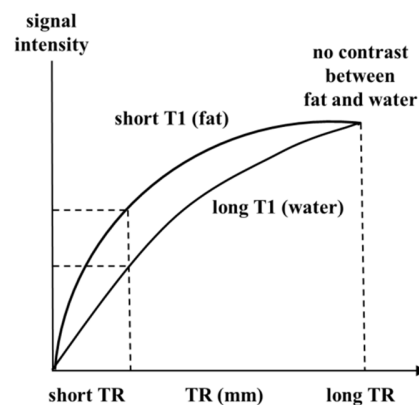
Figure 3.8: T1 weighting *(From Catherine Westbrook and Carolyn Kaut, 1993. MRI in Practice 2nd edition. Blackwell Science Oxford.).*

2. T2 weighting: image wherein the contrast id determined by the differences in the T2 times between fat and water. The TE controls the amount of T2 decay that is allowed to occur before the signal is received. To achieve T2 weighting, the TE must be long enough to give both fat and water time to decay (Fig. 3.9).
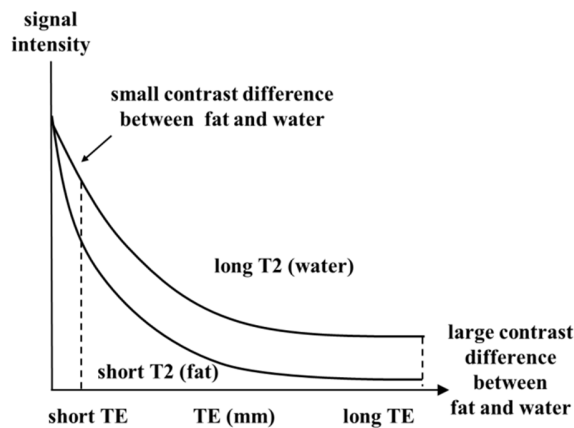
Figure 3.9: T2 weighting *(From Catherine Westbrook and Carolyn Kaut, 1993. MRI in Practice 2nd edition. Blackwell Science Oxford.).*

3. Proton density weighting: image wherein the difference in the numbers of protons per unit volume in the patient is the main determining factor in forming image contrast. In order to achieve proton density weighting, the effects of T1 and T2 contrast must be diminished, so that proton density weighting can dominate. That implies a long TR and a short TE.

4. T2* decay: when the RF excitation pulse is removed, the relaxation and decay processes occur immediately. This decay is faster than T2 decay since it is a combination of two effects, (1) T2 decay itself and (2) dephasing due to magnetic field inhomogeneities (areas within the magnetic field that do not exactly match the external magnetic field strength) (*Westbrook and Kaut, 1993*).

3.2.3   Magnetic Resonance Imaging acquisition parameters

There are many parameters available to the operator when setting up a sequence. The choice of pulse sequence determines the weighting and the quality of the images. The timing parameters selected specifically determine the weighting of the images.

- TR determines the amount of T1 and proton density weighting.

- Flip angle controls the amount of T1 and proton density weighting.

- TE controls the amount of T2 weighting.

The quality of the images is controlled by many factors including.

1. Spatial resolution

The spatial resolution is the ability to distinguish between two points as separate and distinct, and is controlled by the voxel size. Small voxels result in good spatial resolution as small structures can be easily differentiated. Large voxels, on the other hand, result in low spatial resolution, as small structures are not resolved so well. In large voxels, individual signal intensities are averaged together and not represented as distinct within the voxel. This results in partial valuing. The voxel size is affected by:

a. slice thickness - reducing the slice thickness therefore increases spatial resolution;

b. FoV- the matrix determines the number of pixels in the FoV. Small pixels increase spatial resolution. Increasing the matrix therefore increases the spatial resolution;

c. number of pixels or matrix - the size of the FoV also determines the pixel dimensions. A large FoV results in large pixels, whereas a small FoV produces small pixels. Increasing the FoV size therefore decreases the spatial resolution.

2. Scan time

The scan time is the time to complete data acquisition. Scan times are important in maintaining image quality, as long scan times give the patient more of a chance to move during the acquisition. Any movement of the patient will probably degrade the images. As multiple slices are selected during a 2D and 3D volumetric acquisition, movement during these types of acquisition affects all the slices. During a sequential acquisition, movement of the patient only affects those slices that are acquired while the patient is moving.

Type of acquisitions

There are basically three ways of acquiring data:

- sequential acquisition;

- two-dimensional volumetric acquisition;

- Three-dimensional volumetric.

Both the first two acquisition types acquire data in separate slices; the difference between the two consists in the way the K space is filled. On the contrary, three-dimensional volumetric acquires data from an entire volume of tissue, rather than in separate slices. The advantage of the latter acquisition type is that many slices can be obtained (typically 28, 64 or 128) without slice gap (the slice are contiguous). The other main advantage of volumes is that, as data is collected from a slab, the slab can be manipulated to look at the anatomy within the volume in any plane and at any angle of obliquity.

The disadvantages of volume imaging are that, in general, the scan times associated with them are relatively long. For this reason, they are usually used in conjunction with faster pulse sequences. Moreover to obtain equal resolution in every plane and at every angle of obliquity, each voxel should be symmetrical (isotropy). That is to say, that the voxel should have equal dimensions in every plane. If this is not true, the volume has poorer resolution in the planes other than the one in which it was acquired. Volume imaging has many potential applications, but it is widely used for imaging of joints where anatomy is often confusing and not strictly in plane (*Westbrook and Kaut, 1993*).

CHAPTER 4

SCAPULAR AND HUMERAL ANATOMICAL COORDINATE SYSTEMS

1) <u>Calderone M.</u>, Cereatti A., Rosso C., Costantino S., Conti M., Della Croce U., "Anatomical coordinate systems for high-resolution scapula and humerus models", Gait & Posture, 2013, 37S1:S24-S25.

2) <u>Calderone M.</u>, Cereatti A., Conti M., Della Croce U. Comparative evaluation of scapular and humeral coordinate systems based on biomedical images of the gleno-humeral joint", Journal of Biomechanics 47(3):736-741, 2013.

3) <u>Calderone M.</u>, Cereatti A., Merella E., Della Croce U., "Anatomical landmarks position estimation in incomplete 3D humerus models", presented at 3rd Congress National Group of Bioengineering, Rome, Italy, June 26th-29th, 2012.

Scapular and humeral anatomical coordinate systems (ACSs) identification represent a prerequisite for the assessment of the gleno-humeral displacements. Many different conventions exist in literature for defining both scapular and humeral ACS, including the currently standard proposed by the International Society of Biomechanics (ISB) (Wu et al., 2005). The latter definition, as other in literature, is based on the use of selected anatomical landmarks (ALs) (Pearl et al., 1992; van der Helm et al., 1997; Novotny et al., 2000; Veeger et al., 2000; Wu et al., 2005; Kedgley et al., 2010; Ludewig et al., 2010; Verstraeten et al., 2013), other definitions require the identification of anatomical regions (ARs) (Sahara et al., 2007; Amadi et al., 2008; Amadi et al., 2009) to be defined. In the present section we will focus on the different ACSs proposed in literature in order to highlight the advantages and disadvantages of each definition.

4.1   Literature review

ALs and ARs required to define the different ACSs (Fig. 4.1)

HHC: Center of the humeral head

GT: Greater tubercle

LT: Lesser tubercle

AN: Anatomical neck

MEc: Medial epicondyle (central)

LE: Lateral epicondyle

TS: Trigonium Spinae scapula

AA: Angulus Acromialis

IA: Inferior Angle

G: Glenoid

CP: Tip of Coracoid Process

LB: Lateral Border

SS: Root of Scapula Spine
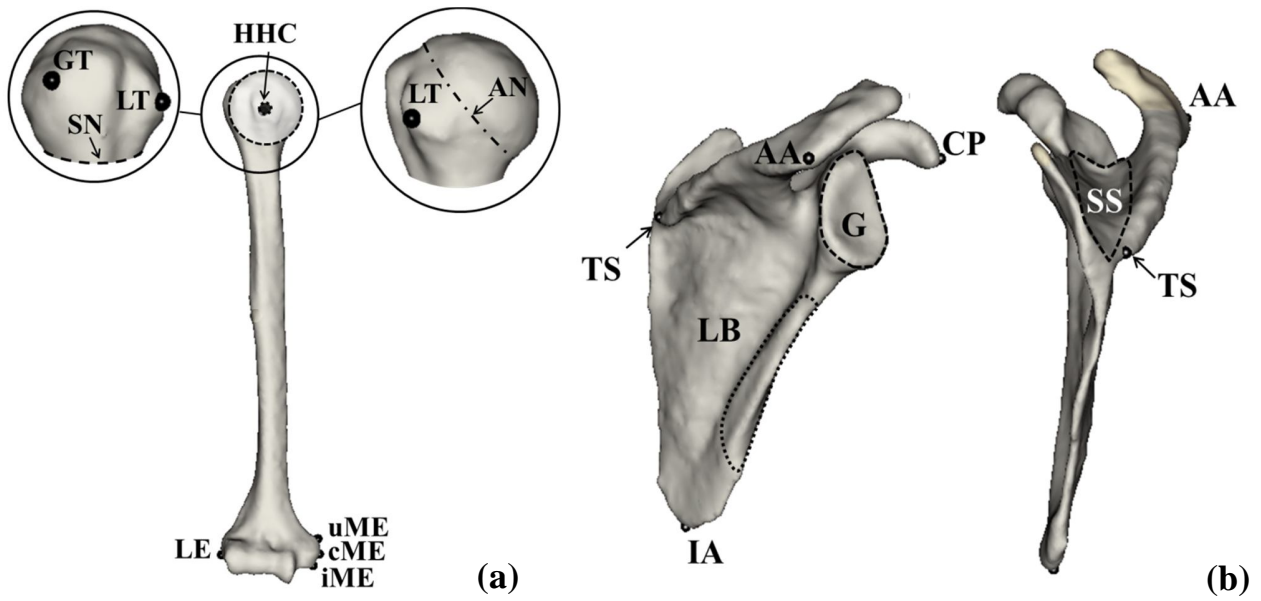
Figure 0: Humeral (a) and scapular (b) ALs and ARs.

Humeral ACS definitions

van der Helm et al. (1996) (Fig. 4.2) - The origin coincides with HHC. The Y axis is oriented as the line connecting HHC and E (midpoint of LE and MEc). The Z axis is directed as the line perpendicular to Y and the line connecting LE and ME, pointing backward. The X axis is the line perpendicular to Y and Z axes.
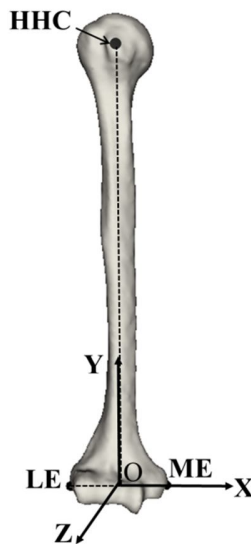
Figure 4.2: Humeral ACS (van der Helm et al., 1996).

Road et al. (1998) - The isolation of the proximal portion of the humerus (Fig. 4.3) is required. The latter AR was obtained by performing a radial cut by means of a sphere centered in the humeral head center HHC and of fixed radius (slightly larger than the best fit spherical surface). The origin and the three axes coincide with the centroid and principal axes of the isolated proximal humerus respectively.
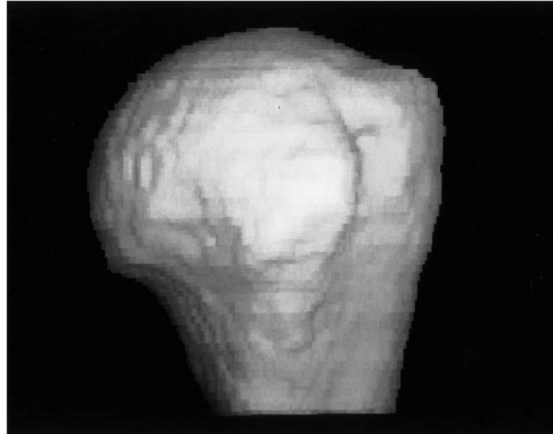
Figure 4.3: Proximal humerus (Road et al., 1998).

Novotny et al. (2000) (Fig. 4.4) - The origin coincides with HHC. The X axis is directed parallel to the proximal humeral shaft centerline. The Z axis is directed from the medial to lateral epicondyle and the Y axis was directed to result in a right-handed coordinate system.
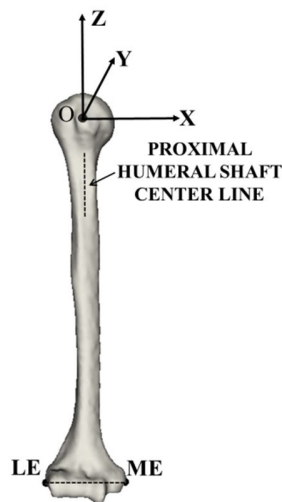
Figure 4.4: Humeral ACS (Novotny et al., 2000).

Wu et al. (2005, standard ISB) (Fig. 4.5) - The origin coincides with HHC. The Y axis is the line connecting HHC to the midpoint of the lateral and medial epicondyles (LE, MEc) and pointing to HHC. The X axis is the line perpendicular to the plane formed by LE, ME, and HHC, pointing anteriorly and the Z axis is defined as the cross product between X and Y axes.
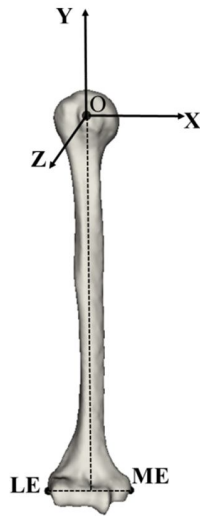
Figure 4.5: Humeral ACS (Wu et al., 2005).

Sahara et al. (2007) (Fig. 4.6) - The origin coincides with the HHC. The Y axis is orthogonal to the anatomical neck plane pointing superiorly. The X axis is equal to the cross product between Y and the canal axis. The Z axis is defined as the cross-product between X and Y axes.
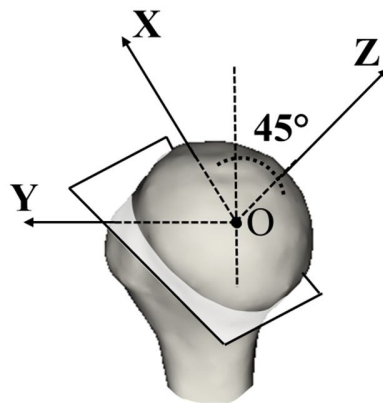
Figure 4.6: Humeral ACS (Sahara et al., 2007).

Amadi et al (2009) (Fig. 4.7) - The origin coincides with the HHC. The Y axis is oriented as the canal axis pointing superiorly. The canal axis coincides with the best fitting line to the center of the humeral shaft cross sections selected from 10 to 60 mm distal to the surgical neck. The X axis is equal to the cross-product between Y and the oriented line from HHC to GT. The Z axis is defined as the cross product between X and Y axes.
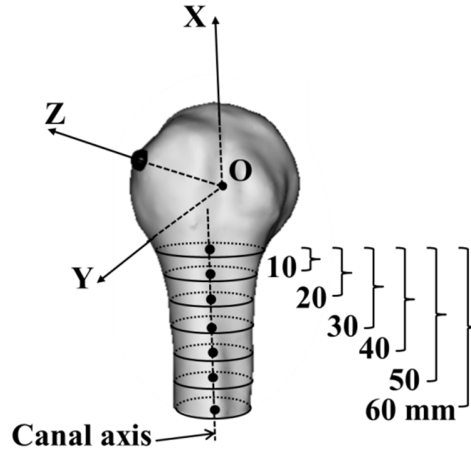
Lee et al. (2010) (Fig. 4.8) - It is based on digitized points along the articular margin of the humeral head where the articular cartilage ends (Fig. 4.8). The following parameters are required:

$\overrightarrow{p}$: is the average position of all the digitized humeral head articular margin points $\overrightarrow{(p} = \frac{1}{m}\sum_{i=1}^{m}\overrightarrow{p}_i$ were m is the number of digitized points);

$\overrightarrow{n}_i$: is the normal vector of the each triangle. It is computed by equation reported below;

s_i: is the ratio of the area (Q_i) of a triangle $\Delta(\overrightarrow{p}, \overrightarrow{p}_i, \overrightarrow{p}_{i+1})$ to the total area of all triangles (Q);

e_i: is the centroid of each triangle($\overrightarrow{e}_i = (\overrightarrow{p} + \overrightarrow{p}_i + \overrightarrow{p}_{i+1})/3$);

$\vec{O}_4$: is the true geometric centroid of the elliptical humeral head articular border. It computed as the average values of all triangles constructed from the average position ($\overrightarrow{p}$), the point ($\overrightarrow{p}_i$), and (i + 1) the point ($\overrightarrow{p}_{i+1}$). Numerically $\vec{O}_4$ was defined as the average of the centroids of all triangles ($\vec{O}_4 = \sum_{i=1}^{m}[\overrightarrow{e}_i \times s_i]{=}\overrightarrow{p}_{HHC}$).

$\overrightarrow{n}_i = (\overrightarrow{p}_i - \overrightarrow{p}_{HHC}) \times (\overrightarrow{p}_{i+1} - \overrightarrow{p}_{HHC})/(|(\overrightarrow{p}_i - \overrightarrow{p}\|\overrightarrow{p}_{i+1} - \overrightarrow{p}|)$.

$\vec{n}$: is the normal vector of the articular margin plane. It is determined by averaging the normal directions of all triangles ($\overrightarrow{n} = \frac{1}{m}\sum_{i=1}^{m}\overrightarrow{n}_i$).

The origin coincides with$\vec{O}_4$. Z axis is defined as the normal direction of the humeral head resection plane ($\vec{n}$). X axis is oriented as the vector connecting ($\vec{O}_4$) and the superior point of the humeral head resection surface. Y axis is the axes resulting from the cross product of the Z and X axes.
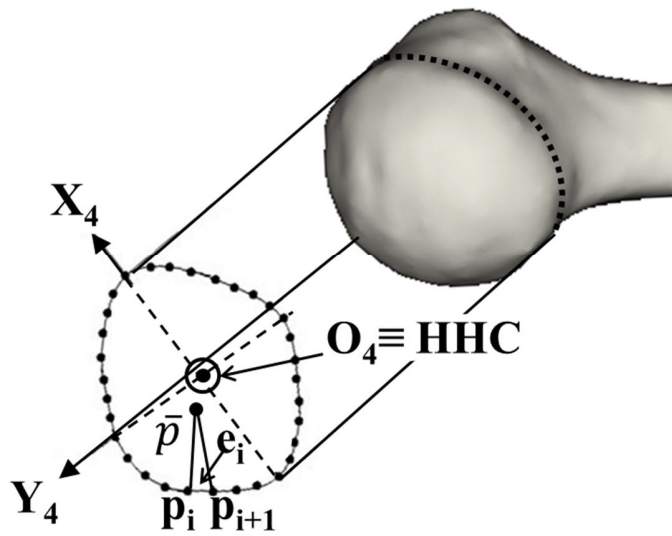
Figure 4.8: Humeral ACS (Lee et al., 2010).

Scapular ACS definitions

Pearl et al. (1992) (Fig. 4.9) – Origin coincides with P. The Z axis is oriented as the line connecting P and TS, pointing to P. The X axis is directed as the line perpendicular to the plane formed by AI, TS and P, pointing forward. The Y axis is defined as the common line perpendicular to the X and the Z axes, pointing upward.
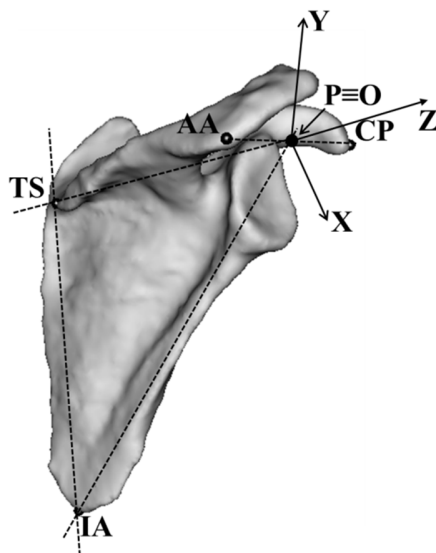
Figure 4.9: Scapular ACS (Pearl et al., 1992).

40

van der Helm (1996) (Fig. 4.10)- The origin coincides with AC. The X axis is oriented as the line connecting AC and TS, pointing to AC. The Z axis is directed as the cross product of X axis and line connecting AI and AC pointing downward. The Y axis is defined as the common line perpendicular to the Z and the X axes, pointing upward.
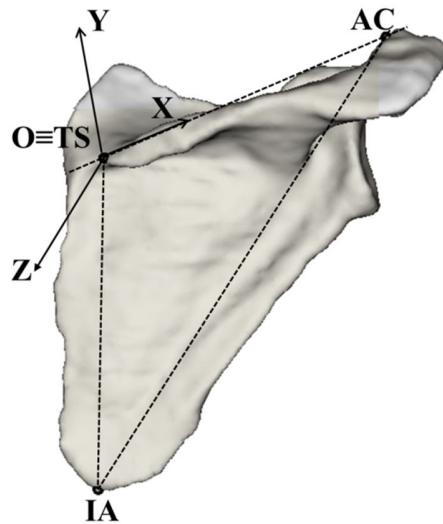
Figure 4.10: Scapular ACS (van der Helm et al., 1996).

Road et al. (1998) - The origin and the three axes coincide with the centroid and principal axes of the isolated glenoid surface (Fig. 4.11) respectively.
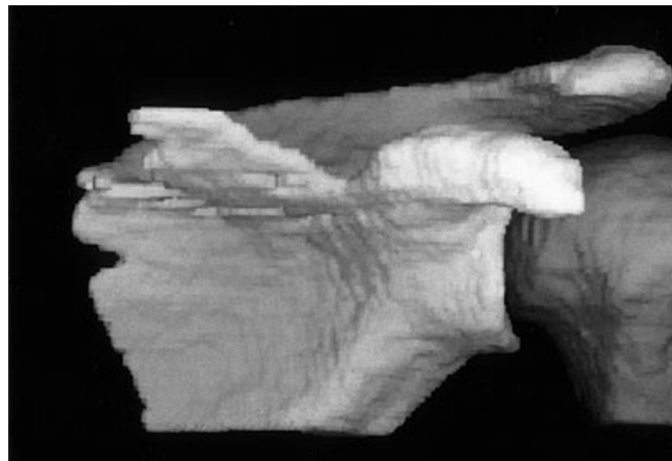
Figure 01: Glenoid surface obtained by means of an automatic process based on the computation of parameters related to the MRI images (Road et al., 1998).

Novotny et al. (2000) (Fig. 4.12) - The Z axis is directed superiorly from the most inferior aspect of the glenoid to the biceps tendon insertion. The X axis is directed laterally along the line making the shortest distance from the Z axis to the center of a sphere fit to the glenoid surface, and the Y axis is

directed to result in a right-handed coordinate system. The origin coincides with the intersection of the X and Z axes.
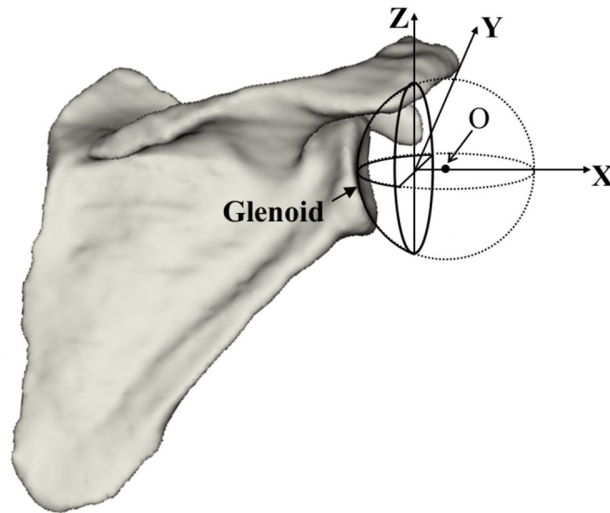
Figure 02: Scapular ACS (Novotny et al., 2000).

Wu et al. (2005) (Fig. 4.13) - The Z axis is oriented as the line connecting AA and TS, pointing to AA. The X axis is directed as the line perpendicular to the plane formed by AI, AA, pointing forward. The Y axis is defined as the common line perpendicular to the X and the Z axes, pointing upward.
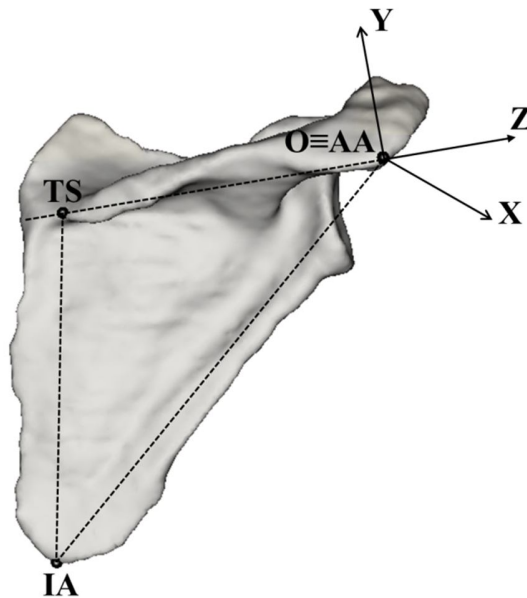
Figure 03: Scapular ACS (Wu et al., 2005).

Sahara et al. (2007) (Fig 4.14) - The scapular origin coincides with K. The Z axis is oriented as the line orthogonal to the plane pointing to the right. The X axis direction is defined as the line orthogonal to the Z axis, passing through the closest point of the glenoid margin and pointing anteriorly. The Y axis is defined as the cross-product between Z and X axes.
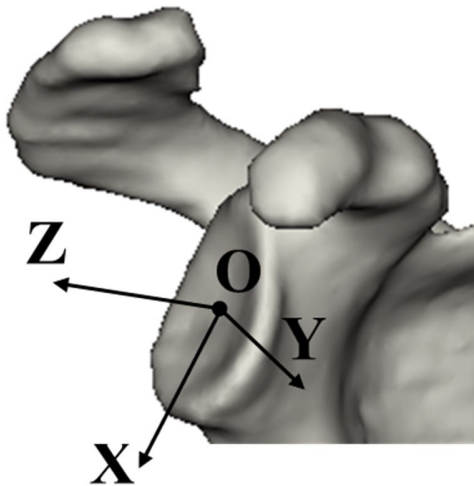
Figure 04: Scapular ACS (Sahara et al., 2007).

Amadi et al. (2008) (Fig. 4.15) - The origin is not specified. The Z axis is oriented as the line passing through the centre of the root of the scapular spine and pointing to the right, X axis is anteriorly directed and it is defined as the cross-product of Z axis and a line, superiorly directed, through the centre of the ridge of the scapular lateral border. The Y axis is defined as the cross-product between Z and X axes.
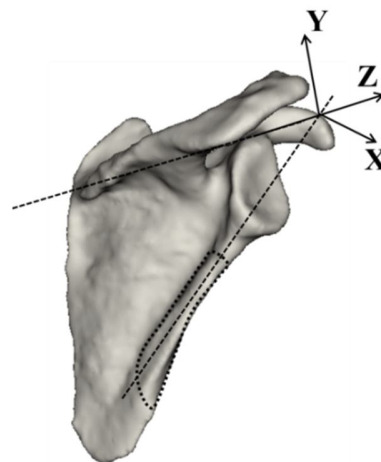
Figure 4.15: Scapular ACS (Amadi et al., 2008).

43

Kedgley et al. (2010) (Fig. 4.16) - The origin coincides with AA. The Z axis is oriented as the line connecting TS and AA, pointing to AA. The Y axis direction is defined as the cross product between the oriented line from CP to AA and the Z axis. The X is defined as the cross-product between Y and Z axes.
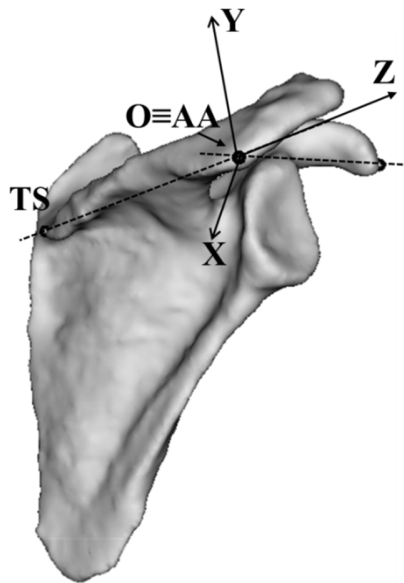
Figure 4.16: Scapular ACS (Kedgley et al., 2010).

Ludewing et al (2010) (Fig. 4.17) - The origin is not specified. The Z axis is directed as the line perpendicular to the glenoid plane. The Y axis is directed superiorly toward the superior glenoid tubercle. The X axis is directed anteriorly perpendicular to the other two axes.
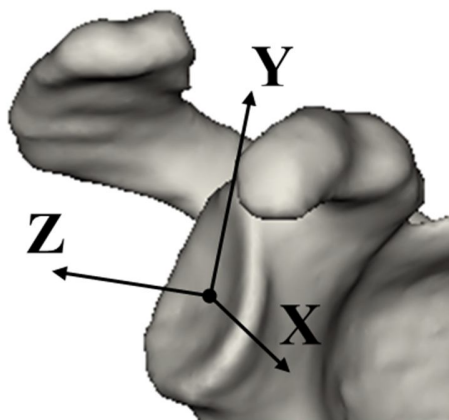
Figure 4.17: Scapular ACS (Ludewing et al., 2010).

Lee et al. (2010) (Fig. 4.18) - the definition of the preliminary ACS is require: the pre-ACS is built on the supero-inferior (SI) axis defined by the intersection of the superior glenoid rim with the glenoid-coracoid confluence (S, Fig. 4.18), and the intersection of the inferior glenoid rim with the infero-lateral margin of the scapula (I, Fig. 4.18). Anterior and posterior ALs of the glenoid were defined as the anterior and posterior intersections (A and P in Fig. 4.18) of the bony glenoid rim with a perpendicular plane bisecting the S–I bony line. The bisecting point of the SI is the origin $(\overrightarrow{O'}_3)$ of the preliminary glenoid coordinate system (pre-ACS, X′, Y′ and Z′). With $\overrightarrow{O'}_3$, the anterior and posterior landmarks (A, P) and the superior landmark (S), the pre-ACS was determined by the right-hand rule-based Cartesian coordinate system.

O_{pg}: the origin of the pre-GCS coincident with $\overrightarrow{O'}_3$.

X_{pg}: the vector parallel to $\overrightarrow{AP}$ and passing O_{pg}.

Y_{pg}: $\overrightarrow{SI}$.

Z_{pg}: the axis defined as the cross product of the X_{pg} and Y_{pg}-axes.

The ACS was determined by translating the origin of the pre-GCS (O_{pg}) to the bottom of the glenoid surface. This bottom level of the glenoid surface was determined by numerically finding the point $(\vec{g}_h)$ which has the least distance from the origin of the pre-GCS among the points $(\vec{g}_i)$ digitized along the concave SI glenoid surface.

The vertical depth of the glenoid $\Delta_t = \left| \overrightarrow{O'}_3 - \vec{g}_h \cdot \vec{k}_3 \right|$) was expressed as the distance from the origin of the pre-ACS to the point $(\vec{g}_i)$ along the Z-direction of the pre-ACS where $(\vec{k}_3)$ is the unit vector along the Z_{pg}.
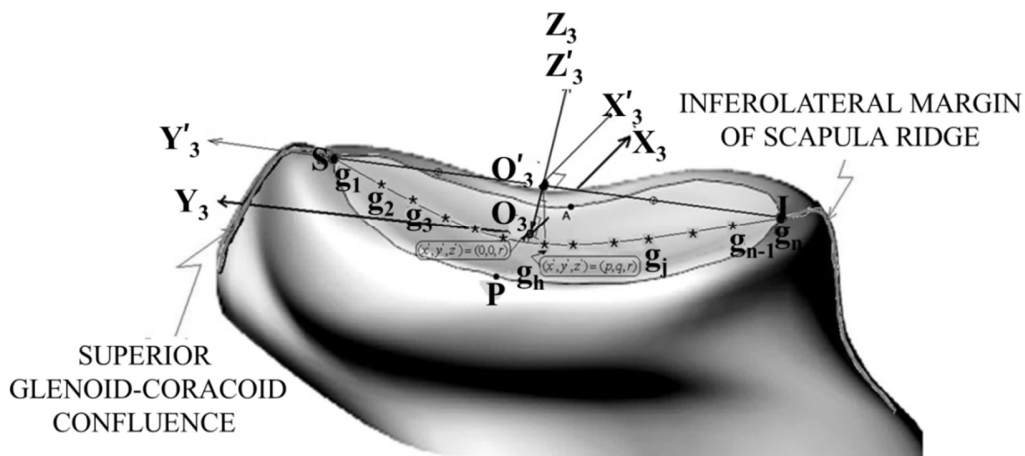
Figure 4.18: Scapular ACS (Lee et al., 2010).

45

Verstraeten et al. (2013) (Fig. 4.19) - The origin is defined as the center of the circle defined by the three selected glenoid points. The Z axis is oriented as the line orthogonal to the circle plane and pointing to the right. The Y axis direction is defined as the line orthogonal to the Z axis, passing through the inferior point of the glenoid margin and pointing superiorly. The X axis is defined as the cross-product between Y and Z axes.
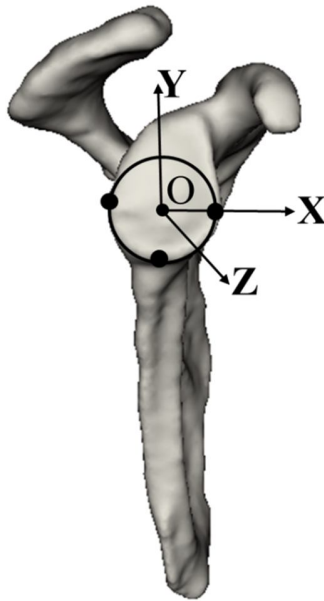
Figure 4.19: Scapular ACS (Verstraeten et al., 2013).

The principal limitation of most of the ACSs in literature (Pearl et al. 1992; van der Helm et al., 1996; Novotny et al., 2000; Amadi et al., 2008; Kedgley et al., 2010) including the currently standard proposed by the ISB (Wu et al., 2005), is the need to have access to ALs sited both in the proximal and distal portion of the bone models. These ACS are not suitable to be used with high resolution models obtained from MR clinical images, because, due to their restricted FoV, this technique prevent the acquisition of the complete bone model. Moreover these definitions do not define a specific glenoid ACS that is crucial for assessing the humeral movement with respect to the glenoid (Lee et al., 2010). On the contrary the ACSs proposed by Rohad et al. (1998), Novotny et al. (2000), Sahara et al. (2007), and Verstraeten et al. (2012) in addition to being constructed on the glenoid, because the latter is always included in the FoV, they could be implemented also with 3D models obtained from MR clinical images.

However, the ACS proposed by Rohad et al. (1998) and based on principal axis to be consistent and yield accurate motion information, it is essential that the shapes of the surface of the bone determined at various joint positions are as similar as possible, may therefore depend on the 3D model.

Novotny et al. (2000) as Verstraten et al. (2012) used a sphere to represent the glenoid, instead the glenoid appear like a pear-shaped (Iannotti et al., 1992). Consequently, due to the variability of the glenoid shape the axes direction may show an intersubjective variability. The main limitation of the scapular ACS proposed by Sahara et al. (2007) is the difficulty of implementation and the need for manual adjustments.

An additional issue is represented by the use of information which may be morphologically variable between different samples as for Lee at al. (2010) which proposed a specimen-specific ACS definition and based on information not easily identifiable on 3D bone models obtained from magnetic resonance images. This is true also for the definition of the humeral coordinate system proposed by Sahara et al. (2007), which is based on the anatomical neck of the humerus. Some anatomical study had reported the intersubjective variability in the neck-shaft angle (125°-150°, Iannotti et al., 2007), which is the angle subtended by the central intramedullary axis of the humeral shaft and a line perpendicular to the base of the joint segment (humeral anatomical neck); accordingly the variability in the anatomical neck inclination influences the orientation of the coordinate system based on it. Moreover, the identification of the anatomical neck used in this proposal does not take in to account of the intersubjective variability of this AR. With regard to the scapular ACS, the problem related to the intersubjective variability has been overcome by Amadi et al. (2009), who have proposed the best body-fixed coordinate system based on ALs and ARs that are least susceptible to scapular morphometric variability. Nevertheless, this definition is based on the identification of anatomical regions which are not easy to identify from MRI, that are not readily accessible and that could not be included in the FoV.

Among the different definitions proposed for the humeral ACS, the most robust method for defining an ACS is based on the use of the HHC and epicondylar axis (Amadi et al., 2009; Wu et al., 2005), as for the humeral ACS proposed in the ISB recommendation (Wu et al., 2005). Unfortunately, as previous highlighted it can be used only if the entire bone are included in the FoV of clinical bio-imaging techniques. The use of the proximal humerus to define a robust ACS has been proven by Amadi et al. (2009). This humeral ACS was defined to be most closely oriented as that ACS using the epicondylar and humeral canal and to be applied to a standard shoulder CT scan. The CT scan, however, has a larger FoV and a higher spatial resolution with respect to the MR scan, therefore, once again it cannot be used with 3D high resolution models obtained from MR clinical images.

To overcome the limitation associated to the ACS exiting in literature two different approaches have been proposed.

4.2 Proposal for a novel humerus and scapula anatomical coordinate system definition

4.2.1 Introduction

The scapular and humeral ACS definitions proposed in the literature are based either on the identification of ALs (Pearl et al., 1992; van der Helm et al., 1997; Novotny et al., 2000; Veeger et al., 2000; Wu et al., 2005; Kedgley et al., 2010; Ludewig et al., 2010; Verstraeten et al., 2013), or of ARs (Sahara et al., 2007; Amadi et al., 2008b; Amadi et al., 2009). Generally, the spatial locations of the abovementioned morphological parameters are identified by manual palpation or visual inspection of 3D digital models of the bones obtained from biomedical images (Salvia et al., 2009). The size of the reconstructed portion of the bone and the resolution of the images used to reconstruct it determine the applicability of a specific ACS.

Considering that technologies allowing for the highest spatial resolution are based on ionizing radiation, such as computer-tomography scanning (CT), dual fluoroscopy, it would be ideal to limit the bone portions to be exposed (Lee CH et al., 2008). A restricted FoV allows MR scans to be faster, to have a finer spatial resolution and a higher tolerance to motion artifacts (Smith et al., 2012). To this extent, it would be desirable to have ACSs readily applicable when limited scapula and humerus bone portions are included in the FoV.

Moreover, to meet the requirements of intra- and inter-operator repeatability, the ACS definition should be based on ALs (or ARs), which are easy to identify, irrespective of the bone morphology acquisition tool used and least susceptible to the physiological morphometric variability (Amadi et al., 2008b). In addition, ACSs should be consistent with the anatomical cardinal directions to be clinically interpretable (Amadi et al., 2008b; Amadi et al., 2009; Ludewig et al., 2010).The primary aim of this study is to present ACS definitions for both scapula and humerus to be used when only their portions near the gleno-humeral joint fall in the FoV (Fig. 4.20) and fulfilling the abovementioned requirements. The sensitivity of the newly proposed ACS definitions to bone morphological variation was assessed along with a preliminary analysis of the inter- and intra - operator repeatability associated to the uncertainty in the ALs (and ARs) identification and ACS consistency with the anatomical cardinal directions. A comparison with alternative ACS definitions found in the literature, which do not require the entire scapula and humerus models, was also performed.
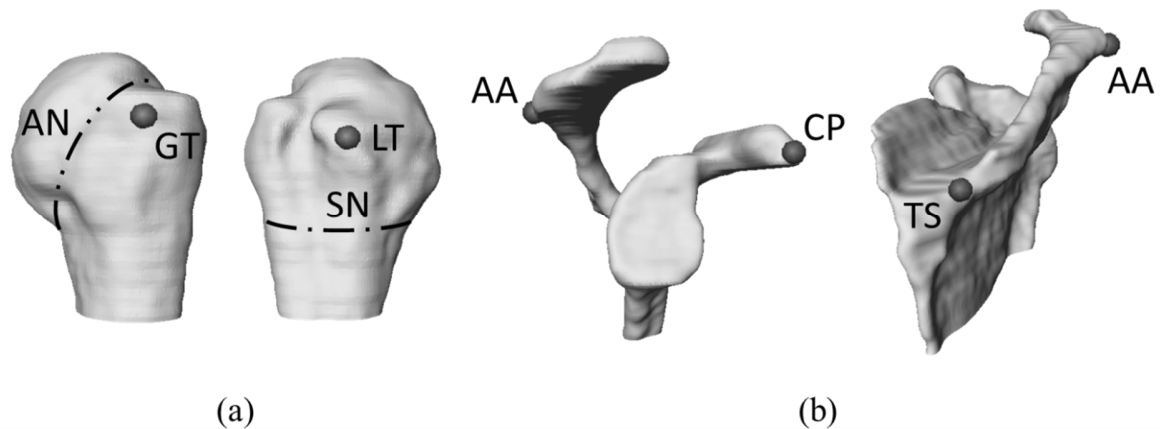
Figure 4.20: Bony scapular and humeral portions hypothesized to be available from MR images. The greater tubercle (GT), the lesser tubercle (LT), the anatomical neck (AN) and surgical neck (SN) for the right humerus are reported in (a); The acromial angle (AA), the root of scapular spine (TS) and tip of coracoid process (CP) are reported for the right scapula (b).

4.2.2 Materials and methods

Twenty healthy asymptomatic subjects (9 females, 31 ±8 y.o.) were enrolled for this study and signed an informed consent. The study was approved by the local Institutional Review Board. MR scans of the whole right humerus and scapula were obtained by using a 1.5 T MR scanner (Philips Intera Achieva version 1.7). Spin Echo imaging sequences were used (axial T1-W: TR 660 ms; TE 18 ms; flip angle 90 deg; Contiguous Slice Thickness 4 mm, FoV 280 mm). Bone contours were identified using a semiautomatic segmentation procedure. 3D reconstructions of the entire scapular and humeral bones were obtained using the AMIRA image processing software (Visualization Sciences Group, v.5.4).

In the following ACS definitions, right-handed ACSs are considered, anatomical planes are defined with respect to the standing subject in the anatomical position (Cappozzo et al., 1995; Wu et al., 2005).

Proposal for the scapular and humeral ACS

Scapular ACS - The glenoid margin, and consequently its surface, is manually isolated from the scapular model. The scapular origin (Os) coincides with the centroid (K) of the glenoid, calculated as the average of the coordinates of the vertices forming the triangular meshes. A plane (α) is then fitted to the glenoid margin points (Amadi et al., 2008a). The Zs axis is oriented as the line orthogonal to α pointing to the right in accordance with Amadi et al. (2008a). An ellipse is fitted to the projections on α of the glenoid margin points. The Xs and Ys axes are oriented as the minor and major axes of the ellipse, pointing anteriorly and upward, respectively (Fig. 4.21).

49
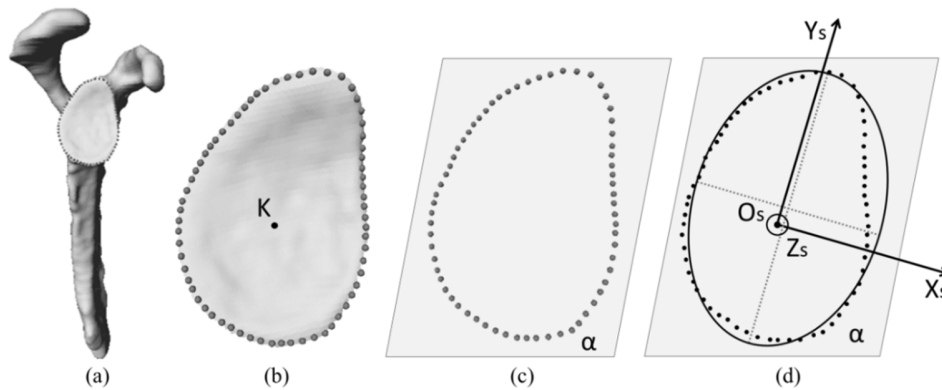
Figure 4.21: The novel scapular ACS definition. Glenoid margin is manually identified from the reconstructed glenoid model (a, b); the plane α is fitted to the selected glenoid points (c); an ellipse is fitted to the points of the glenoid margin projected on α. The ACS for a right scapula is also shown (d).

Humeral ACS - The humeral ACS origin (Oh) coincides with the center of the best fitting sphere to the humeral head (Gamage and Lasenby, 2002). The Yh axis is oriented as the canal axis identified by the least square regression line connecting the centers of the humeral shaft cross section (C1: surgical neck; C2: at a distance of 10 mm from C1, C3 at a distance of 20 mm from C1) pointing upwards. The Xh axis is oriented as the line orthogonal to the Yh axis, passing to LT and pointing anteriorly. The Zh is equal to the cross-product between the Xh and Yh axes (Fig. 4.22).
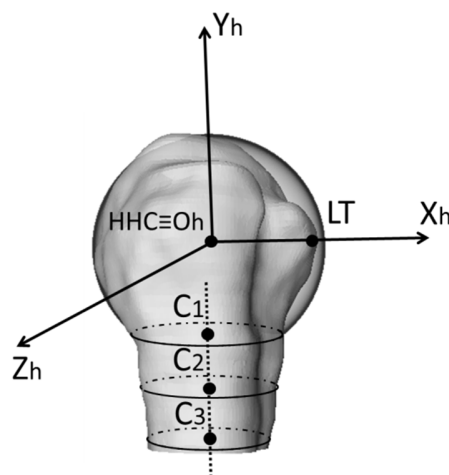
Figure 4.22: The novel humeral ACS. A sphere is fitted to the spherical portion of the humeral head for the identification of the HHC; the centers of the humeral shaft cross-section (C1, C2, C3) are used to identify the canal axis; the lesser tubercle (LT) and the resultant ACS for a right humerus are also shown.

ACSs selected for comparison

The novels ACS definitions were compared to the definitions proposed by Sahara et al. (2007) and Amadi et al. (2009) for the humerus (Fig. 4.23), Sahara et al. (2007), Kedgley et al. (2010), Verstraeten

et al. (2013) for the scapula (Fig. 4.24). Both scapular and humeral ACS have been described in the paragraph 4.1.
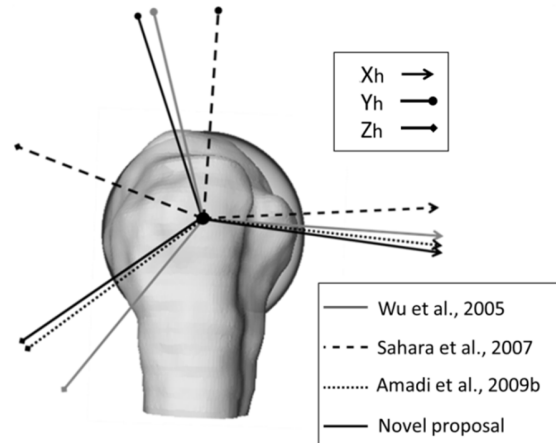
Figure 4.23: Humeral ACSs selected for comparison and reference humeral ACS (Wu et al., 2005) for an arbitrary selected humerus. The Y_h axis of the ACS of Amadi et al., 2009 is not visible since it coincides with the Y_h axis of the novel proposal.
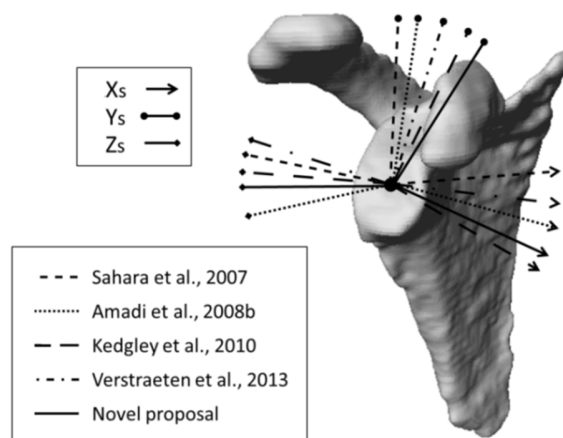
Figure 4.24: Scapular ACSs selected for comparison and reference scapular ACS (Amadi et al., 2008b) for an arbitrary selected right scapula. For sake of clarity, all the origins were made to coincide with the origin adopted in the novel proposal.

As regard the scapular ACS proposed by Sahara et al. (2007), since the instructions provided for the identification of the flat central region of the glenoid were ambiguous ("… defined as 3D contiguous meshes including the central mesh and the meshes under 25-30° angles from the central one"), the flat region was identified as follows. An inverted right circular cone with the axis coinciding to the normal to α (see proposal for the scapular and humeral ACS-Scapular ACS), with an aperture equals to 150° and with the apex coinciding with the closest point of the glenoid surface from the centroid K of the glenoid, is determined. The points of the glenoid surface not included in the cone were selected as the "flat" area of the glenoid. A plane is then fitted to the points belonging to the flat area (Fig. 4.25).
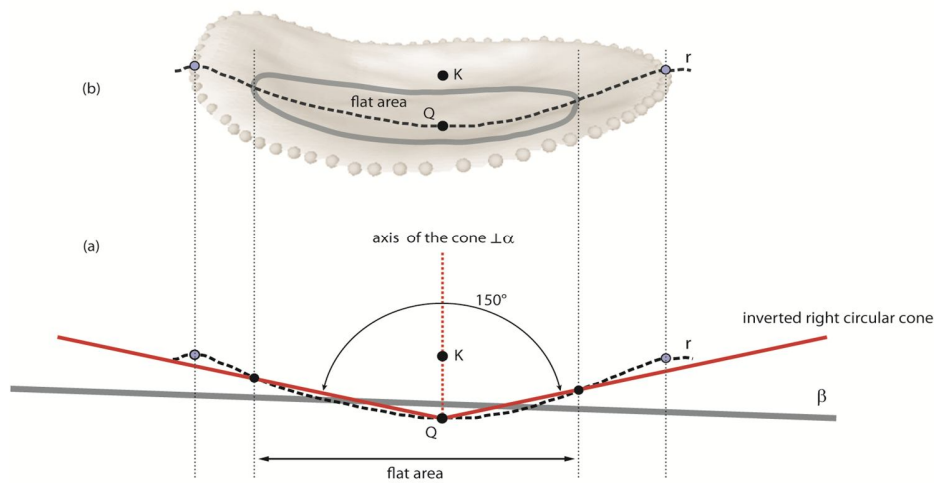
Figure 4.25: The glenoid surface, the centroid K of the glenoid and the closest point Q of the glenoid surface from the centroid K are shown (a). A two-dimensional schematic representation of the glenoid surface as seen in a frontal section (plane containing the line r) is depicted in (b). An inverted right circular cone with the axis coinciding to the normal to the best fitting plane α to the glenoid margin points, with an aperture equals to 150° and with the apex coinciding with the Q, is determined. The points of the glenoid surface not included in the cone were selected as the flat area of the glenoid. A plane α is then fitted to the points belonging to the flat area.

For both the humeral ACSs proposed by Sahara et al. (2007) and Amadi et al. (2009) the procedure to identify the canal axis was the same used for the novel ACS proposed in this study. This adjustment was performed because the small size of the reconstructed portion of the bone derived by MR clinical images.

Sensitivity to bone morphological variability

To assess the sensitivity of the various ACS definitions to the bone morphometric variability, the reconstructed 3D bone models need to be appropriately superimposed. Amadi and colleagues carried out an extensive analysis aimed at the identification of the axes the least sensitive to scapular morphological variations and used those axes to define an ACS which minimizes specimen variability (Amadi et al., 2008b). For the humerus, the most robust method for defining an ACS is based on the use of the HHC and epicondylar axis (Amadi et al., 2009; Wu et al., 2005). Based on the aforementioned considerations, the reconstructed bone models were superimposed by aligning the scapulae using the ACS proposed by Amadi et al. (2008b) and the humeri using the ACS definition proposed in Wu et al. (2005) (both the scapular and humeral ACS proposed by Amadi et al., 2008b and Wu et al., 2006 respectively, have been described in the paragraph 4.1). The ACSs proposed by Amadi et al. (2008b) and Wu et al. (2005) were used as reference for the assessment of bone morphological variability but since they require the scapular lateral border and the complete humeral bone models to be implemented, they were not included in the comparative evaluation. From the aligned scapulae and humeri, for each selected ACS definition, the X, Y and Z mean axes were computed. The angular

deviations $\theta^i_{x,y,z}$, between the ACS axes of the *i-th* (i = 1,.., 20) scapular and humeral bones and the corresponding mean axes, were calculated. The overall ACS sensitivity to the morphological bone variations was evaluated for each ACS definition and direction by calculating the mean absolute angular deviation values $MAD^\theta_{x,y,z} = \frac{1}{20}\sum_{i=1}^{20}\left|\theta^i_{x,y,z}\right|$ and the corresponding standard deviation values. Significant differences between the $MAD^\theta_{x,y,z}$ values found in correspondence of the proposed scapular and humeral ACS definitions and those selected for evaluation were analyzed by performing pairwise comparisons using the Wilcoxon rank-sum test for non-normal sample distributions (three and two pairwise comparisons for the scapular and humeral ACSs, respectively). The level of significance was determined using the Holm-Bonferroni method for adjusted p-values (alpha = 0.05). Statistical analyses were performed using IBM SPSS statistics, version 21 (SPSS Inc., Chicago, IL, USA).

Intra- and inter-operator repeatability

To preliminarily investigate the sensitivity of the various ACS definitions to the uncertainty associated to the identification of the ALs and ARs location, for an arbitrary selected scapula and humerus model, the calibration procedure was performed seven times by the same operator in seven separate days (intra-operator repeatability) and one time by seven different operators (inter-operator repeatability). All operators had experience in ALs (ARs) identification and the visual inspection was performed following the guidelines given to examiners (Van Sint Jan, 2005; Van Sint Jan and Della Croce, 2005). For each calibration, the corresponding scapular and humeral ACSs were computed and for each ACS definition, the $MAD^\theta_{x,y,z}$ values from the corresponding mean axes were calculated along with the corresponding standard deviation values. Since the assessment of the inter- and intra-rater reliability with statistical power would require the design of a specific study (Walter et al., 1998), for this preliminary evaluation only descriptive statistics are reported.

Scapular and humeral ACSs anatomical cardinal directions consistency.

The aim of this specific analysis was to assess the angular offsets between the ACS definitions analyzed and the anatomical cardinal directions and therefore their clinical interpretability. For the scapula, the angular deviations were computed with respect the ACS proposed by Amadi and colleagues since the latter ACS definition was developed with the aim of minimizing the axes deviation from the plane of the scapular blade and it is closely related to clinical coordinate systems (Amadi et al., 2008b; Ludewig et al., 2010). For the humerus, we referred to the ACS definition proposed in Wu

et al. (2005) since it is based on the epicondylar and the longitudinal axes which define the standard anatomical planes. For each scapula, the angles $\phi^i_{x,y,z}$ between the scapular axes identified in correspondence of the various definitions selected for comparison and the corresponding axes defined by Amadi et al. (2008b) were computed and the $MAD^\theta_{x,y,z}$ values and the corresponding standard deviation values estimated. Similarly, the same calculations were repeated for each humerus with respect to the ACS definition described in Wu et al. (2005). The same statistical analysis described above (in the section sensitivity to bone morphological variability) was used to analyze statistical differences among the various ACS definitions.

4.2.3 Results

Data relative to the sensitivity of the ACS definitions to the bone morphological variability are reported in Table 4.1. For the scapular ACS, our proposal showed for all three axes $MAD^\theta_{x,y,z}$ values very similar to those found for Kedgley et al. (2010). Despite the differences observed in the $MAD^\theta_{x,y,z}$ values among the compared methods, the only statistically significant difference was observed for the Yh between our proposal and the ACS proposed by Sahara et al. (2007) and Verstraeten et al. (2013) (adjusted p equals to 0.003 and 0.006, respectively). For the humeral ACS, the $MAD^\theta_{x,y,z}$ values found for our ACS were similar to those found for the ACS presented in Amadi et al. (2009). Since the definition of Yh axis is the same in Amadi et al. (2009) and in our ACS, the corresponding MAD^θ_y values were identical. ACS variability for the ACS presented in Sahara et al. (2007) was the largest for all three axes and statistically significant differences from our ACS were found for both Xh and Yh (adjusted p equals to 0.038 and 0.01, respectively).

ACS definition	*Scapula*			*Humerus*		
	X_s (deg)	Y_s (deg)	Z_s (deg)	X_h (deg)	Y_h (deg)	Z_h (deg)
Sahara et al. (2007)	13.0 (6.7)	13.9* (7.0)	10.0 (4.3)	13.6* (9.7)	9.5 (6.8)	10.5 (6.5
Amadi et al. (2009)	-	-	-	7.2 (4.0)	4.0 (1.8)	7.4 (3.8)
Kedgley et al. (2010)	8.3 (3.6)	7.8 (3.6)	8.1 (5.1)	-	-	-
Verstraeten et al. (2013)	11.2 (7.0)	14.2* (5.8)	9.5 (5.2)	-	-	-
Novel proposal	8.0 (3.3)	8.3 (3.3)	8.3 (3.3)	7.1 (3.4)	4.0 (1.8)	7.1 (3.4)

Table 4.1: Mean absolute angular deviation values $MAD^\theta_{x,y,z}$ (and standard deviation values) for each ACS definition and axis direction computed over 20 scapular and humerus bone models. The symbol (*) indicates a significant difference with respect to the novel proposal.

Data relative to the sensitivity of ACSs definitions analyzed to the uncertainty associated to the ALs and ARs identification are reported in Table 4.2 and Table 4.3.

	Scapula			Humerus		
ACS definition	Xs (deg)	Ys (deg)	Zs (deg)	Xh (deg)	Yh (deg)	Zh (deg)
Sahara et al. (2007)	2.7 (2.4)	2.8 (2.4)	0.7 (0.3)	4.2 (2.9)	2.9 (2.0)	3.1 (2.1)
Amadi et al. (2009)	-	-	-	3.6 (1.7)	0.3 (0.3)	3.6 (1.7)
Kedgley et al. (2010)	0.5 (0.3)	0.4 (0.3)	0.4 (0.3)	-	-	-
Verstraeten et al. (2013)	3.7 (1.9)	3.7 (1.9)	0.9 (0.9)	-	-	-
Novel proposal	0.3 (0.1)	0.3 (0.1)	0.2 (0.1)	0.4 (0.3)	0.3 (0.3)	0.4 (0.3)

Table 4.2: Intra-operator repeatability for the ACS definitions, associated to the identification of the ALs and ARs location, in terms of mean absolute angular deviation values $MAD^{\theta}_{x,y,z}$ (and standard deviation values) for each ACS definition and axis direction.

	Scapula			Humerus		
ACS definition	Xs (deg)	Ys (deg)	Zs (deg)	Xh (deg)	Yh (deg)	Zh (deg)
Sahara et al. (2007)	3.2 (2.6)	3.3 (2.6)	0.6 (0.6)	7.8 (6.6)	5.8 (4.4)	5.4 (4.7)
Amadi et al. (2009)	-	-	-	5.2 (2.8)	0.8 (0.3)	5.2 (2.8)
Kedgley et al. (2010)	1.3 (1.0)	1.1 (0,5)	1.2 (1.2)	-	-	-
Verstraeten et al. (2013)	5.8 (2.8)	6.0 (2.9)	1.4 (1.1)	-	-	-
Novel proposal	1.5 (0.6)	1.4 (0.7)	0.7 (0.3)	3.3 (0.8)	0.8 (0.3)	3.3 (0.8)

Table 4.3: Inter-operator repeatability for the ACS definitions, associated to the identification of the ALs and ARs location, in terms of mean absolute angular deviation values $MAD^{\theta}_{x,y,z}$ (and standard deviation values) for each ACS definition and axis direction.

The scapular ACS proposed in the present study showed an intra- and inter-operator precision ranging between 0.3 deg to 1.5 deg for all axes. A comparable repeatability was observed for the definition proposed in Kedgley et al. (2010) which varied, for all axes, between 0.4 deg to 1.3 deg. The highest intra and inter-operator variability was found for Xs and Ys axes of the scapular definition proposed by Verstraeten et al. (2013). For the humerus, our ACS showed the highest intra- and inter-operator precision with $MAD^{\theta}_{x,y,z}$ values between 0.3 deg and 3.3 deg for all axes. The humerus ACS proposed in Amadi et al. (2009) appeared to be characterized by a high repeatability in the identification of the humerus longitudinal axis Yh but not for the Xh and Zh ($MAD^{\theta}_{x,z}$ values equal to 3.6 deg and 5.2 deg for the intra and inter-operator repeatability, respectively). The $MAD^{\theta}_{x,y,z}$ values for the humerus ACS described in Sahara et al. (2007) varied between 2.9 deg to 4.2 deg and between 5.4 deg to 7.8 deg for the intra- and inter-operator repeatability, respectively. Results relative to the scapular and humeral ACS consistency with the anatomical cardinal directions are reported in Table 4.4. The $MAD^{\phi}_{x,y,z}$ values for the scapular ACS proposed in this study were significantly smaller than those reported in Sahara et

al. (2007) and in Verstraeten, et al. (2013) for the Ys axis (adjusted p equals to 0.001 and 0.032, respectively), and smaller than those in Kedgley et al. (2010) and Verstraeten, et al. (2013) for the Zs axis (adjusted p equals to 0.002 and 0.01, respectively). The $MAD^{\phi}_{x,y,z}$ values for the humerus were similar to those found for Amadi et al. (2009) and significantly smaller than Sahara et al. (2007) for Ys and Zs axes (adjusted p value equals to 0.00).

	Scapula			Humerus		
ACS definition	Xs (deg)	Ys (deg)	Zs (deg)	Xh (deg)	Yh (deg)	Zh (deg)
Sahara et al. (2007)	16.7 (9.2)	21.6* (9.2)	15.2 (7.1)	15.4 (13.6)	46.5* (2.1)	49.5*(5.4)
Amadi et al. (2009)	-	-	-	8.1 (4.0)	6.1 (3.0)	8.8 (3.9)
Kedgley et al. (2010)	14.7 (6.9)	12.9 (6.3)	17.7* (8.7)	-	-	-
Verstraeten et al. (2013)	12.7 (8.0)	25.9* (9.8)	22.8* (9.4)	-	-	-
Novel proposal	11.1 (5.5)	15.0 (7.0)	13.9 (5.9)	8.2 (4.5)	6.1 (3.0)	8.6 (4.6)

Table 4.4: Mean absolute angular deviation values $MAD^{\phi}_{x,y,z}$ (and standard deviation values) for both scapular and humeral ACSs definitions with respect the corresponding axes defined by Amadi et al. (2008b) and Wu et al. (2005) respectively. The symbol (*) indicates a significant difference with respect to the novel proposal.

4.2.4 Discussion

The use of bio-imaging techniques represents a powerful tool for high resolution joint biomechanical analysis (Esfandiarpour et al., 2009). 3D models of the bone surface can be derived from the 2D segmented images, acquired using either CT or MR scans, employing different image processing software commercially available. For a given 3D bone model, the level of repeatability associated to the ACS identification is determined by the intrinsic uncertainty characterizing the AL definitions (Della Croce et al., 1999) and the sensitivity of the ACS construction rules to the ALs location errors (Della Croce et al., 2003). As extensively documented in the literature, the precision with which the various ALs can be identified depends on the morphological features of the bone area within the AL is located (Salvia et al., 2009; Donati et al., 2008; Della Croce et al., 1999; Van Sint Jan, 2007). The level of detail with which the bone surface can be reconstructed is determined by the spatial and contrast resolution associated to the bio-imaging technique employed and it is likely to influence the precision with which ALs and ARs can be identified. In general, CT scans allow for a more distinct segmentation of the contours of the bones with respect to MR scans and therefore for a higher resolution of the bone surface description (Lee YS et al., 2008).
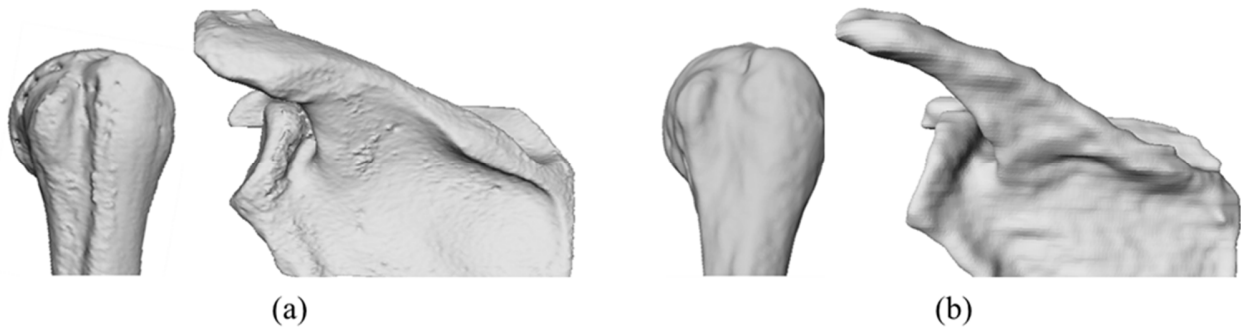
Figure 4.26: Example of right scapula and humerus models reconstructed from MR (a) and CT images (b). The bones reported in the picture belong to different subjects.

Therefore, the intra- and inter-operator repeatability obtained using scapular and humeral bone models derived from MR images is expected to be worse than that obtained from CT images (Amadi et al.,2008b) (Fig. 4.26). Furthermore, the MRI acquisition parameters, such as the slice thickness, employed in the study, were similar to those used in standard clinical MR images of the shoulder joint (Lee and Lang, 2000).

In the present study, we focused on the ACS definitions proposed in the literature for the humerus and scapula based on the identification of ALs and ARs located in the proximity of the GHJ and which are generally included even in images with a small FoV. Overall, our ACS scapular definition proposal and that presented in Kedgley et al. (2010) were found to be the least sensitive to the morphometric variability and, from a preliminary investigation, they were characterized by a high intra- and inter-operator repeatability. The strength points of the scapular ACS proposed by Kedgley et al. (2010) are the simple implementation and its compliance with the ISB standard (Kedgley et al., 2010). On the other hand, while the scapular ACS proposed in the present study is based on the glenoid, which is always included in the scan FoV and clearly visible, sometimes the most superior aspects of the scapula, required for the ACS definition of Kedgley et al. (2010), such as the root of the scapular spine or the tip of the coracoids process, are poorly visible and they are not always guaranteed to appear in standard clinical MR scans.

With regards to the humerus, the sensitivity to morphological variability between our definition and the ACS proposed by Amadi et al. (2009) was found to be very similar and smaller than Sahara et al. (2007). It is key to acknowledge that in the work of Amadi et al. (2009), conducted on 21 CT scans of humeri, the HHC-LT axis was taken into consideration for comparative purposes but then discarded in favor of an axis passing through the GT since the HHC-GT axis was nearly in the same direction of the elbow epicondylar axis and presented a slightly lower variability. The choice to include LT in our definition of the humeral

ACS, instead of GT as proposed by Amadi et al. (2009) did not increase either the morphological variability or the anatomy consistency and it was justified by the simpler identification of LT with respect to GT when the bone model is reconstructed from MR images. In fact, LT is smaller and more prominent than GT (Botte, 2002). This may explain the lower intra-and inter-operator repeatability observed for the humeral ACS proposed by Amadi et al. (2009). The largest dispersion of the humeral ACS proposed in Sahara et al. (2007) is possibly due to the morphological variability of the anatomical neck plane (neck-shaft angle between 125 deg and 150 deg) (Iannotti et al., 2007), which would affect the axes direction. For the scapula, substantial differences in the axes directions were observed between the ACS definitions analyzed and that proposed by Amadi et al. (2008b). This implies that attention should be paid when comparing the scapular motion as derived by different ACS definitions (Ludewig et al., 2010; Xu et al., 2012). The ACS proposed in the present study for the humerus showed angular deviation from the anatomical cardinal directions smaller than 8.6 deg for all three axes. Differences in the axes direction among alternative ACS definitions can lead to significantly different joint kinematics (Kedgley et al., 2010), unless appropriate transformations are applied (Xu et al., 2012).

An evaluation of the clinically significant differences associated to the adoption of different ACS definition would require an analysis of the joint kinematic outcomes. However, the latter evaluation was beyond the scope of the present study and it advocates for further research. Another limitation is in regards to the methodology employed for the assessment of the intra- and inter-operator ACS repeatability, a conclusive assessment would have required the design of a specific reliability study by defining the optimal number of observations (operators) and number of subjects (bone models) according to a preliminary statistical power calculation. In the present study, we proposed ACS definitions for the scapula and humerus based on the extraction of ALs and ARs easy to identify and which can be applied when a limited portion of the gleno-humeral joint is available as it may occur in standard shoulder clinical exams. However, while the use of contours or surfaces for the creation of ACSs allow exploiting redundant information and circumventing the errors inherent in the identification of single fiducial points, this approach can be more time-consuming for the operator.

4.3   An alternative method for the anatomical coordinate system definition on incomplete 3D bone model: an application to the humerus

4.3.1   Introduction

Standard MRI is a powerful tool in those clinical applications where the joint motion can be analyzed in quasi-static conditions (F. Esfandiarpour et al., 2009) and small displacements need to be detected.

However, due to its limited field of view, often, only portions of the 3D model of the analyzed bones can be reconstructed, while complete bone models are needed to use ISB recommendations.

This problem could be overcome by obtaining the missing ALs by matching the MRI-based portion of the subject specific 3D bone model (SBP), to a template of a complete bone model (TBC) on which the relevant ALs have been previously identified. Established algorithms exist for surface matching, popular ones being based on the Iterative Closest Point (ICP) algorithm (Besl et al., 1992) for which an initial guess of the transformation between the bone meshes is required. The reliability of the above mentioned registration exercise would depend on the size of SBP and the similarity level between SBP and TBC morphologies. In this preliminary study, the feasibility and the assessment of the level of accuracy and repeatability of the procedure for the ALs estimate when applied to the proximal portion of the human humerus, was evaluated. To this purpose, two experimental scenarios which can be encountered in the clinical practice were simulated. First, the ALs estimate procedure was tested to different SBPs characterized by different extents (expressed as percentage of the humerus length) using as TBC the bone applied to SBP and TBC belonging to different subjects.

4.3.2   Materials and methods

Data sets

Three left humeri were scanned and the 3D corresponding mesh models reconstructed (*TBC*1, 2, 3). From each TBC, three SBP were generated by isolating different proximal portions identified as percentage of the humerus length (14%, 16%, 20%) (14%, 16%, 20% 1, 2, 3 SBP). These values were chosen to simulate different sizes of the MRI acquisition volume. On each TBC, the following ALs were identified by an expert: lateral and medial epicondyle (LE, ME), greater and lesser tubercle (GT, LT) and the geometrical center of the humerus head (HHC). HHC was identified by fitting a sphere to the humeral head.

Procedure for the estimation of the ALs on the SBP

To estimate the position vectors of both LE and ME, with respect to the SBP point set, the next steps are followed:

1) *Registration of first approximation* - Three anatomical landmarks GT, LT, and HHC were manually identified by an operator on the SBP (Fig. 4.27a). Using the three pairs of corresponding points, TBC and SBP were uniformly scaled, registered and expressed in a common reference frame.

2) *TBC iso-shaping* - A TBC iso-shape was automatically created by isolating a portion from the whole TBC using a separation plane coinciding with the most distal slice plane of the SBP (Fig. 4.27b).

3) *Final registration and LE and ME position estimation* - ICP algorithm was employed to refine the registration between SBP and the iso-shaped TBC portion. At this stage, the position vectors of both LE and ME, identified on the TBC, were expressed in the same system of reference of the SBP point set (Fig.4.27)
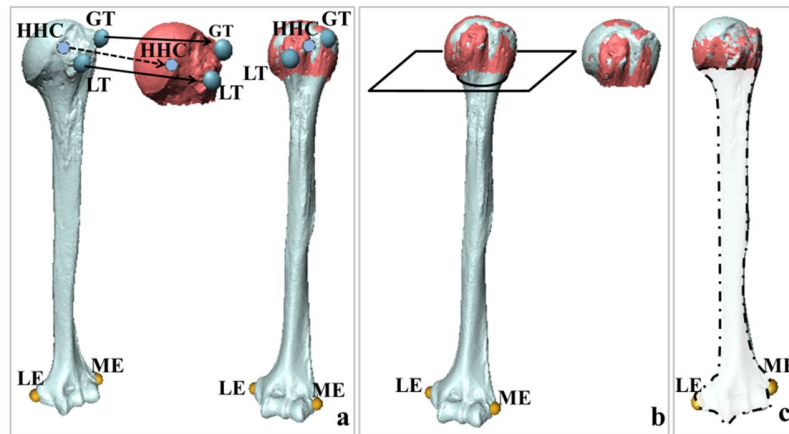
Figure 4.27: Registration procedure. TBC (gray) to SPB (red) registration of first approximation (a). TBC iso-shaping (b). Final registration (c).

Application 1: SBP and TBC of the same subject

Each 14%, 16%, 20% 1, 2, 3 *SBP* was matched to the corresponding *TBC* (Table 4.5). For *SPB*116%, the ALs estimate procedure was performed three times by the same operator to verify the method sensitivity to the registration of first approximation.

Application 2: SBP and TBC of different subjects

Each 14%, 16%, 20% 1, 2, 3 *SBP* was matched with the two TBC belonging to different subjects (Table 4.5). For *SPB*2 16%, the ALs estimate procedure was repeated three times by the same operator, using as template *TBC*1.

Data analysis

Since the SBPs were generated from the corresponding TBC, the true positions of both LE and ME for each SBP were known and used as ground truth for evaluating the magnitude of the errors associated to the ALs estimation procedure. Humerus ACSs were defined from both the estimated and the true LE and ME positions and their relative orientation (α, β, γ) was computed using the Euler angles representation suggested by Grood and Suntay (1983) (Grood et al., 1983).

	TBC_1	TBC_2	TBC_3
$SPB_1^{14\%}$	X	X	X
$SPB_1^{16\%}$	xxx	X	X
$SPB_1^{20\%}$	X	X	X
$SPB_2^{14\%}$	X	X	X
$SPB_2^{16\%}$	xxx	X	X
$SPB_2^{20\%}$	X	X	X
$SPB_3^{14\%}$	X	X	X
$SPB_3^{16\%}$	X	X	X
$SPB_3^{20\%}$	X	X	X

Table 4.5: Experimental scenarios. Different combinations of SBP and TBC tested. In light gray and dark gray are reported Application 1 and Application 2, respectively. The symbol xxx is referred to the combination which was tested three times.

4.3.3 Results

When SBP and TBC belonged to the same subject, the errors associated to the ACSs definition were negligible for all different SBP extents analyzed (14%, 16%, 20%) and were lower than 0.1 deg for all angles (α, β, γ). Errors on the ACS identification, due to variability with which GT, LT, HHC were manually identified during the registration of first approximation, ranged, over the three repetitions, between 0.1-0.4 deg, 0.0-0.1 deg and 0.0-0.2 deg for α, β and γ, respectively. On the contrary, when the TBC and the SBP belonged to different subjects, the errors in the ACS definition increased for all angular components and ranged, over the different TBC-SBP combinations (Table 4.5), from 0.2-1.9 deg for α, 2.7-19.0 deg for β, 0.3-4.3 deg for γ. By estimating the ALs for different registrations of first approximation (*SPB*2 16%-*TBC*1), ACSs estimation errors varied, over the three repetitions, from 0.5-0.9 deg for α, 13.5-16.3 deg for β, 1.1- 1.8 deg for γ.

4.3.4 Conclusion

A general method for the estimate of the position of missing ALs on incomplete 3D bone model was presented. The methodology was applied and preliminarily tested on 3D bone models relative to the proximal portion of the human humerus. Preliminary results have shown that this method can be successfully employed when the portion of the 3D model of the bone, SBP, and the template, TBC, refer to the same subject. Under this condition, even with a limited portion of the SBP of the humerus (14% of the humerus length) it is possible to accurately estimate the position of the missing ALs. Moreover, the manual identification of the ALs, necessary for the registration of first approximation, and the TBC iso-shaping procedure did not appear to be critical. On the contrary, the performance of the method was unsatisfying when tested on SBPs and TBCs of different subjects. In this case, errors associated to the

ACS identification were up to 2 deg, 19 deg and 4 deg for α, β and γ, respectively. The large variability observed for the tested SBP-TBC combinations confirmed that the accuracy of the method is heavily affected by the degree of similarity between the morphology of the SBP and that of the template selected for the matching. The largest errors found for β can be explained by the high level of symmetry of the proximal portion about the humerus long axis and the variability characterizing the angle of humeral torsion (Cowgill et al., 2007). The validity of present study is limited by the low number of samples analyzed. However, our preliminary results may suggest the critical role played by morphological variability. This issue might be faced using appropriate statistical models (Heimann et al., 2009) or by selecting from large databases the template most morphologically similar to the portion of the 3D model of the bone. The applicability and the evaluation of this approach to different type of bones, such as the scapula, calls for further and specific analysis.

CHAPTER 5

MAGNETIC RESONANCE IMAGING BASED METHODOLOGY FOR ESTIMATION OF GLENO-HUMERAL JOINT TRANSLATIONS

1) Calderone M., Cereatti A., Rosso C., Della Croce U. "In vivo evaluation of gleno-humeral joint translations in loaded and unloaded conditions", Proceedings of XXIV National Congress of SIAMOC, Pisa, Italy, 2013.

2) Cereatti A., Calderone M., Buckland D.M., Muller A.M., Della Croce U., Rosso C. "In vivo gleno-humeral translation under external loading in an open MRI setup", Proceedings of XXIV ISB Congress, Natal, Brazil 2013.

3) Cereatti A., Calderone M., Buckland M.D., Buettnerb A., Della Croce U., Rosso C. "In vivo gleno-humeral translation under external loading in an open MRI setup". Journal of Biomechanics (submitted).

(This chapter was written on the basis of the article "In vivo gleno-humeral translation under external loading in an open-MRI setup" Cereatti A., Calderone M., Buckland M.D., Buettnerb A., Della Croce U., Rosso C. Journal of Biomechanics, submitted).

5.1 Introduction

The *in vivo* assessment of the GHJ instability is crucial in orthopedic research since it is instrumental in understanding and thus preventing primary and repeated shoulder dislocations (Mallon and Speer, 1995). The evaluation of the GHJ laxity requires the ability of accurately measuring the linear displacement of the HHC with respect to the glenoid resulting from shoulder movements and/or from the applications of external forces. *In vivo* experiments for the assessment of shoulder laxity under the application of anterior forces have been proposed in the literature (Sauers et al., 2001; McQuade and Murthi, 2004). However, while the use of skin mounted sensors may be acceptable for quantifying the relative changes in translation, it cannot provide an accurate description of the HHC position with respect to the glenoid. In fact, the deformation of the soft tissues surrounding the scapula and humerus bones hampers reaching the level of accuracy required for the analysis of the small displacements involved (Anglin et al., 2000; Hill et al., 2007; Veeger and van der Helm, 2007). An alternative approach is offered by the use of technologies based on ionizing radiation such as CT (Baeyens et al., 2001), biplanar X-rays (Lagacé et al., 2012), fluoroscopy (San Juan and Karduna, 2010) or a combination of dual-plane fluoroscopy and 3D bone models derived from CT or MRI (Bey et al., 2006; Nishinaka et al., 2008; Massimini et al., 2012). Major limitations of such techniques include the image geometric distortion and invasiveness due to the radiation exposure. A further alternative, which could provide an acceptable level of accuracy and that is innocuous for patients, is the use of MRI (von Eisenhart-Rothe et al., 2010). GHJ translations have been investigated both in healthy subjects (Rohad et al., 1998; Graichen et al., 2000; Sahara et al., 2007) and patients (von Eisenhart-Rothe et al., 2002; Chhadia et al., 2010) using MRI. However, none of the latter *in vivo* studies analyzed the GHJ translations under the action of selected external forces. Conversely, extensive analyses of the biomechanical role of soft tissues and articular surfaces as joint constraints under the application of selected external forces has been conducted on cadavers (Alberta et al., 2006; Marquardt et al., 2006; Su et al, 2009). However, the translation of the *in vitro* results to the *in vivo* condition should be approached with caution due to the lack of tone of the mono and bi-articular muscles involved. The primary aim of this study was thus to develop a MRI based methodology for an accurate *in vivo*

63

evaluation of the GHJ translation under a loaded condition. The secondary aim was to gather normative data on healthy subjects to use for further comparison on patients population.

5.2   Materials and methods

5.2.1   Subjects selection

Thirteen shoulders of ten healthy subjects (5 females; age 28.5 ± 3.2 years [mean ± standard deviation, SD]; height 1.76 ± 0.9 m; weight 68.3 ± 8.4 kg) with no previous shoulder injury and no congenital joint laxity were analyzed. The study was approved by the local Institutional Review Board of Basel and an informed consent was obtained from all subjects prior to enrollment.

5.2.2   Experimental set-up

A horizontal open-MR scanner (Philips Panorama HFO, 1 Tesla, Fig. 5.1) and a custom-built device (Fig. 5.2, Fig. 5.3) for the shoulder loading were used.

Figure 5.1: Philips Panorama HFO, 1 Tesla.

The device is composed by a wooden goniometer (Fig. 5.2a) to fix the trunk of the subject and which allow to firmly positioning the forearm of the subject at different degree of abduction by means of a Velcro strap, a carbon lever used to transmit the force to the arm and a load (Fig. 5.2b) which define the magnitude of the force applied.
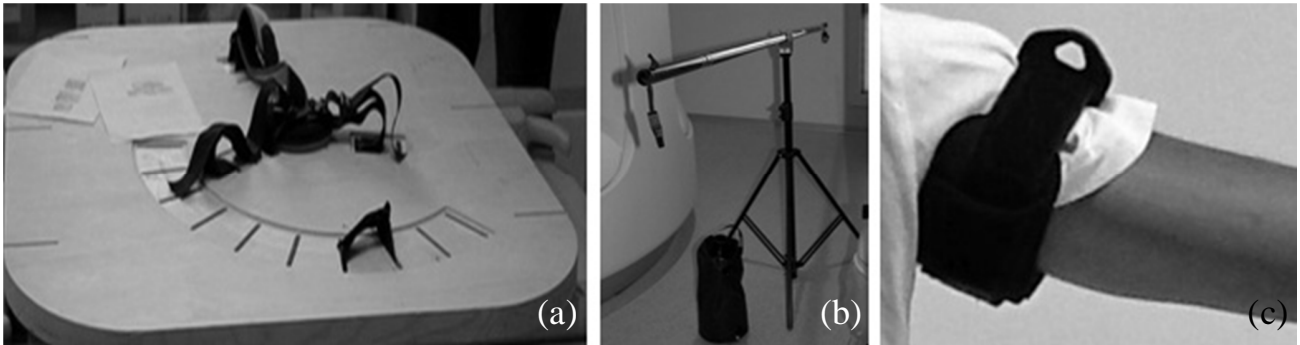
Figure 5.2: Custom-built device for shoulder loading. Wooden goniometer (a); lever and weight (b); Velcro strap to attach the lever to the arm (c).

The intensity of the external force was fixed at 20 N plus the weight of the arm (2.55% and 2.71% of the body mass (Kg) for female and male respectively) (de Leva et al., 1996). The force was aligned to the gravity and anteriorly directed. The lever was attached to the proximal portion of the humerus through a Velcro strap (Fig. 5.2c). Scans were performed using 3D T2-W Spin Echo imaging sequences (TR 1.4 s; TE 50 ms; flip angle 90 deg; interslice gap 1.5 mm, slice thickness 3 mm, FoV 180 mm).

Figure 5.3: Detail of the experimental set-up employed to apply the anterior force to the subject humerus in the MRI scanner.

5.2.3   Experimental protocol

Acquisition

The following acquisitions were collected while the subject was asked to relax as much as possible:

1)   15 deg of arm abduction without external load (15-w/o, Fig. 5.4a);

2)   15 deg of arm abduction with the external load (15-w, Fig. 5.4b);

3)   90 deg of arm abduction without external load (90-w/o, Fig. 5.4c);

4)   90 deg of arm abduction with the external load (90-w, Fig. 5.4d).

Recordings were made with the subject in the supine position between the two gantries of the MRI system with the hand of the tested arm facing up representing 90 deg of external rotation. The thoraco-humeral angle was adjusted by using the wooden goniometer. The acquisition time for each scan was approximately 12 minutes.
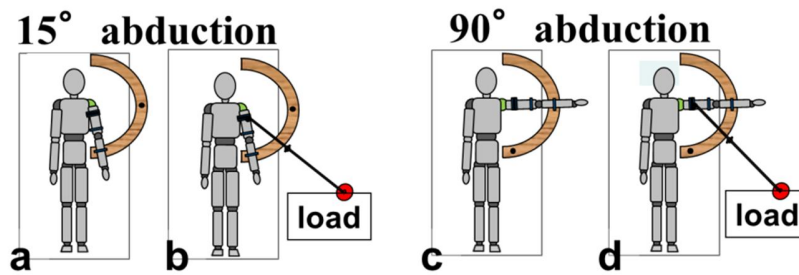
Figure 5.4: Acquisition: 15 deg of arm abduction without external load (a); 15 deg of arm abduction with the external load (b); 90 deg of arm abduction without external load (c); 90 deg of arm abduction with the external load (d).

Estimation of GHJ displacements

From each MR acquisition, 3D scapula and humerus models were obtained through a semiautomatic segmentation (Fig. 5.5) performed by a single skilled operator using the software AMIRA (v.5, Visage Imaging Inc., San Diego, CA, USA). The scapula and humerus anatomical ACSs were defined according to the definitions proposed in Calderone et al. (2013).
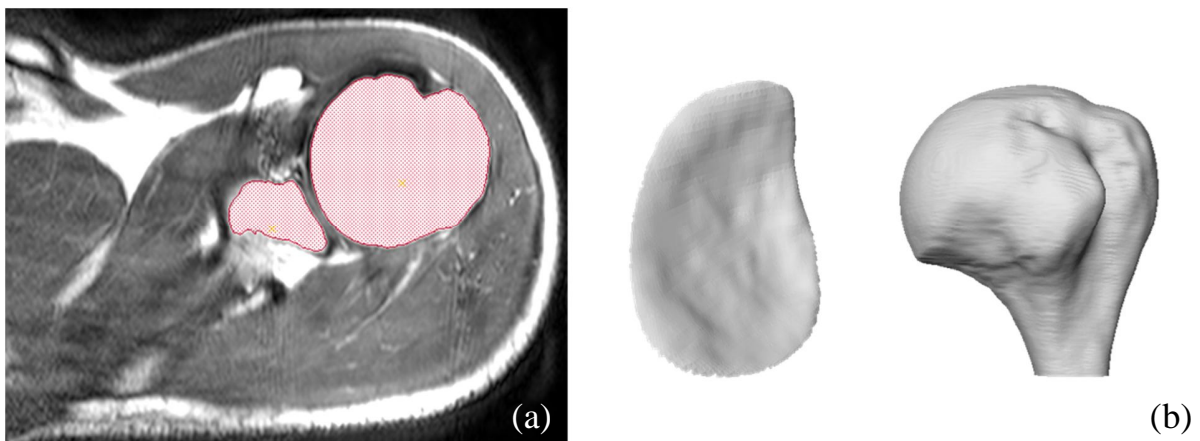
Figure 5.5: Image segmentation (a) and 3D scapula and humerus models reconstructed (b).

Following the latter guidelines, the humeral ACS origin coincides with the HHC and it is determined as the center of the best fitting sphere to the spherical portion of the humeral head (Veeger, 2000). For each shoulder, four distinct pairs of humerus and scapula models of the same bone were obtained for the acquisitions (15-w/o, 90-w/o, 15-w, and 90-w). To minimize repeatability errors associated with the ACSs identification procedure, these were defined by the same operator on the humerus and scapula

models reconstructed in correspondence of an arbitrary acquisition (15-w/o) referred to as bone templates (Fig. 5.6). The latter templates, carrying the ACSs, were then optimally registered to the remaining scapula and humerus models of the same shoulder by means of the iterative closest point technique (Besl and McKay, 1992) and the ACSs transferred to them (Fig. 5.6). For each acquisition, the positions of the HHC with respect to the relevant scapula ACS were estimated. The GHJ translational components were computed as the HHC displacements in the following conditions: (1) between 15-w/o and 15-w, (2) between 90-w/o and 90-w; (3) between 15-w/o and 90-w/o. From the anterior-posterior (A-P), the superior-inferior (S-I) and the medio-lateral (M-L) components, both 3D and 2D displacement (A-P, S-I plane) were computed.
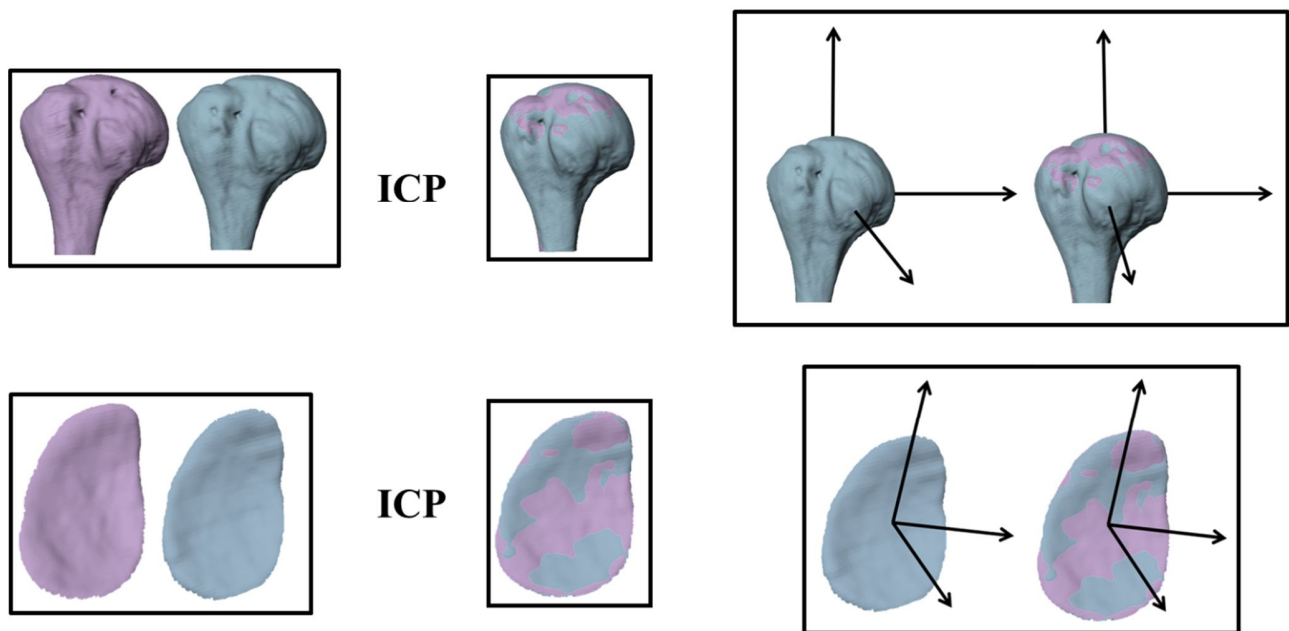
Figure 5.6: Registration of the humerus and scapula models by means of the iterative closest point technique and ACSs transfer.

5.2.4 Repeatability assessment

To assess the level of precision associated with the GHJ translation estimates, the MR images, relative to two arbitrary selected shoulders (1 right male and 1 left female) were segmented and processed by the same operator four times in four separate days. Repeated estimates of the GHJ translations for the different conditions (15-w/o and 15-w, 90-w/o and 90-w, 15-w/o and 90-w/o) were performed and the SD values computed.

5.2.5 Statistical analysis

A test for normality of the GHJ translational components over the subjects indicated that none of them was normally distributed. Therefore, their dispersion was described using a five number summary technique. To determine if there were differences 100 in the GHJ translation components for each of the different analyzed conditions, a Friedman's multiple comparison test for dependent samples was applied. Post-hoc pairwise comparisons were then performed by using the Wilcoxon rank-sum test for non-normal sample distributions. The level of significance was determined using the Holm-Bonferroni correction for adjusted p-values (α= 0.05). Differences between GHJ translations estimated between 15-w/o and 15-w and between 90-w/o and 90-w were analyzed by performing pairwise comparisons using the Wilcoxon rank-sum test for non-normal sample distributions. Statistical analyses were performed using IBM SPSS statistics, version 21 (SPSS Inc., Chicago, IL, USA).

5.3 Results

As an example, HHC positions for the different shoulder acquisitions relative to a subject are shown in
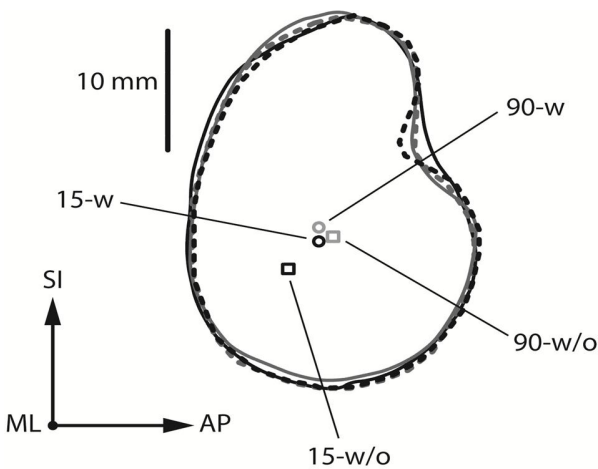
Figure 5.7: Projections onto the (A-P, S-I) scapula plane of the glenoid margins and the HHC positions for the four conditions analyzed for an arbitrary selected subject.

Fig. 5.7. Descriptive statistics of the GHJ translations for the analyzed conditions is reported in Fig. 5.8. The results for each shoulder are reported in table 5.1. The smallest GHJ translations were observed along the M-L direction (p < 0.03) in all conditions. No significant differences were found in the GHJ translation components at 15 deg and 90 deg of arm abduction in the loaded condition. The precision assessment of the GHJ translations across the analyzed conditions and the two subjects revealed SD values below 0.22 mm, 0.33 mm, 0.17 mm for the A-P, S-I and ML directions, respectively, and below 0.17 mm for the 3D translations.
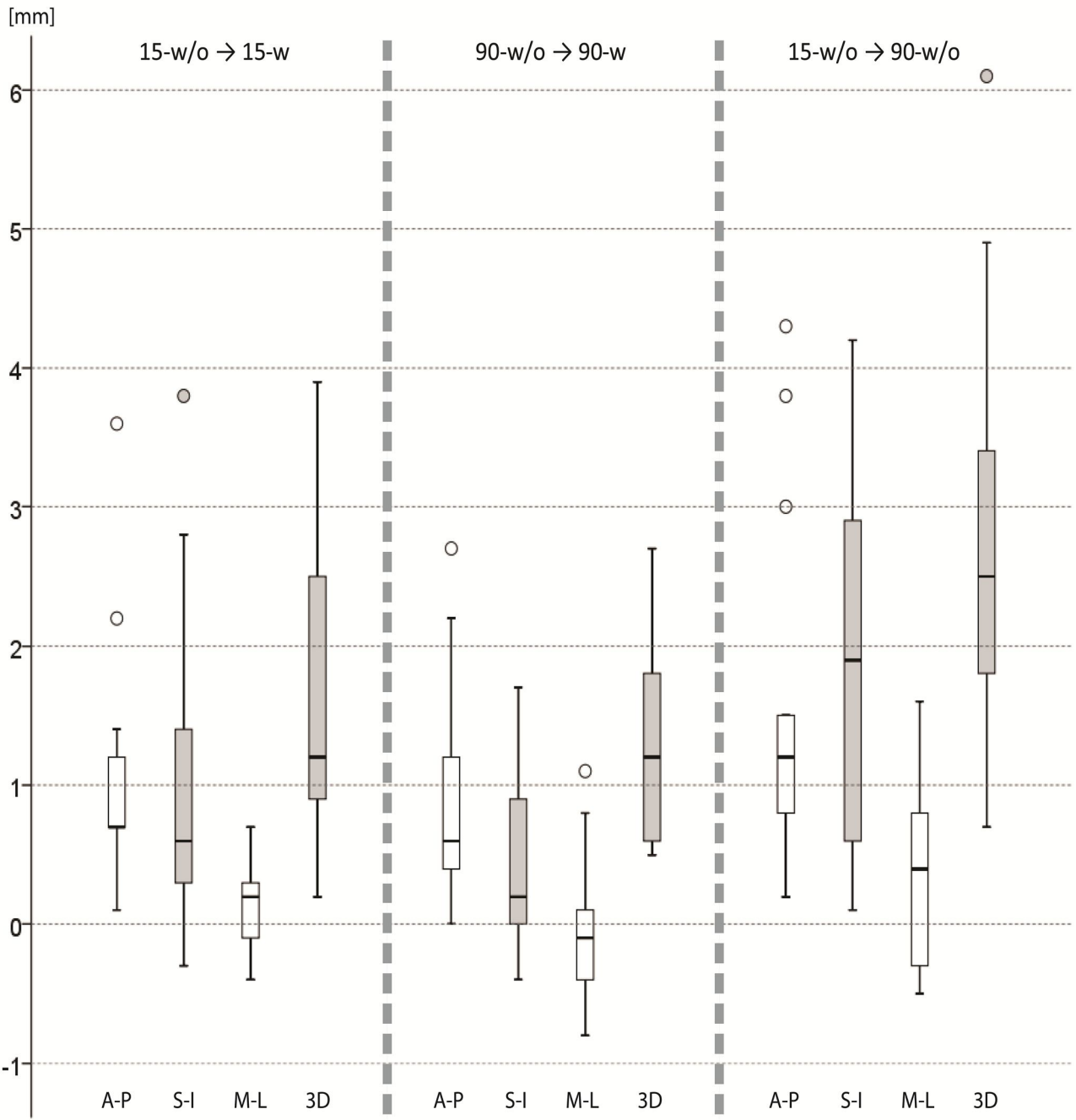
Figure 5.8: Minimum, first quartile, median, third quartiles and maximum values of the gleno-humeral joint center translations components (A-P, S-I, M-L) and of the 3D displacement for the following conditions: 1) between 15-w/o and 15-w; 2) between 90-w/o and 90-w; 3) between 15-w/o and 90-w/o. The outliers are shown by circles and represent cases that have values more than three times the height of the boxes.

	15-w/o to 15-w (mm)					90-w/o to 90-w (mm)					15-w/o to 90-w/o (mm)				
Subject	A-P	S-I	M-L	3D	2D	A-P	S-I	M-L	3D	2D	A-P	S-I	M-L	3D	2D
S1-left	0.7	0.4	0.1	0.8	0.8	1.2	-0.3	-0.4	1.3	1.3	3.8	3.2	-0.2	4.9	4.9
S1-right	2.2	2.8	0.3	3.5	3.5	2.2	-0.4	-0.1	2.2	2.2	1.1	2.3	0.4	2.5	2.5
S2-left	0.7	0.3	-0.4	0.9	0.8	0.5	0.0	-0.3	0.6	0.5	1.5	0.8	0.5	1.8	1.7
S3-left	1.1	0.3	-0.1	1.2	1.2	2.7	0.1	0.4	2.7	2.7	0.5	0.3	-0.4	0.7	0.6
S3-right	1.4	0.5	-0.1	1.5	1.5	0.4	0.2	0.1	0.5	0.5	0.2	0.1	0.9	0.9	0.2
S4-left	3.6	0.9	0.7	3.8	3.7	0.6	0.9	0.1	1.1	1.1	1.2	1.9	-0.3	2.3	2.3
S4-right	0.7	3.8	0.2	3.9	3.9	1.2	1.1	-0.8	1.8	1.7	4.3	4.2	0.8	6.1	6.0
S5-right	1.0	-0.3	-0.4	1.1	1.0	0.4	-0.3	-0.4	0.6	0.5	1.5	1.6	-0.5	2.3	2.2
S6-rigth	0.2	0.6	0.4	0.7	0.6	0.6	0.7	0.8	1.2	0.9	3.0	0.6	-0.5	3.1	3.0
S7-left	0.2	1.4	0.4	1.5	1.4	0.3	1.0	1.1	1.5	1.0	1.2	2.9	1.2	3.4	3.2
S8-rigth	0.7	0.8	-0.1	0.9	0.8	0.0	0.3	-0.5	0.6	0.3	0.6	3.1	1.6	3.6	3.2
S9-left	1.2	2.1	0.2	2.5	2.4	1.2	1.7	-0.1	2.1	2.1	1.2	2.8	0.2	3.1	3.1
S10-right	0.1	-0.1	0.2	0.2	0.2	0.3	0.1	-0.3	0.5	0.4	0.8	0.5	0.5	1.0	0.9
MEAN	1.1	1.0	0.1	1.7	1.7	0.9	0.4	0.0	1.3	1.2	1.6	1.9	0.3	2.7	2.6
SD	0.9	1.2	0.3	1.3	1.3	0.8	0.6	0.5	0.7	0.8	1.3	1.3	0.7	1.6	1.6

Table 5.1: GHJ translation of each shoulder, Mean and SD values averaged across subjects for the three conditions.

5.4   Discussion

The methodology presented allowed to accurately assess the GHJ translation *in vivo* under the application of an anterior directed force. The intensity of the anterior load was set to 20 N (Alberta et al., 2006; Marquardt et al., 2006; Su et al., 2009) plus the weight of the arm to remove differences in the loading condition among subjects associated to the gravity contribution. The GHJ stability was tested under moderately low loading condition in order to avoid patient's discomfort as the same methodology will be applied to analyze pathological shoulders. When no load was applied, from 15 deg to 90 deg of arm abduction, the gleno-humeral joint center (GHJC) translated both anteriorly and superiorly, while significant smaller displacements were observed in the M-L direction. In particular, the estimated anterior translations were within the ranges observed in similar *in vivo* studies (Table 5.2). Conversely, no clear trend has emerged from the literature on the GHJ translations in the S-I direction (Table 5.2).

Authors	Shoulder range of abduction	Direction (mm)		Muscle activity	Methodology
		A (+)/P (-)	S(+)/I(-)		
Graichen et al., 2000	30 - 90 deg	0.9	0.7	No	Horizontal open MR
Von Eisenhart-Rothe et al., 2002	30 - 90 deg	0.7 ± 0.6	1.3 ±1.1	No	Horizontal open MR
Sahara et al., 2007	0 - 90 deg	2.4 ± 2.6	0.5	Yes	Vertical open MR
Nishinaka et al., 2008	15 - 90 deg	-	0.9	Yes	Mono planar fluoroscopy
Massimini et al., 2012	0 - 90 deg	3.2 ± 2.8	0.3 ± 2.1	Yes	Biplanar fluoroscopy
Matsuki et al., 2012	0 - 90 deg	-	2.1	Yes	Monoplanar fluoroscopy
Our study	15 - 90 deg	1.6 ± 1.3	1.9 ± 1.3	No	Horizontal open MR

Table 5.2: GHJ translations (mean ± SD) along the A-P and S-I scapula axes estimated by different authors during in vivo experiments using different methodologies.

To the authors' knowledge, this is the first study investigating the GHJ translation *in vivo* as consequence of the application of an anterior directed force using bio-imaging techniques. When interpreting the GHJ translation components, it is important to keep in mind that the force direction (aligned to the gravity) did not necessarily coincide with the direction of the scapula A-P axis (Calderone et al., 2013). This circumstance explains the occurrence of HHC translation component different from zero along the S-I direction. Under the application of an anterior force of 20 N, the HHC moved, on average, with respect to the glenoid 1.7 ± 1.3 mm and 1.3 ± 0.7 mm at 15 deg and 90 deg of arm abduction, respectively. Despite the slightly larger GHJ translation at 15 deg, no statistically significant differences were found in the GHJ laxity for the two analyzed arm positions. The translations observed *in vivo* in our study were significantly smaller than those observed in previous cadaver studies under the application of an anterior load of 20 N. Alberta and colleagues (Alberta et al., 2006) tested six cadaver shoulders with an intact capsule and all muscles removed and found an anterior translation of 13.4 ± 2.0 mm at 90 deg of shoulder abduction. Smaller translations (6.8 ± 2.4 mm and 5.1 ± 3.1 mm at 0 deg and 90 deg of gleno-humeral abduction, respectively) were found by Marquardt et al. (2006) on twelve cadaveric shoulders with all soft tissues removed except for the tendons of the rotator cuff, the pectoralis major and the deltoid muscle. Adopting a more realistic

cadaveric model in which the rotator cuff tendons were individually loaded, Su et al., (2009) found an average translation of 2.0 ± 0.5 mm at 45 deg of gleno-humeral abduction. The discrepancies between *in vivo* and *in vitro* conditions can be ascribed to various factors such as the total or partial lack of the shoulder muscles and differences in muscular tone. In this regard, it is interesting to note that the GHJ translation measured when simulating the muscle tone (Su et al., 2009) were quite similar to the *in vivo* results herein presented. The level of precision associated to the GHJ translation estimates provided by the proposed MR-based methodology was acceptable (< 0.33 mm) and it is expected to be at least of one order of magnitude smaller than the GHJ translations. It is worth noting that, in order to increase the segmentation reproducibility and minimize the errors in the GHJ translation estimates, all shoulders were segmented by the same operator. The use of an MRI offers both advantages and limitations compared to alternative bio-imaging techniques such as CT or fluoroscopy. The main advantages are related to the complete non-invasiveness of the exam and the potentiality of visualizing and identifying soft tissues abnormalities in the GHJ (Rohad, 1998). A first limitation is that the joint analysis is restricted to static conditions, while dual fluoroscopy or single plane fluoroscopy combined with CT bone model allow to evaluate GHJ kinematics in dynamic conditions (Nishinaka et al., 2008; Massimini et al., 2012; Matsuki et al., 2012). Secondly, whereas using CT-based images, the segmentation is automatic, in MR images, the segmentation is mainly performed manually, it is time consuming and requires a high level of expertise. Furthermore, the reliability of the GHJ translation estimates is highly dependent on the quality of the reconstructed bone models. The one-Tesla horizontal open-MRI scanner used for this study, along with an appropriate imaging sequence, guaranteed for good quality images, however MR scanner with a lower magnetic field could not be suitable for such analysis. In conclusion, the MRI-based methodology allowed to analyze GHJ translations under loaded conditions within an acceptable level of reliability and to detect changes in GHJ translations which are clinically significant (Bey et al., 2006).

CONCLUSIONS

The present doctoral research was focused on developing and testing a Magnetic Resonance Imaging methodology for *in vivo* estimation of the GHJ translations with and without an external load.

A thorough review of the literature has highlighted that very limited data relative to gleno-humeral joint translations in healthy subjects resulting from the applications of external forces are available. Moreover, no studies investigating the GHJ translations *in vivo* as consequence of the application of an anterior directed force using bio-imaging techniques have been proposed so far. In particular, only few studies have been conducted using open MRI to estimate GHJ translations, but none of these have analyzed the shoulder under loaded condition. The developed methodology proposed in this research doctoral thesis represents a feasible tool for the assessment of the GHJ laxity because of the noninvasiveness for the patients and the possibility to measure the GHJ displacements *in vivo* under the application of an anterior directed force using a technique which provides an acceptable level of accuracy.

The results obtained in the present thesis were found to be different from those obtained in studies conducted on cadaver; in particular the translations in loaded conditions were smaller than those observed on cadaver. This discrepancy can be ascribed to the lack of muscular tone of the latter. On the other hand, the number of subjects analyzed in this study is too small to reach a definitive conclusion. In this regard, it was found that the GHJ translation measured when simulating the muscle tone were quite similar to the *in vivo* results presented in this study.

Results provided in this research project can be used to define normative reference data about the anterior translations of the gleno-humeral joint. This information can be useful when different pathological populations need to be evaluated. Another important aspect which tackles in this research project was the definition of the scapula and humerus anatomical coordinate systems. In fact, the quantification of the GHJ translations requires the definition of the scapular and humeral ACSs, which can be used with incomplete bone models derived from MR images. The large majority of the ACSs definitions proposed in the literature for both scapula and humerus are based on the use of selected anatomical landmarks or anatomical regions located both in the proximal and distal portion of the bone models. These ACSs are not suitable to be used with high resolution models obtained from MR clinical images, because, due to their restricted field of view, this technique prevents the acquisition of the

complete bone model. To guarantee a high level of precision in the GHJ translations estimate novel humeral and scapular ACSs were defined in order to meet a number of strict criteria: they were defined using ALs and ARs, easy to identify irrespective of the bone morphology acquisition techniques used and least susceptible to the physiological morphometric variability.

ACKNOWLEDGMENTS

REFERENCES

Abboud J.A., Soslowsky L.J. Interplay of the static and dynamic restraints in gleno-humeral instability. Clin Orthop Relat Res (400): 48-57, 2002.

Alberta F.G., Elattrache N.S., Mihata T., McGarry M.H., Tibone J.E., Lee T.Q. Arthroscopic anteroinferior suture plication resulting in decreased gleno-humeral translation 203 and external rotation. Study of a cadaver model. Journal of Bone and Joint Surgery (Am) 204 88:179-87, 2006.

Amadi H.O., Banerjee S., Hansen U.N., Wallace A.L., Bull A.M.J., 2008a. An optimized method for quantifying glenoid orientation. Int. J. Shoulder Surg. 2:25–29, 2008a.

Amadi H.O., Hansen U.N., Wallace A.L., Bull A.M.J. A scapular coordinate frame for clinical and kinematic analyses. J. Biomech. 41:2144–2149, 2008b.

Amadi H.O., Hansen U.N., Bull A.M. A numerical tool for the reconstruction of the physiological kinematics of the gleno-humeral joint. Proc. Inst. Mech. Eng. Part H J. Eng. Med.223:833–837, 2009a.

Amadi H.O., Majed A., Emery R.J.H., Bull A.M.J. A humeral coordinate system for in vivo 3D kinematics of the gleno-humeral joint. J. Musculoskeletal Res. 12:169–174, 2009b.

Anglin C and Wyss U.P., Review of arm motion analyses. Proceedings of the Institution of Mechanical Engineers. Part H, Journal of engineering in medicine 214: 541-555, 2000.

Anderst W., Zauel R., Bishop J., Demps E., Tashman S. Validation of three-dimensional model-based tibio-femoral tracking during running. Medical engineering & physics, 31(1):10–6, 2009.

Baeyens J.P., Van Roy P., De Schepper A., Declercq G., Clarijs J.P. Gleno-humeral joint kinematics related to minor anterior instability of the shoulder at the end of the late preparatory phase of throwing. Clinical Biomechanics 16:752-757, 2001.

Bey M.J., Zauel R., Brock S.K., Tashman S. Validation of a new model-based tracking technique for measuring three-dimensional, in vivo gleno-humeral joint kinematics. Journal of Biomechanical Engineering 128:604-609, 2006.

Besl P, McKay N. A method for Registration of 3-D Shapes. IEEE Transactions on Pattern Analysis and Machine Intelligence 14: 239-256,1992.

Bourne D.A., Choo A.M., Regan W.D., Macintyre D.L., Oxland T.R. The Placement of Skin Surface Markers for Non-Invasive Measurement of Scapular Kinematics Affects Accuracy and Reliability. Ann Biomed Eng., 2010.

Borstad J.D., Ludewig P.M. Comparison of scapula kinematics between elevation and lowering of the arm in the scapular plane. Clin Biomech 17:650–659, 2002.

Brandsson S., Karlsson J., Sward L., Kartus J., Eriksson B.I, Kärrholm J. Kinematics and laxity of the knee joint after anterior cruciate ligament reconstruction: pre- and postoperative radiostereometric studies. Am J Sports Med., 2002.

Burkhart S.S. Fluoroscopic Comparison of Kinematic Patterns in Massive Rotator Cuff Tears. A Suspension Bridge Model. Clin Orthop Relat Res. 284:144–152, 1992.

Bull A.M., Amis A.A. Accuracy of an electromagnetic tracking device. J Biomech.30(8):857-859, 1997.

Bull A.M.J., Amis A. A. Knee joint motion: description and measurement. Proc Inst Mech Eng [H] 212:357–372, 1998.

Botte M.J. Skeletal anatomy. In: Doyle, J.R., Botte M.J. (Eds.), Surgical Anatomy of the Hand and Upper Extremity. Lippincott Williams and Wilkins, Philadelphia, 19–23, 2002.

Calderone M., Cereatti A., Conti M., Della Croce U. Comparative evaluation of scapular and humeral coordinate systems based on biomedical images of the gleno-humeral joint. Journal of Biomechanics 47 (3):736-741, 2013.

Cappozzo A., Catani F., Della Croce U., Leardini A. Position and orientation in space of bones during movement: anatomical frame definition and determination. Clin.Biomech10:171–178, 1995.

Chhadia, A.M., Goldberg, B.A., Hutchinson, M.R. Abnormal translation in SLAP lesions on magnetic resonance imaging abducted externally rotated view. Arthroscopy 26:19- 25, 2010.

de Groot J.H. The shoulder: a kinematic and dynamic analysis of motion and loading. PhD thesis, Delft University of Technology, Delft, The Netherlands, 1998.

de Groot J.H. The scapulo-humeral rhythm: Effects of 2-D roentgen projection. Clin Biomech 14(1): 63-68, 1999.

de Leva P. Adjustments to Zatsiorsky-Seluyanov's segment inertia parameters. Journal of Biomechanics 29:1223-1230, 1996.

de Luca C.J., Forrest W.J. Force analysis of individual muscles acting simultaneously on the shoulder during isometric abduction. J Biomech 6:385–393, 1973.

Della Croce U., Cappozzo A., Kerrigan D.C. Pelvis and lower limb anatomical landmark calibration precision and its propagation to bone geometry and joint angles. Med. Biol. Eng. Comput. 37:155–161, 1999.

Della Croce U., Camomilla V., Leardini A., Cappozzo A. Femoral anatomical frame: assessment of various definitions. Med. Eng. Phys. 25:425–431, 2003.

Dempster W.T. Mechanisms of shoulder movement. Arch Phys Med Rehabil 46:49-70, 1965.

Dennis D.A., Mahfouz M.R., Komistek R.D., Hoff W. In vivo determination of normal and anterior cruciate ligament-deficient knee kinematics. Journal of biomechanics, 38(2):241–53, 2005.

Donati M., Camomilla V., Vannozzi G., Cappozzo A. Anatomical frame identification and reconstruction for repeatable lower limb joint kinematics estimates. J.Biomech. 41; 2219–2226, 2008.

Doody SG, Freedman L, Waterland JC: Shoulder movements during abduction in the scapular plane. Arch Phys Med Rehabil 51:595-604, 1970.

Everaert D.G., Spaepen A.J., Wouters M.J., Stappaerts K.H., Oostendorp R.A. Measuring small linear displacements with a three-dimensional video motion analysis system: determining its accuracy and precision. Arch. Phys. Med. Rehabil. 80:1082-1089, 1999.

Esfandiarpour F., Olyaei G.R., ShakouriRad A., Farahmand F., Talebian S., Makhsous, M., Parnianpour M. Reliability of determination of bony landmarks of the distal femur on MR images and MRI based 3D models. Iran. J. Radiol.6: 225–230, 2009.

Fleisig, G.S., Andrews, J.R., Dillman, C.J., and Escamilla, R.F., 1995, "Kinetics of baseball pitching with implications about injury mechanisms," Am J Sports Med, 23(2): 233-239, 1995.

Foxlin, E., Harrington, M., & Altshuler, Y. Miniature 6-DOF inertial system for tracking HMDs. Proceedings of SPIE: Helmet and Head-Mounted Display III, 3362, 1998.

Freedman L., Munro R.R. Abduction of the arm in the scapular plane: scapular gleno-humeral movements. J Bone Joint Surg 48-A: 1503–1510, 1966.

Gamage, S.S.H.U., Lasenby J. New least squares solutions for estimating the average centre of rotation and the axis of rotation. J. Biomech. 35:87–93, 2002.

Gerber C, Nyffeler R.W. Classification of Gleno-humeral Joint Instability. Clin Orthop 400:65–76, 2002.

Graichen, H., Bonel, H., Stammberger, T., Heuck, A., Englmeier, K.H., Reiser, M., Eckstein, F. A technique for determining the spatial relationship between the rotator cu! and the subacromial space in arm abduction using MRI and 3D image processing.Magnetic Research in Medicine 40, 640-643, 1998.

Graichen H, Stammberger T, Bonel H, Englmeier, K.H, Reiser M, Eckstein F. Gleno-humeral translation during active and passive elevation of the shoulder - a 3D open-MRI study. J Biomech. 33(5):609-613, 2000.

Grossman M.G., Tibone J.E. McGarry M.H., Schneider D.J., Veneziani S., Lee T.Q. A Cadaveric Model of the Throwing Shoulder: A Possible Etiology of Superior Labrum Anterior-to-Posterior Lesions. Bone Joint Surg Am. 87:824-831, 2005.

Grumet R.C, Bach B.R, Provencher M.T. Arthroscopic stabilization for first-time versus recurrent shoulder instability. Arthroscopy 26(2):239-248, 2010.

Halder A.M., Zhao K.D., Odriscoll S.W., Morrey B.F., An K.N. Dynamic Contributions to Superior Shoulder Stability. J Orthop Res. 2001; 19(2):206–212, 2001.

Halder A.M., Kuhl S.G., Zobitz M.E., Larson D., An K.N. Effects of the glenoid labrum and gleno-humeral abduction on stability of the shoulder joint through concavity-compression: an in vitro study. J Bone Joint Surg Am 83:1062–1069, 2001.

Hallström E., Kärrholm.J. Shoulder Rhythm in Patients and Controls, Dynamic RSA during active and passive abduction, 2009.

Harryman D.T.II, Sidles J.A., Clark J.M., McQuade K.J., Gibb T.D., Matsen F.A.III (1990) Translation of the humeral head on the glenoid with passive gleno-humeral motion. J Bone Joint Surg 72-A:1334–1343, 1990.

Harryman D.T.II, Sidles J.A., Harris S.L., Matsen F.A.III (1992) The role of the rotator interval capsule in passive motion and stability of the shoulder. J Bone Joint Surg 74-A: 53–66, 1992.

Hart D.L., Carmichael S.W. Biomechanics of the shoulder. J Orthop Sports Phys Ther. 6(4):229-234, 1985.

Hawkins R.J., Neer C.S.II, Pianta R.M., Mendoza F.X. Locked posterior dislocation of the shoulder. J Bone Joint Surg Am 69:9–18, 1987.

Hawkins R.J., Hobeika P.E. Physical examination of the shoulder. Orthopedics 6:59-64, 1983.

Herman G.T., Foundamentals of computerized tomography. Image reconstruction from projection, 2nd edition. Springer, 2009.

Hill A.M., Bull A.M.J., Urwin M., Aichroth P., Wallace A.L. Potential clinical application of electron beam computed tomography to dynamic imaging of the shoulder. British Elbow and Shoulder Society, Wigan, 2003.

Hill A.M., Bull A.M.J, Amadi H., Aichroth P., Wallace A.L. Quantitative dynamic electron beam computed tomography imaging of the shoulder rhythm in real-time. International Congress on Surgery of the Shoulder, Washington, 2004.

Hill A.M., Bull, A.M., Dallalana, R.J., Wallace, A.L., Johnson, G.R. Gleno-humeral motion: review of measurement techniques. Knee Surgery, Sports Traumatology, Arthroscopy 15:1137-1143, 2007.

Hodge D.K., Beaulieu C.F., Thabit G.H., Gold G.E., Bergman A.G., Butts R.K., Dillingham M.F., Herfkens R.J. Dynamic MR imaging and stress testing in gleno-humeral instability: comparison with normal shoulders and clinical/surgical findings. J Magn Reson Imaging 13:748–756, 2001.

Holden J.P., Orsini J.A., Siegel K.L., Kepple T.M., Gerber L.H., and Stanhope S.J. ''Surface Movement Errors in Shank Kinematics and Knee Kinetics During Gait,'' Gait & Posture, 5:217–227, 1997.

Howell S.M., Galinat B.J. The glenoid-labral socket: a constrained articular surface. Clin Orthop 243:122–5, 1989.

Iannotti J.P., Gabriel J.P., Schneck S.L: The normal gleno-humeral relationships. An anatomical study of one hundred and forty shoulders. J Bone Joint Surg Am 74:491-500, 1992.

Iannotti J.P., Williams G.R. Total shoulder arthroplasty. Orthop Clin North Am 29(3):377–91, 1998.

Iannotti J.P., Williams G.R., eds. Disorders of the shoulder: Diagnosis and management. Philadelphia: Lippincott Williams & Wilkin, 1999.

Iannotti J.P., Lippitt S.B., Williams G.R. Variation in neck-shaft angle: influence in prosthetic design. Am. J. Orthop. 36:9–14, 2007.

Inman V., Saunder J., Abbot L. Observations on the function of the shoulder joint. J Bone Joint Surg 26:1, 1944.

Johnston T.B. The movements of the shoulder joint. A plea for the use of the 'Plane of the Scapula' as the plane of reference for movements occurring at the humero-scapular joint. Br J Surg 25:252–260, 1937.

Kaltenborn F. Mobilization of the Extremity Joints. Examination and Basic Treatment Techniques. Oslo, Olaf Bokhandel, 1980.

Karduna A.R., Williams G.R., Williams J.L., Iannotti J.P. Kinematics of the gleno-humeral joint: influences of muscle forces, ligamentous constraints, and articular geometry. J Orthop Res 14:986–993, 1996.

Karduna A.R., Williams G.R., Williams J.L., Iannotti J.P. Gleno-humeral joint translations before and after total shoulder arthroplasty. A study in cadavera J Bone Joint Surg 79-A:1166–1174, 1997.

Karduna A.R., McClure P.W., Michener L.A. Scapular kinematics: effects of altering the Euler angle sequence of rotations. J Biomech 33:1063–1068, 2000.

Karrholm J., Selvik G., Elmqvist L.G., Hansson L.I., and Jonsson H. Three-Dimensional Instability of the Anterior Cruciate Deficient Knee. J. Bone Jt. Surg., 70-B: 777–783, 1988.

Karrholm J. Roentgen Stereophotogrammetry. Review of Orthopedic Applications. Acta Orthop. Scand. 60:491–503, 1989.

Kedgley A.E., Dunning C.E. Analternativedefinition of the scapular coordinate system for use with RSA. J. Biomech.43:1527–1531, 2010.

Kelley M, Clark W: Orthopedic Therapy of the Shoulder. Philadelphia, JB Lippincott, 1995.

Kessel L., Watson M. The painful arc syndrome. Clinical classification as a guide to management. J Bone Joint Surg Bry 59(2):166-72, 1977.

Kindratenko V. Calibration of electromagnetic tracking devices. Virtual Reality: Research, Development, and Applications, 4:139–150, 1999.

Kindratenko V., Bennett A. Evaluation of rotation correction techniques for electromagnetic position tracking systems. Proceedings of the 6th Eurographics Workshop on Virtual Environments, 13–22, 2000.

Kindratenko V. A Comparison of the Accuracy of an Electromagnetic and a Hybrid Ultrasound-Inertia Position Tracking System. Presence 10(6):657– 663, 2001.

Kiss J., McNally ,E.G., Carr A.J. Measurement of the anteriorposterior translation of the humeral head using MRI. International Orthopaedics 21:77-82, 1997.

Kon Y., Nishinaka N., Gamada K., Tsutsui H., Banks S.A. The influence of handheld weight on the scapulohumeral rhythm. Journal of Shoulder and Elbow Surgery, 2008.

Kibler W.B. The role of the scapula in athletic shoulder function. Am J Sports Med 26:325-337, 1998.

Lafortune M.A., Lambert C.E., Lake M.J. Skin Marker Displacement at the Knee Joint. NACOB II: The Second North American Congress on Biomechanics, Chicago, IL: Pergamon Press, J. Biomech., 26:299, 1992.

Lagacé P.Y., Billuart F., Ohl X., Skalli W., Tétreault P., de Guise J., Hagemeister, N. Analysis of humeral head displacements from sequences of biplanar X-rays: repeatability study and preliminary results in healthy subjects. Computer Methods in Biomechanics and Biomedical Engineering 15:221-9, 2012.

Lam F., Bhatiaa D.N, Mostofib S.B., van Rooyena K., de Beera J.F. Biomechanical considerations of the normal and rotator cuff deficient shoulders and the reverse shoulder prosthesis. Current Orthopaedics 21:40–46, 2007.

Lee Y.S., Lee T.Q. Specimen-Specific Method for Quantifying Gleno-humeral Joint Kinematics. Annals of Biomedical Engineering 38(10): 3226–3236, 2010.

Lee S.U., Lang P.M.R. MR arthrography to identify degenerative and post traumatic diseases in the shoulder joint. Eur. J. Radiol 35:126–135, 2000.

Lee C.H., Goo J.M., Ye H.J., Ye S.J., Park C.M., Chun E.J., Im J.G. Radiation dose modulation techniques in the multi detector CT era: from basics to practice. Radiographics 28:1451–1459, 2008.

Lee Y. S. Seon J.S. Shin V.I., Kim G.H., Jeon M. Anatomical Evaluation of CT-MRI Combined Femoral Model. BioMedical Engineering online 7, 2008.

Lin H.T., Hsu A.T., Chang G.L., Chang Chien J.R., An K.N., Su F.C. Determining the resting position of the gleno-humeral joint in subjects who are healthy. Physical therapy 87(12):1669-1682, 2007.

Lippitt S., Matsen F. Mechanisms of gleno-humeral joint stability. Clin Orthop 291:20, 1993.

Ludewig P.M., Phadke V., Braman J.P., Hassett D.R., Cieminski C.J., LaPrade R.F. Motion of the shoulder complex during multiplanar humeral elevation. J Bone Joint Surg Am. 91(2):378-389, 2009.

Ludewig P. M., Hassett D. R., LaPrade R. F., Camargo P. R., Braman J. P., 2010. Comparison of scapular local coordinate systems. Clin. Biomech.25:415–421, 2010.

Lujan T.J., Lake S.P., Plaizier T.A., Ellis B.J., Weiss J.A.: Simultaneous measurement of three-dimensional joint kinematics and ligament strains witt optical methods. Journal of Biomechanical Engineering 127:193-197, 2005.

Lundberg A. Patterns of motion of the ankle/foot complex. Thesis, Karolinska Institutet, Stockholm, Sweden, 1988.

Lundberg A., Svensson O.K., Németh G,.Selvik G. The axis of rotation of the ankle joint. J Bone Joint Surg [Br]. 71:94-99, 1989.

Mallon W.J., Speer, K.P., 1995. Multidirectional instability: current concepts. Journal of Shoulder and Elbow Surgery 4:54-64, 1995.

Mandalidis D.G., Mc Glone B.S., Quigley R.F., McInerney D., O'Brien M. Digital Fluoroscopic Assessment of the Scapulohumeral Rhythm. Surg Radiol Anat. 21(4):241–246, 1999.

Massimini D.F., Li G., Warner J.P. Gleno-humeral contact kinematics in patients after total shoulder arthroplasty. J Bone Joint Surg Am. 92(4):916-926, 2010.

Massimini D.F., Boyer P.J., Papannagari R., Gill T.J., Warner J.P., Li G. In-vivo gleno-humeral translation and ligament elongation during abduction and abduction with internal and external rotation. Journal of Orthopaedic Surgery and Research 28:7-29, 2012.

Milne A.D., Chess D.G., Johnson J.A., and King G.J. Accuracy of an electromagnetic tracking device: a study of the optimal range and metal interference, J Biomech, 29(6):791-793, 1996.

Marquardt B., Hurschler C., Schneppendahl J., Witt K.A., Pötzl W., Steinbeck J. Quantitative assessment of gleno-humeral translation after anterior shoulder dislocation and subsequent arthroscopic bankart repair. American Journal of Sports Medicine 34:1756-1762, 2006.

Matsen F.A.III, Harryman D.T.II, Sidles J.A. Mechanics of gleno-humeral instability. Clin Sports Med 10:783–788, 1991.

Matsen F.A.III, Lippitt S.B., Sidles J.A., et al. (eds): Practical Evaluation and Management of the Shoulder. Philadelphia, W. B. Saunders, 1994.

Matsen F.A.III, Thomas S.C., Rockwood C.A.Jr. Gleno-humeral instability, in Rockwood CA Jr, Matsen F.A.III (eds): The Shoulder. Second edition. Philadelphia, WB Saunders, 611–754, 1998.

Matsuki K., Matsuki K.O., Yamaguchi S., Ochiai N., Sasho T., Sugaya H., Toyone T., Wada Y., Takahashi K., Banks S.A. Dynamic in vivo gleno-humeral kinematics during scapular plane abduction in healthy shoulders. Journal of Orthopaedic Sports and Physical Therapy 42:96-104, 2012.

McFarland E.G., Torpey B.M., Curl L. A. Evaluation of shoulder laxity. Sports Med 22:264–272, 1996.

McQuade K.J., Dawson J., Smidt G.L. Scapulothoracic muscle fatigue associated with alterations in capulohumeral rhythm kinematics during maximum resistive shoulder elevation. J Orthop Sports Phys Ther. 28(2):74-80, 1998.

McQuade K.J., Murthi A.M., 2004. Anterior gleno-humeral force/translation behavior with and without rotator cuff contraction during clinical stability testing. Clinical Biomechanics 19:10-15, 2004.

Meskers C.G.M., van der Helm F.C.T., Rozendaal L. A., Rozing P. M. In vivo estimation of the gleno-humeral joint rotation center from scapular bony landmarks by linear regression. Journal of Biomechanics 31:93-96, 1998.

Nishinaka N., Tsutsui H., Mihara K., et al. Determination of in vivo gleno-humeral translation using fluoroscopy and shape-matching techniques. J Shoulder Elbow Surg. 17(2):319-322, 2008.

Novotny J.E., Beynnon B.D., Nichols C.E. Modeling the stability of the gleno-humeral joint during external rotation. J. Biomech. 33:345–354, 2000.

Oatis C.A. Kinesiology: The Mechanics and Pathomechanics of Human Movement. Philadelphia, Lippincott Williams & Wilkins, 2004.

O'Brien S.J., Neves M.C., Arnoczky S.P. The anatomy and histology of the inferior gleno-humeral ligament complex of the shoulder. Am J Sports Med 18:449, 1990.

O'Brien S.J., Schwartz R.S., Warren R.F., Torzilli P.A. Capsular restraints to anterior-posterior motion of the abducted shoulder: a biomechanical study. J Shoulder Elbow Surg 4:298– 308, 1995.

O'Connell P.W., Nuber G.W., Mileski R.A., Lautenschlager E. The contribution of the gleno-humeral ligaments to anterior stability of the shoulder joint. Am J Sports Med 18:579–84, 1990.

Payne L.Z., Deng X.H., Craig E.V., Torzilli P.A., Warren R.F. The Combined Dynamic and Static Contributions to Subacromial Impingement. A Biomechanical Analysis. Am J Sports Med. 25(6):801–808, 1997.

Pearl M.L., Jackins S., Lippitt S.B., Sidles J.A.., Matsen F.A.Humeroscapular positions in a shoulder range-of-motion-examination. J. Shoulder Elbow Surg. 1:296–305, 1992.

Peat M. Functional Anatomy of the Shoulder Complex. Physical Therapy 66:1855-1865, 1986.

Pfirrmann C.W., Huser M., Szekely G., Hodler J., Gerber C. Evaluation of Complex Joint Motion With Computer-Based Analysis of Fluoroscopic Sequences. Invest Radiol. 37(2):73–76, 2002.

Poppen N.K., Walker P.S. Normal and abnormal motion of the shoulder. J Bone Joint Surg 58-A:195–201, 1976.

Raab F., Blood E., Steioner T., & Jones, H. Magnetic position and orientation tracking system. IEEE Transactions on Aerospace and Electronic Systems, 15(5):709–718, 1979.

Randelli M., Gambrioli P.L. Gleno-humeral osteometry by computed tomography in normal and unstable shoulders. Clin Orthop 208:151, 1986.

Reinschmidt C., van den Bogert A.J., Nigg B.M., Lundberg A., Murphy N. Effect of Skin Movement on the Analysis of Skeletal Knee Joint Motion During Running. J. Biomech., 30: 729–732, 1997.

Remia L.F., Ravalin R.V., Lemly K.S., McGarry M.H., Kvitne R.S., Lee T.Q. Biomechanical evaluation of multidirectional gleno-humeral instability and repair. Clin Orthop Relat Res. 416:225-236, 2003.

Rhoad R.C., Klimkiewicz J.J., Williams G.R., Kesmodel S.B., Udupa J.K., Kneeland J.B., Iannotti J.P. A new in vivo technique for three-dimensional shoulder kinematics analysis. Skeletal Radiology 27: 92-97, 1998.

Robinson C.M., Howes J., Murdoch H., Will E., Graham C. Functional outcome and risk of recurrent instability after primary traumatic anterior shoulder dislocation in young patients. J Bone Joint Surg Am. 88(11):2326-2336, 2006.

Ryd L., Yuan X., Löfgren H. Methods for determining the accuracy of radiostereometric analysis (RSA). Acta Orthop Scand. 71:403- 408, 2000.

Saari T., Carlsson L., Karlsson J., Kärrholm J. Knee kniematics in medial arthrosis. Dynamic radiostereometry during active extension and weight-bearing. J Biomech. 38:285-292, 2005.

San Juan J.G., Karduna A.R. Measuring humeral head translation using fluoroscopy:a validation study. Journal of Biomechanics 43:771-774, 2010.

Saha A.K. Dynamic stability of the gleno-humeral joint. Acta Orthop Scand 42:491–505, 1971.

Saha A.K. Mechanism of shoulder movements and a plea for the recognition of ''Zero Position'' of gleno-humeral joint. Indian J Surg 12:153–165, 1950.

Sahara W., Sugamoto K., Murai M., Tanaka H., Yoshikawa H. The three-dimensional motions of gleno-humeral joint under semi-loaded condition during arm abduction using vertically open MRI. Clin Biomech 22(3):304-312, 2007.

Salvia P., Jan S.V., Crouan A., Vanderkerken L., Moiseev F., Sholukha V., Mahieu C., Snoeck O., Rooze M. Precision of shoulder anatomical landmark calibration by two approaches: a CAST-like protocol and a new anatomical palpator method.GaitPosture 29:587–591, 2009.

Sauers E.L., Borsa P.A., Herling D.E., Stanley R.D. Instrumented measurement of gleno-humeral joint laxity: reliability and normative data. Knee Surg, Sports Traumatol, Arthrosc 9:34–41, 2001.

Schiffern S.C., Rozencwaig R., Antoniou J., Richardson M.L., Matsen F.AIII. Anteroposterior Centering of the Humeral Head on the Glenoid In Vivo. Am J Sports Med 30:382, Am J Sports Med, 2002.

Selvik G., Alberius P., Aronson A.S. A roentgen stereophotogrammetric system. Construction, calibration and technical accuracy. Acta Radiol Diagn (Stockh) 24: 343-352, 1983.

Selvik, G. Roentgen Stereophotogrammetric Analysis. Acta Radiol., 31:113–126, 1990.

Sharkey N.A., Marder R.A. The Rotator Cuff Opposes Superior Translation of the Humeral Head. Am J Sports Med. 23(3):270–275, 1995.

Simonet W.T., Melton L.J., 3rd, Cofield RH, Ilstrup DM. Incidence of anterior shoulder dislocation in Olmsted County, Minnesota. Clin Orthop Relat Res. (186):186-191, 1984.

Smith T.B., Nayak, K.S. Reduced field of view MRI with rapid, B1-robustouter volume suppression. Magn. Reson. Med. 67:1316–1323, 2012.

Standring S.Gray's Anatomy of the human body, 40th Edition. The Anatomical Basis of clinical Practice, Expert Consult. Elsevier, Philadelphia, 2008.

Stanley R.D. Instrumented measurement of gleno-humeral joint laxity: reliability and normative data. Knee Surgery, Sports Traumatology, Arthroscopy 9:34-41, 2001.

Su W.R., Budoff J.E., Luo Z.P. The effect of anterosuperior rotator cuff tears on gleno-humeral translation. Arthroscopy 25:282-289, 2009.

Tashman S., Anderst V.In-Vivo Measurement of dynamic Joint Motion Using High Speed Biplane Radiography and CT: Application to Canine ACL Deficiency. Journal of Biomechanical Engineering 125:238-245, 2003.

Torry M.R., Shelburne K.B., Peterson D.S., Giphart J.E., Krong J.P., Myers C., Steadman J.R., Woo S.L.Y. Knee Kinematic Profiles During Drop Landings: A Biplane Fluoroscopy Study. Med Sci Sports Exerc, 43(3):533–41, 2010.

Uvehammer J., Kärrholm J., Brandsson S. In vivo kinematics of total knee arthroplasty. Concave versus posterior-stabilised tibial joint surface. J Bone Joint Surg Br. 82(4):499-505, 2000.

van Andel C., van Hutten K., Eversdijk M., Veeger D., Harlaar J. Recording scapular motion using an acromion marker cluster. Gait Posture. 29(1):123-128., 2009.

von Eisenhart-Rothe R.M., Jager A., Englmeier K.H., Vogl T.J., Graichen H. Relevance of Arm Position and Muscle Activity on Three-Dimensional Gleno-humeral Translation in Patients With Traumatic and Atraumatic Shoulder Instability. Am J Sports Med. 30(4):514–522., 2002.

van Andel C, van Hutten K, Eversdijk M, Veeger D, Harlaar J. Recording scapular motion using an acromion marker cluster. Gait Posture 29(1):123-128, 2009.

VandenBerghe G., Hoenecke H.R., Fronek J. Gleno-humeral Joint Instability. The Orthopedic Approach. Seminars in musculoskeletal radiology 9(1), 2005.

van der Helm F.C.T.A standardized protocol for motion recordings of the shoulder. In:Veeger, H.E.J.,vanderHelm, F.C.T., Rozing, P.M.(Eds.). Proceedings of the First Conference of the International Shoulder Group, 1997.

Van SintJan S. Introducing anatomical and physiological accuracy in computerizing anthropometry for increasing the clinical usefulness of modeling system. Phys. Rehab. Med.17:249–274, 2005.

Van SintJan S., DellaCroce U. Identifying the location of human skeletal landmarks: why standardized definitions are necessary—a proposal. Clin. Biomech. 20:659–660, 2005.

Van Sint Jan S. Color Atlas of skeletal landmark definitions. In: Churchill Livingstone (Ed.), Guidelines for Reproducible Manual and Virtual Palpations.Elsevier, Edinburg, 2007.

Veeger H.E. The position of the rotation center of the gleno-humeral joint. J. Biomech.33:1711–1715, 2000.

Veeger, H.E., van der Helm, F.C. Shoulder function: the perfect compromise between mobility and stability. Journal of Biomechanics 40:2119-2129, 2007.

Verstraeten T., Deschepper E., Jacxsens M., Walravens S., DeConinck B., Pouliart N., De Wilde L.F. Determination of a reference system for the three-dimensional study of the gleno-humeral relationship. Skeletal Radiol.42:1–11, 2013.

von Eisenhart-Rothe, R.M., Jäger, A., Englmeier, K.H., Vogl, T.J., Graichen, H. Relevance of arm position and muscle activity on three dimensional gleno-humeral translation in patients withtraumatic and atraumatic shoulder instability. American Journal of Sports Medicine 30:514-522, 2002.

von Eisenhart-Rothe, R.M., Hinterwimmer, S., Graichen, H. Simultaneous 3D assessment of gleno-humeral shape, humeral head centering, and scapular positioning in atraumatic shoulder instability: a magnetic resonance-based in vivo analysis. American Journal of Sports Medicine 38:375-382, 2010.

Walter S.D., Eliasziw M., Donner A. Sample size and optimal designs for reliability studies.Stat.Med.17:101–110, 1998.

Westbrook C. and Kaut C. MRI in Practice, 2nd edition.Blackwell Science Oxford, 1993.

Werner C.M., Nyffeler R.W, Jacob H.A, Gerber C. The effect of capsular tightening on humeral head translations. J Orthop Res 22:194-201, 2004.

Wu G., vanderHelm F.C.T., Veeger H.E.J., Makhsous M., VanRoy P., Anglin C., Nagels J., Karduna A.R., McQuade K., Wang X., Werner F.W., Buchholz B. ISB recommendation on the definitions of joint coordinate systems of various joints for the reporting of human joint motion-part II: shoulder, elbow, wrist and hand. J. Biomech. 38:981–992, 2005.

Publications

Journals

Bianco A., <u>Calderone M.</u>, Cacciotti I. Electrospun PHBV/PEO co-solution blends: microstructure, thermal and mechanical properties, Mater Sci. Eng. C. 33(3):1067-77, 2013.

Cacciotti I., <u>Calderone M.</u>, Bianco A. Tailoring the properties of electrospun PHBV mats: Co-solution blending and selective removal of PEO, European Polymer Journal 49 (10):3210–3222, 2013.

<u>Calderone M.</u>, Cereatti A., Conti M., Della Croce U. Comparative evaluation of scapular and humeral coordinate systems based on biomedical images of the gleno-humeral joint", Journal of Biomechanics 47(3):736-741, 2013.

Cereatti A., <u>Calderone M.</u>, Buckland M.D., Buettnerb A., Della Croce U., Rosso C. In vivo gleno-humeral translation under external loading in an open MRI setup. Journal of Biomechanics (submitted).

Abstracts

<u>Calderone M.</u>, Cereatti A., Merella E., Della Croce U. Anatomical landmarks position estimation in incomplete 3D humerus models, presented at 3rd Congress National Group of Bioengineering, Rome, Italy, June 26th-29th, 2012.

<u>Calderone M.</u>, Cereatti A., Rosso C., Costantino S., Conti M., Della Croce U. Anatomical coordinate systems for high-resolution scapula and humerus models, Gait & Posture, 2013, 37S1:S24-S25.

Cereatti A., <u>Calderone M.</u>, Buckland D.M, Muller A.M., Della Croce U., Rosso C. In vivo gleno-humeral translation under external loading in an open MRI setup, Proceedings of XXIV ISB Congress, Natal, Brazil 2013.

<u>Calderone M.</u>, Cereatti A., Rosso C., Della Croce U. In vivo evaluation of gleno-humeral joint translations in loaded and unloaded conditions, Proceedings of XXIV National Congress of SIAMOC, Pisa, Italy, 2013